Miriam Kosik

nr albumu: 502897

Praca doktorska

na kierunku fizyka

Tight-binding framework to study optical properties of graphene nanoantennas with adatoms

Promotor pracy doktorskiej:

dr hab. Karolina Słowik, prof. UMK

Promotor pomocniczy:

dr Marta Pelc

Toruń 2022

Contents

Preface

The dissertation which lies before you has been written in the course of my PhD studies at the Faculty of Physics, Astronomy and Informatics at the Nicolaus Copernicus University in Toruń. It contains a summary of results from the research project in which I was engaged during the time of my PhD programme.

I have decided to write the text using the plural first person pronoun *we*. The motivation is that the framework introduced in this thesis is due to a joint effort of several people and a large part of the presented content is the result of discussions with my supervisors and our co-workers from the Karlsruhe Institute of Technology (KIT) and Donostia International Physics Center (DIPC).

My main responsibilities in the project involved topics related to quantum optics and quantum dynamics. In particular, I investigated how to include the adatom into the system and explored processes occurring in it (like Rabi oscillations or spontaneous emission). I also devoted a lot of work to the numerical implementation of the framework, as well as to code maintenance, refactoring and documentation, which I hope will make it accessible and easy to extend for future users.

The framework presented in this thesis would not exist in this form without the help of many people. First of all, I would like to thank my supervisors, Karolina and Marta, for their help in formulating research questions, and for their guidance and support during the entire course of my PhD studies. Furthermore, I thank dr Andrés Ayuela from DIPC for all discussions and sharing his knowledge of graphene physics. I would also like to thank prof. Carsten Rockstuhl and Marvin Müller from KIT for their invaluable contributions to the parts concerning classical optics, plasmonics and electromagnetism, especially on including the external field and calculating the absorption spectra. Additionally, I would like to thank Marvin for our close collaboration on the code implementation, which I found very satisfying and fruitful.

Introduction

Since its discovery in 2004, graphene has been experiencing constant attention due to its numerous unconventional physical properties, especially optical, electronic and plasmonic ones. Graphene is able to sustain plasmon polaritons with relatively long lifetimes as compared to those of noble metal nanostructures and offers the exceptional possibility to tune their properties after the nanostructure has been fabricated, by means of doping or electrostatic gating of the material. Cutting graphene into finite nano-sized flakes allows to bring the resonant plasmonic frequencies into the optical range of the electromagnetic spectrum, which can be especially interesting for applications, since this is the range where many atoms and molecules are optically active.

Exciting plasmon polaritons in metallic nanostructures hugely impacts the electromagnetic density of states in their surroundings. Such modified density of states may impact optical properties of adjacent atomic systems and can be used to enhance the strength of their interaction with light. Since graphene plasmon polaritons show extraordinary properties in terms of energy confinement, lifetime and tunability, they can be used to bring light-matter interaction close to its extreme.

The aim of this thesis is to introduce a mathematical model, which describes hybrid systems consisting of graphene nanoflakes coupled to adjacent atoms (adatoms). To achieve this, one has to keep in mind several things. First of all, a proper description of small graphene nanoflakes requires a quantum-mechanical approach. Additionally, the extreme concentration of electromagnetic energy near plasmonic nanostructures suggests that atomic systems coupled to plasmonic graphene flakes should be positioned extremely close, at distances for which tunnelling effects might become meaningful. Moreover, the physical properties of graphene are strongly determined by its honeycomb-like structure. Hence, any impurity placed on the surface of a graphene sheet perturbs this regular lattice, which gives rise to significant changes in the electronic, optical and transport

properties of this material.

The thesis will introduce a framework for modelling hybrid systems consisting of graphene nanoflakes coupled to adatoms, which takes into account all the aspects mentioned above. The purpose of the model is to describe the adatom's influence on the optical properties and dynamics of a graphene nanoflake, as well as the back-action from the latter. The presentation of the model will be supported by its exemplary application to simple hybrid systems.

Rigorous quantum-mechanical description of electron dynamics in this case should exploit many-body approaches. In the simplest but also the coarsest of them, each electron is modelled in a Hilbert space of the size equal to the doubled number of atomic sites in the graphene flake $2N$ (the factor 2 comes from the fact that spin is incorporated and there are two available orbitals per site for each electron), while the space of all N_e electrons has the size of $\binom{2N}{N_e}$ (we distribute N_e electrons on $2N$ spin-orbitals). However, graphene flakes which are active in the optical regime have sizes corresponding to a few hundred atoms, making such straightforward approach difficult to use in practice. Let us consider three nanoflakes without doping ($N_e = N$) to demonstrate how badly the dimension scales with the size of the system: for a simple benzene ring, the dimension is $\binom{6}{3} = 20$, for an 18-atom triangular flake it already becomes $\binom{18}{9} = 48620$ and for a 100-atom nanoflake it would be $\binom{100}{50} \approx 10^{29}$.

In the second-quantisation picture, the attempt to exactly specify which state is occupied by which particle is replaced by a less demanding one, evaluating the *number* of particles occupying each site. Even though the Hilbert space size scaling is significantly reduced, it is still exponential and reads as 2^N. A treatment of flakes with a few hundred atoms remains computationally challenging.

To model the electron dynamics in such large structures, our framework has been based on the single-particle density-matrix approach, in which the size of the Hilbert space scales linearly with the number of atomic sites in the graphene nanoflake N. The advantages and challenges of this approach are presented in Chapters 3 and 4, where the model is introduced in detail.

The thesis is structured as follows: Chapter 1 contains fundamental facts from graphene physics, Chapter 2 introduces the formalism used in quantum optics to describe the dynamics of two-level systems. Chapter 3 introduces the general model to describe optical

and electronic properties of finite graphene flakes and presents most important predictions of physical properties of graphene nanoflakes obtained in this framework. In Chapter 4, the model is extended to account also for the presence of adatoms near graphene flakes. It is applied to an exemplary hybrid system to demonstrate canonical effects like Rabi oscillations and spontaneous emission in the adatom. The summary and outlook of the thesis lists problems which could be treated with the developed model as well as its possible extensions.

Chapter 1

Electronic and optical properties of graphene

Graphene is a one-atom-thick allotrope of carbon, which is increasingly gaining attention of scientists and technology developers due to its numerous unusual properties with promising application potential. It is a gapless semiconductor and at the same time one of the best conductors of electricity on Earth, which remains capable of conducting even at the limit of zero temperature and zero carrier concentration with a finite conductivity value of $\sim 4e^2/h$ [1]. It exhibits high carrier mobility of around $1332.4\,\mathrm{cm^2/Vs}$ and low resistivity of $0.7\,\mathrm{k\Omega}$ at room temperature [2]. Charge carriers in graphene obey linear dispersion relation, thus mimicking massless relativistic particles (so-called massless Dirac fermions). This results in the observation of very peculiar electronic properties like anomalous integer quantum Hall effect, the Klein paradox, absence of localisation [3].

Graphene has a remarkable intrinsic tensile strength of 130 GPa and a Young's modulus close to 1 TPa [4], which means it has the tensile stiffness of diamond but at the same time it is lighter than aluminium. Graphene is highly thermally conductive with a thermal conductivity of around 4000 W/mK [5]. It is considered to be completely impermeable to gases and liquids, even a single helium atom cannot pass through a defect-free monolayer graphene sheet [6]. Graphene also represents a conceptually new class of materials, so-called two-dimensional materials, and it is very attractive for the fabrication of mixed-dimensional van der Waals heterostructures [7].

However, the wonderful properties cannot be effectively exploited without the means to synthesise high-quality, large-area graphene. First stable samples of high-quality

graphene have been fabricated in 2004 [8], which was a big surprise considering the common belief at that time, that truly two-dimensional crystals cannot exist in a stable form [9]. The discovery led to a Nobel Prize in Physics for Andre Geim and Konstantin Novoselov awarded in 2010 *for groundbreaking experiments regarding the two-dimensional material graphene.* Since then, countless graphene production techniques have been invented, amongst which the most prominent are: various variants of exfoliation [10, 11], epitaxy [12], using a CO_2 infrared laser [13], nanotube slicing [14], hydrothermal self-assembly [15]. Nevertheless, the production of large sheets of high-quality defect-free graphene still remains a challenge [16].

In this chapter, we present the chemical structure and fundamental properties of graphene. In particular, we introduce the tight-binding approximation, which is later used throughout the thesis for modelling graphene.

1.1 Structure
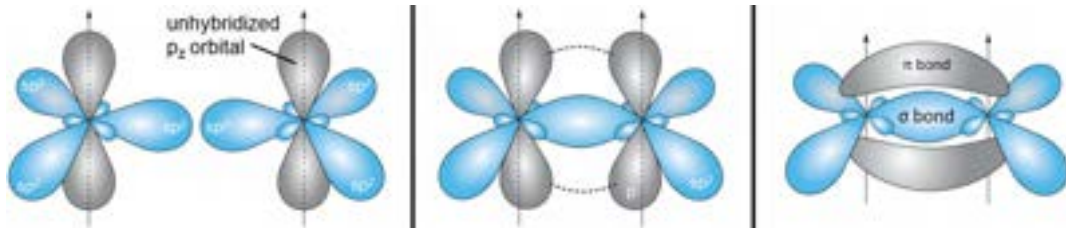
Figure 1.1: Two sp^2-hybridised carbon atoms can bond via the sp^2 orbitals, which creates a strong bond called σ, and also very weakly via the unhybridised p_z orbitals, which creates so called π bonds. Adapted from Ref. 17.

Carbon is a chemical element with an atomic number of six, meaning there are six electrons in a neutral carbon atom. A free carbon atom in vacuum has its energy levels determined by the ground-state electron configuration: $1s^2 \, 2s^2 \, 2p^2$. However, if we take two or more carbon atoms and put them near each other, their atomic orbitals can mix into new hybrid orbitals, which will be more energetically favourable. This process is called hybridisation and it leads to the creation of chemical bonds. Carbon can exhibit three types of hybridisation: sp, sp^2 and sp^3.

Graphene is built of sp^2-hybridised carbon orbitals, which means that the s orbital in the second shell mixes with two of the p orbitals and one p orbital remains unhybridised

(Fig. 1.1). The sp^2-hybridised orbitals can create strong bonds with other sp^2-hybridised carbon atoms. The bonds that are created this way are called σ bonds. Three of the four valence electrons in graphene are used to create these strong bonds with neighbouring atoms in the plane.

The fourth valence electron is considered to be in the unhybridised $2p_z$ state. The overlap between the p_z orbitals and the other orbitals is zero by symmetry. Therefore, the p_z electrons can be treated independently from the electrons that create the σ bonds. They can interact weakly with other p_z electrons creating so called π bonds and therefore they are also called π electrons.

The three electrons that constitute the σ bonds do not play a role in the conductivity of graphene because they are energetically distant by about ± 1 eV from the Fermi level. The electrons that are responsible for the good conductivity of graphene are the highly mobile π electrons in the p_z orbitals. We treat graphene in the π-electron approximation, meaning we take into account one conduction electron per atom.

The strong σ bonds create a rhombic lattice with two atoms in the unit cell, which results in a honeycomb-like atomic structure characteristic for graphene, as shown in Fig. 1.2. The two atoms in the unit cell are shown in the figure as yellow and blue dots. The colour of the dots distinguishes two sublattices, labelled with letters A and B. The lattice constant $a = 2.46$ Å. The two lattice vectors can be written as:

$$\vec{a}_1 = \frac{a}{2}\left(\sqrt{3}, 1\right) \qquad \vec{a}_2 = \frac{a}{2}\left(\sqrt{3}, -1\right). \tag{1.1}$$

The vectors connecting nearest neighbours in real space read:

$$\vec{\delta}_1 = \frac{a}{2}\left(\frac{1}{\sqrt{3}}, 1\right), \qquad \vec{\delta}_2 = \frac{a}{2}\left(\frac{1}{\sqrt{3}}, -1\right), \qquad \vec{\delta}_3 = a\left(-\frac{1}{\sqrt{3}}, 0\right). \tag{1.2}$$

The reciprocal lattice of graphene is also a rhombic lattice. The first Brillouin zone, which is a rhombus, is presented in Fig. 1.2b. The reciprocal lattice vectors are given by:

$$\vec{b}_1 = \frac{2\pi}{3a}\left(1, \sqrt{3}\right) \qquad \vec{b}_2 = \frac{2\pi}{3a}\left(1, -\sqrt{3}\right). \tag{1.3}$$

Two high-symmetry points in the reciprocal space are the Dirac points K and K', which are located at the coordinates:

$$\vec{K} = \frac{2\pi}{3\sqrt{3}a}\left(\sqrt{3}, 1\right) \qquad \vec{K}' = \frac{2\pi}{3\sqrt{3}a}\left(\sqrt{3}, -1\right). \tag{1.4}$$
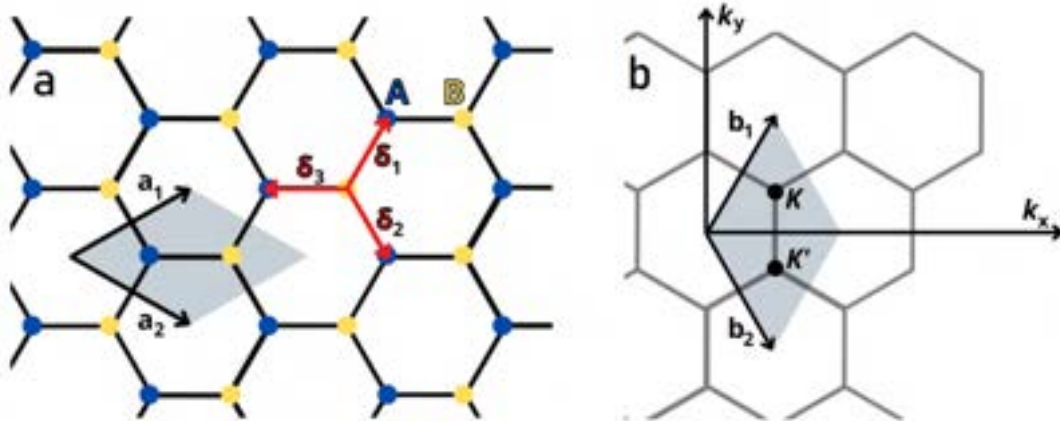
Figure 1.2: a) Lattice structure of graphene. Blue and yellow dots represent atoms of two distinct sublattices. The unit cell is marked as a grey rhombus. b) First Brillouin zone corresponding to the lattice marked in grey. The Dirac cones are located at the K and K' points.

1.2 Tight-binding model for graphene

In solid-state physics, the tight-binding model is an approach to the calculation of the electronic band structure using energy eigenstates approximated as a superposition of wave functions for isolated atoms located at each atomic site [18]. The term "tight-binding" comes from the assumption that the electrons are tightly bound to the atom to which they belong, meaning they have limited interaction with states and potentials on surrounding atoms of the solid. Graphene has been studied theoretically with the use of the tight-binding model already in 1947 by P. R. Wallace, who used it as a starting point for studying graphite. He predicted the electronic properties of a graphene layer and calculated its band dispersion [19]. A nearest-neighbour tight-binding Hamiltonian, which takes into account only the π orbital on each atom, is a simple model which describes well the electronic properties of graphene. The π electrons are the ones that are conducting and highly mobile, they determine graphene's optical and electronic properties, therefore it is sufficient to include only these in the model and neglect the influence of σ electrons. Besides the mathematical simplicity and intuitive interpretation, an additional advantage of the approach is that it is computationally inexpensive and therefore is suitable for simulating larger structures, such as large flakes of graphene.

If we consider only the nearest-neighbour interactions, the tight-binding Hamiltonian

reads:

$$H = -t \sum_{<i,j>} \left(a_i^\dagger b_j + b_j^\dagger a_i \right), \tag{1.5}$$

where $a_i^\dagger$ (a_i) is the creation (annihilation) operator of an electron at position $\boldsymbol{r}_i$ (on site i) of the sublattice A, and $b_j^\dagger$ (b_j) is the creation (annihilation) operator of an electron at position $\boldsymbol{r}_j$ (on site j) of the sublattice B, the triangular brackets denote summing over nearest neighbours only and t is the nearest-neighbour hopping energy. In the thesis, $t = 2.66\,\mathrm{eV}$ is used as the value for the hopping parameter between the neighbouring sites in graphene. This value is based on experiments on extended graphene sheets and is commonly used in literature [18, 20].

Looking at the honeycomb graphene lattice, one can note that the three nearest neighbours of an electron from sublattice A always belong to sublattice B and vice-versa. Using this fact, we can rewrite the Hamiltonian as:

$$H = -t \sum_{i \in A} \sum_{\substack{\delta \in \\ \{\delta_1, \delta_2, \delta_3\}}} \left(a_i^\dagger b_{i+\delta} + b_{i+\delta}^\dagger a_i \right). \tag{1.6}$$

We need to diagonalise the Hamiltonian given by Eq. 1.5. Since we have a translation invariant system, it is convenient to make a transformation to the Fourier space. The electron creation operators can be expressed in the reciprocal Fourier space as:

$$a_i^\dagger = \frac{1}{\sqrt{N}} \sum_{\boldsymbol{k} \in \mathrm{IBZ}} e^{i\boldsymbol{k}\boldsymbol{r}_i} a_k^\dagger \qquad b_j^\dagger = \frac{1}{\sqrt{N}} \sum_{\boldsymbol{k} \in \mathrm{IBZ}} e^{i\boldsymbol{k}\boldsymbol{r}_j} b_k^\dagger, \tag{1.7}$$

where N is the number of unit cells in the lattice and IBZ denotes the first Brillouin zone. The non-vanishing anticommutation relations are:

$$\left\{ a_k, a_{k'}^\dagger \right\} = \left\{ b_k, b_{k'}^\dagger \right\} = \delta_{kk'} \tag{1.8}$$

and the rest are zero. Relations 1.8 result from the fermionic nature of electrons and account for the Pauli exclusion principle. Using this fact, we can rewrite the Hamiltonian from Eq. 1.5:

$$H = -\frac{t}{N} \sum_{j \in A} \sum_{\boldsymbol{\delta}, \boldsymbol{k}, \boldsymbol{k'}} \left[e^{i(\boldsymbol{k}-\boldsymbol{k'})\boldsymbol{r}_j} e^{-i\boldsymbol{k'}\boldsymbol{\delta}} a_k^\dagger b_{k'} + h.c. \right] = -t \sum_{\boldsymbol{\delta}, \boldsymbol{k}} \left(e^{-i\boldsymbol{k}\boldsymbol{\delta}} a_k^\dagger b_k + e^{i\boldsymbol{k}\boldsymbol{\delta}} b_k^\dagger a_k \right), \tag{1.9}$$

where we used the fact that

$$\sum_{i \in A} e^{i(\boldsymbol{k}-\boldsymbol{k'})\boldsymbol{r}_i} = N\delta_{\boldsymbol{k}\boldsymbol{k'}}. \tag{1.10}$$

12

Defining $\mathbf{\Psi} = (a_k, b_k)^T$ we can express the Hamiltonian as:

$$H = \sum_k \mathbf{\Psi}^\dagger \tilde{H}(\boldsymbol{k})\mathbf{\Psi}, \tag{1.11}$$

where the matrix $\tilde{H}$ called the Bloch Hamiltonian takes the form:

$$\tilde{H} = \begin{bmatrix} 0 & f(\boldsymbol{k}) \\ f^*(\boldsymbol{k}) & 0 \end{bmatrix} \tag{1.12}$$

with

$$f(\boldsymbol{k}) = -t\sum_{\boldsymbol{\delta}} e^{i\boldsymbol{k}\boldsymbol{\delta}} = -t\left(e^{-ik_x a} + 2\,e^{\frac{i}{2}k_x a}\cos\left(\frac{\sqrt{3}}{2}k_y a\right)\right). \tag{1.13}$$

The eigenvalues of the Bloch Hamiltonian give the energies of the system:

$$E_\pm = \sqrt{f(\boldsymbol{k})f^*(\boldsymbol{k})} = \pm|f(\boldsymbol{k})|. \tag{1.14}$$
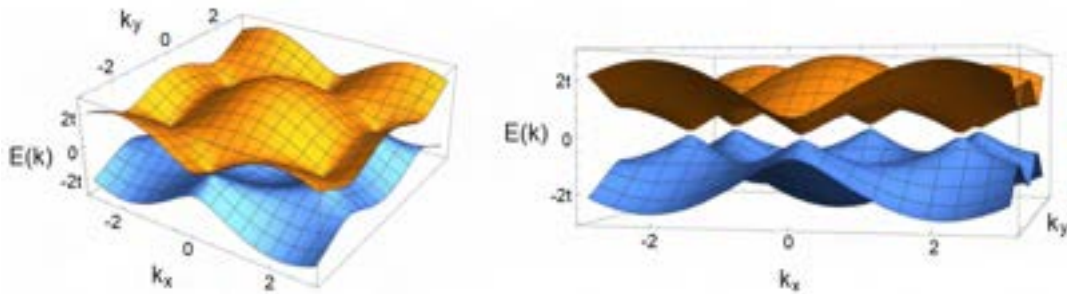
Figure 1.3: Electronic dispersion of single-layer graphene calculated within the nearest-neighbour approximation. The two bands touch each other at Dirac points in the reciprocal space.

The resulting energy values form two symmetric bands, which touch at the high-symmetry points (Fig. 1.3). Therefore, graphene has no band gap and it can be seen as a semimetal. However, the density of states vanishes at these points and from this perspective graphene is sometimes called a gapless semiconductor, depending on the chosen convention.

1.3 Adding electrons: doping and gating

1.3.1 Controlling the conductivity of graphene

As one can see from the energy dispersion relation obtained from the tight-biding model, pristine graphene has a zero-bandgap, since the two bands touch at Dirac points, which

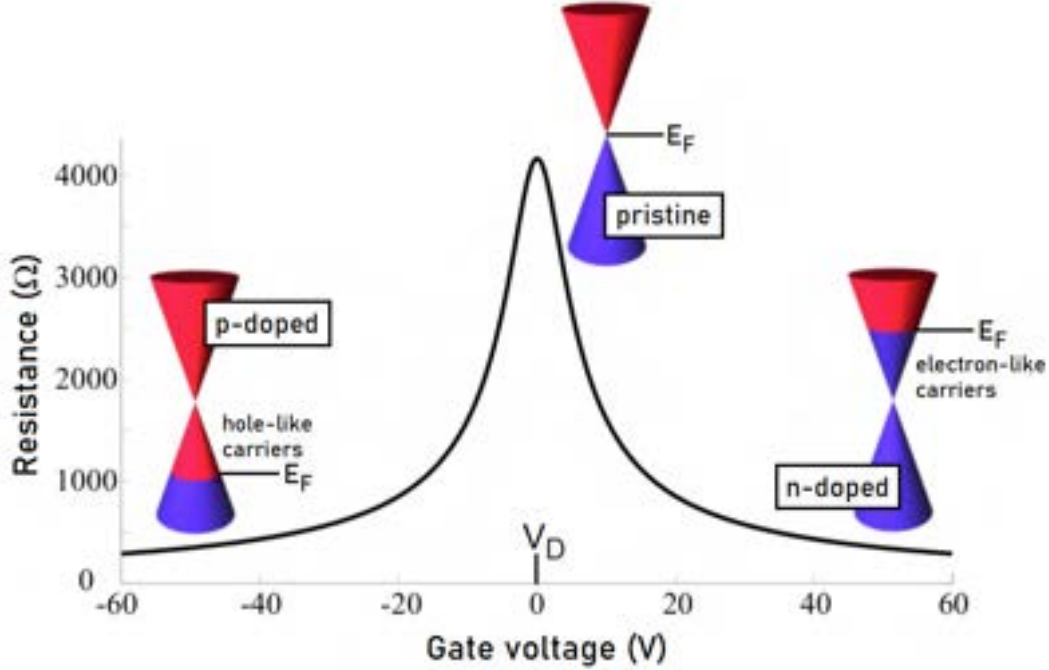Figure 1.4: Theoretical prediction of the resistance as a function of gate voltage for graphene on a SiO$_2$ substrate. V_D marks the point where the resistance reaches its maximum. If the gate voltage is larger than V_D, the graphene is n-doped (electron doped) and if it is smaller, the graphene is p-doped (hole doped). E_F denotes the Fermi energy. Adapted from Ref. 21.

makes it behave like a metallic material. Since the early discovery of graphene, a minimum conductivity at the neutrality point has been theoretically predicted for Dirac electrons in graphene with a value of $\sim 4e^2/h$ [1] and confirmed in charge transport experiments, which revealed that even if the carrier density vanishes at the Dirac point, the conductivity does not go to zero but it remains finite at zero temperature [22].

There are several ways that give reliable control of the type and density of the charge carriers in graphene. By applying a gate voltage to graphene, it is possible to continuously drive the Fermi level away from the Dirac point, thus controlling the type and amount of carriers in the material [8, 23], as shown in Fig. 1.4. Depending on the sign of the applied voltage, graphene is doped with either electrons or with holes, which in both cases leads to the strengthening of metallic properties.

Introducing additional electrons to the system by the means of atomic or molecular doping allows to open a bandgap in single-layer [24] and in bilayer graphene [25, 26]. Another way to control conducting properties is the method of electrostatic field tuning, presented in Fig. 1.5.
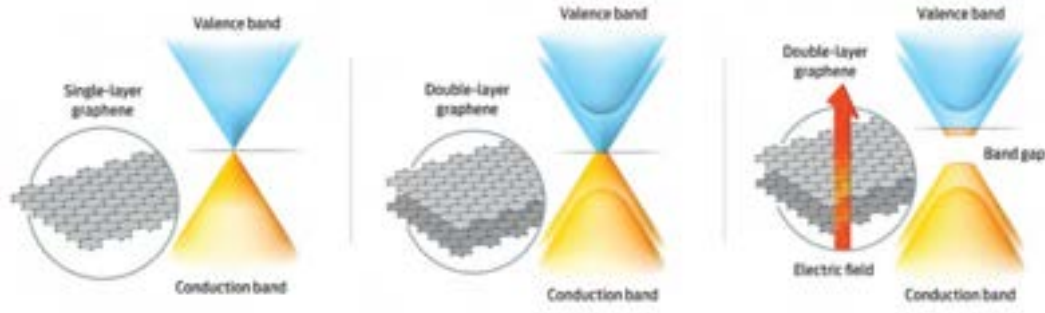
14

Figure 1.5: Band structure of single layer graphene, band structure of bilayer graphene and band gap opening in bilayer graphene caused by electrostatic field tuning. Figure from [27].

1.3.2 Exciting plasmons

Doping graphene has also proven to be a simple and effective way to excite plasmons in this material. Modern plasmonics, which emerged at the turn of the twenty-first century [28, 29], has experienced huge interest in the past two decades with a recent shift of focus toward related quantum processes and applications at the nanoscale. The rapid development of nanostructure fabrication techniques and experimental tools, together with the implementation of powerful numerical modelling based on full-wave electromagnetic simulations, caused an explosion of interest in the field, which was visible over the past decade [30]. Graphene physics has also attracted growing attention in the last years and the number of publications on this subject has escalated quickly during that period.

The link between both these areas of research was established in 2011. One of the first accomplishments in the emerging field of graphene plasmonics was the experimental realisation of surface plasmon-polaritons (SPPs) in engineered graphene micro-ribbon arrays obtained by patterning a pristine graphene sheet. The experiment revealed that graphene plasmon resonances can be tuned over a broad terahertz frequency range by changing micro-ribbon width and in situ electrostatic doping [31]. This seminal work has sparked a lot of interest in graphene nanoplasmonics, paving the way for the investigation of graphene as a novel plasmonic material [32–34].

Doped graphene is capable of sustaining SPPs [33, 35, 36] and its layers have shown similar surface plasmon effects to those of metallic thin films [34, 37]. Having said that, graphene SPPs also exhibit some significant differences with respect to the noble metal plasmons, some of which make them especially promising for applications.

An interesting property of the SPPs in graphene is their tunability - they can be dy-
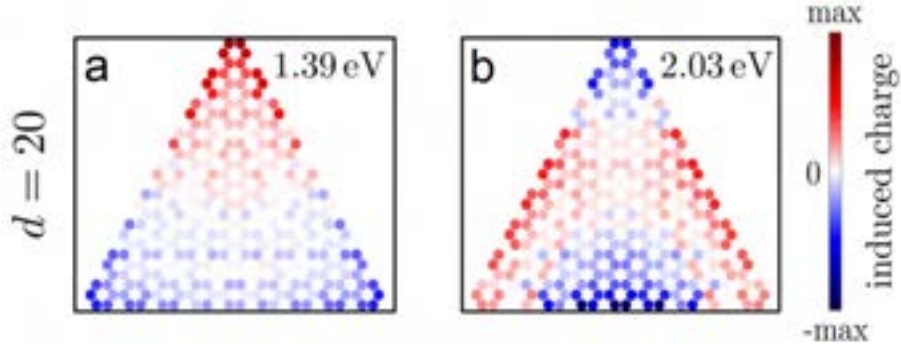
Figure 1.6: Snapshots present the real space induced charge distribution in a triangular 270-atom graphene nanoflake with 20 doping electrons under vertically polarized CW illumination of frequency 1.39 eV (a) and 2.03 eV (b). Snapshots were taken at the time of maximum dipole moment. Adapted from Ref. [40].

namically controlled and tuned through doping or electrical gating [30]. Since the spectral position of plasmonic resonances depends on the interaction energy of the electrons in the system, they are sensitive to the number of doping electrons because the position of the Fermi energy is modified and different states contribute to the resonance. This shift of the absorption peak has been predicted in doped graphene nanoantennas for collective resonances under varying doping conditions [38, 39]. Additionally, electrostatic doping has been used to demonstrate plasmon-frequency tunability and induced optical modulations in the THz and infrared response of graphene [38]. This stands in contrast to traditional metal-based plasmonics, where the tunability of plasmons is usually limited - it can be achieved by controlling the geometry of the metallic nanostructures and their dielectric environment, or by exploring the thickness of thin films of noble-metals. After the fabrication of a metallic nanostructure, it is challenging to control and tune the frequency of its plasmons. Furthermore, graphene surface plasmon-polaritons enable higher levels of spatial confinement than plasmons in noble metals and are predicted to suffer from relatively low losses, therefore having larger lifetimes and propagation lengths, when compared with traditional plasmonic materials [30].

The plasmons in very large graphene sheets are typically located in the far or mid infrared region of the electromagnetic spectrum with energies up to 1 eV [33], usually on the order of tenths or hundredths of eV. A finite flake size allows to shift the plasmons energies to visible energies [41], which is crucial for a wide variety of applications. Fig. 1.6 presents the charge distribution in two plasmonic excitations in triangular graphene nanoflakes.

A vividly discussed topic is the possibility of exciting graphene plasmons in finite flakes by single electrons [39]. This problem is closely related to the more fundamental issue of how a plasmon should be defined and how to distinguish single-particle-like resonances in nanostructures from plasmonic ones [40, 42–44]. Typically, collective charge density oscillation in real space is considered as the basis to classify a specific resonance as plasmonic in nature [44]. However, as we recently pointed out (using the tools presented throughout this thesis), in plasmonic systems that are so small that they require quantum description the real space analysis cannot be the sole basis for decisions on the nature of a resonance [40]. In order to characterize resonances in such systems, one also needs to look carefully at both the absorption spectra of the nanostructure and the coherence dynamics in energy basis.

Early studies found that in graphene nanoantennas, adding a single extra electron can switch on infrared plasmons that were absent from the structure before doping [39]. That said, if we understand the plasmon predominantly as a resonance originating from long-range electron–electron interactions, it seems that a single electron is not able to excite a plasmonic resonance and one needs heavier doping to achieve it [40]. In any case, there is no doubt that graphene, which supports intrinsic tunable plasmons, is a well-suited platform for investigating plasmonic phenomena and it deserves further exploration.

1.4   Adatoms on graphene

The properties of graphene strongly depend on the shape and purity of its lattice. Some predictions can be hard to verify in practice due to impurities and defects. As an example let us take graphene ribbons. Although theoretical calculations for defectless graphene ribbons predict that these should transmit electrons without scattering and their low-temperature conductances should be quantised in integer multiples of e^2/h [45], their experimental realisation is often far from ballistic, meaning that it shows signs of scatterers that disturb the ideal propagation, and the experimentally measured conductance is much smaller than expected [46].

Atoms adsorbed to a crystal lattice are called adatoms. Adatoms can be a nuisance for transport properties, but they can also be seen as a tool for tailoring graphene. The adsorption of atomic hydrogen on graphene opens a gap in the electronic density of

states and therefore it can turn the material into a semiconductor [47]. Remarkably, after dehydrogenation, the metallic properties can be recovered. This offers a reliable method for controlling the electronic properties of this material [48]. Moreover, graphene offers better control over adsorbate addition than ordinary three-dimensional (3D) materials. In 3D metals adatoms are introduced into the material by alloying, which is a random process. In graphene, which is an open surface, adatoms can be controlled with the use of atomic force microscopy to obtain structures with greater precision [49].

Since working with defect- or impurity-free materials is not always possible, it is critical to investigate how defects and impurities affect the electronic properties of graphene and to decide whether their existence in a particular system is desirable and how it can be utilised [50, 51]. A tight-binding model of graphene with adsorbates based on extended Hückel theory was developed in Ref. [46], where it was used to carry out quantum transport calculations for graphene nanoribbons with adsorbates. Possible ways to adsorb an adatom on the graphene lattice, which are based on these calculations, are presented in Fig. 1.7.

In this thesis, we focus on graphene nanoflakes rather than infinite graphene sheets. Moreover, we take an opposite perspective and focus also on how the graphene nanoflake can affect typical processes in two-level systems. We look not only on stationary solutions but also study the dynamics of the hybrid systems.
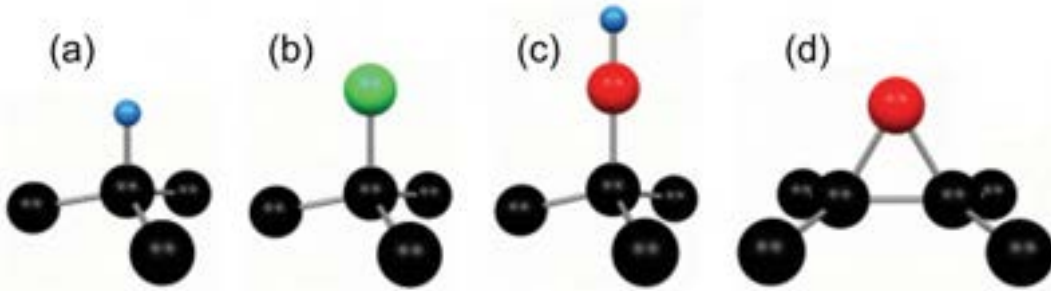
Figure 1.7: Relaxed geometries of adsorbates on graphene. Carbon, hydrogen, fluorine, and oxygen atoms are black, blue, green, and red respectively. (a) Adsorbed hydrogen atom. (b) Adsorbed fluorine. (c) Adsorbed hydroxyl group. (d) Adsorbed oxygen. Adapted from Ref. 46.

Adatoms can attach to graphene in three different positions with respect to the graphene lattice - *top*, *hollow* or *bridge* [52], as shown in Fig. 1.8. If the adatom is coupled to the flake in the *top* position, it affects only one sublattice. *Hollow* and *bridge*

positions influence both sublattices. Throughout this work, we focus on the *top* position of the adatom only, meaning that the adatom will be located over and coupled to one particular graphene site.

Figure 1.8: Three possible adatom positions on an extended graphene sheet are marked with crosses: *top* position (red) on top of a selected carbon site; *bridge* (green) in between a pair of sites and *hollow* (blue) in the middle or above the middle of a hexagon.

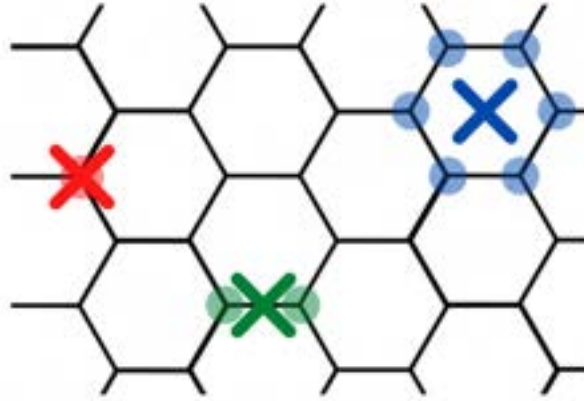## 1.5   Cutting graphene: edge types

Graphene can be cut into many different shapes. Depending on where the cutting lines pass through, the resulting flakes can have various edge types. If we cut along an axis which is connecting two nearest neighbours, the resulting edge type is called *armchair*, and if we cut along a line perpendicular to this one, we get a *zigzag* edge, as presented in Fig. 1.9.

Armchair structures will prove to be of particular interest, since they are non-magnetic and as we will see in further sections, they tend to have a bandgap around the Fermi level. On the contrary, zigzag-edged nanoflakes generally have multiple degenerate levels at zero Fermi energy and they support magnetic edge states [53, 54], which significantly complicates their description and modelling. In this thesis, we focus on graphene nanoflakes of sizes up to 10 nm, since their HOMO-LUMO gaps have frequencies corresponding to those of electromagnetic waves in the optical regime.
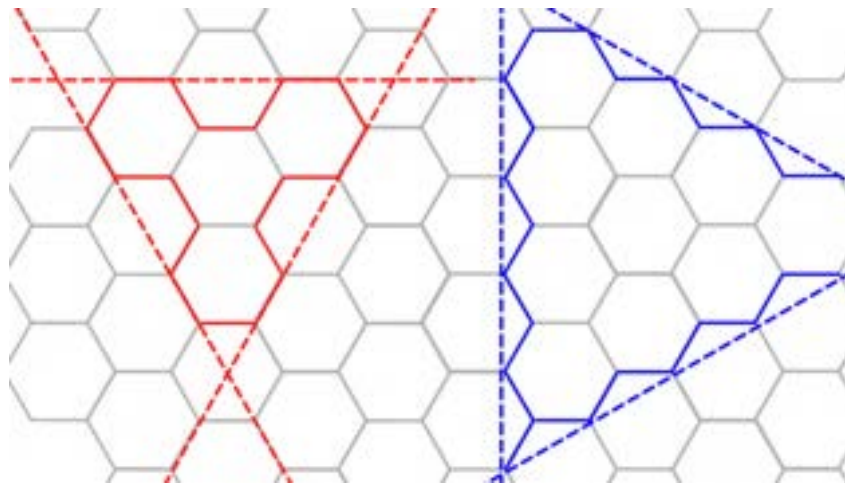
Figure 1.9: Two ways to cut graphene and the resulting edge types: armchair (left) and zigzag (right).

Chapter 2

Interaction of light with atoms

This chapter contains a summary of basic processes which can occur when an atom is irradiated with a light beam resonant with one of its natural frequencies. We will present some commonly used approximations, such as the two-level approximation and the rotating-wave approximation, which allow to find analytical solutions of the evolution equations. With their help we will predict the behaviour of atoms interacting with an external electromagnetic field, which will lead us to the phenomenon of Rabi oscillations. Finally, to describe incoherent or dissipative processes, such as spontaneous emission, we will introduce the density matrix formalism and the Gorini-Kossakowski-Sudarshan-Lindblad equation. The reasoning in this chapter is based mostly on the excellent script written by Daniel A. Steck [55] and on popular quantum optics textbooks by Fox [56], Vogel and Welsch [57] and Haroche and Raimond [58].

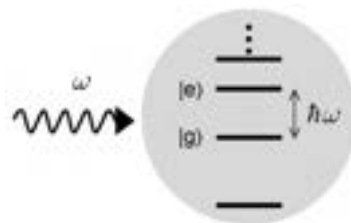Figure 2.1: A visualisation of the two-level atom approximation. When the illumination frequency ω coincides with one of the optical transitions of the atom, we speak about a resonant interaction between the atomic levels involved in this transition and the light field. We can therefore neglect the other atomic levels, which only weakly interact with the incoming light. Figure from [56].

2.1 Two-level atom

In order for a quantum of light to be absorbed or emitted by an atom, its angular frequency ω must be resonant to the energy difference between two quantised energy levels of the atom, of which at least one has to be populated, here denoted as E_e and E_g:

$$E_e - E_g = \hbar\omega. \tag{2.1}$$

In general, an atom can have multiple quantised levels and there is a large number of possible optical transitions between them. The quantum treatment of the interaction between light and atoms, however, is often performed in terms of the two-level atom approximation (Fig. 2.1). This approximation is applicable when the frequency of the incoming light coincides with one of the optical transitions in the atom. In the two-level atom approximation we only consider the pair of states whose energy difference is resonant to the illumination frequency and neglect all the other levels. The atom is then treated as a neutral particle with just two internal levels - the ground state $|g\rangle$ with energy E_g and the excited state $|e\rangle$ with energy E_e.

Mathematically speaking, the two-level atom is represented as a two-dimensional complex Hilbert space. An arbitrary pure state of the system can be represented as a vector in this space:

$$|\Psi\rangle = c_g\,|g\rangle + c_e\,|e\rangle\,, \tag{2.2}$$

with the two energy eigenstates of the atom chosen as the basis vectors:

$$|g\rangle = \begin{pmatrix} 0 \\ 1 \end{pmatrix} \quad \text{and} \quad |e\rangle = \begin{pmatrix} 1 \\ 0 \end{pmatrix}. \tag{2.3}$$

The coefficients c_g and c_e are probability amplitudes. The square of their modulus gives the probability of measuring the system in the state $|g\rangle$ or $|e\rangle$, respectively. In this two-dimensional complex space only four linearly independent operators are possible. A common choice of the operators' form which has a good physical interpretation is:

$$\mathbb{1} = |e\rangle\,\langle e| + |g\rangle\,\langle g|\,, \tag{2.4}$$

$$\hat{\sigma}_z = |e\rangle\,\langle e| - |g\rangle\,\langle g|\,, \tag{2.5}$$

$$\hat{\sigma}_+ = \frac{1}{2}\,(\hat{\sigma}_x + i\,\hat{\sigma}_y) = |e\rangle\,\langle g|\,, \tag{2.6}$$

$$\hat{\sigma}_- = \frac{1}{2}\,(\hat{\sigma}_x - i\,\hat{\sigma}_y) = |g\rangle\,\langle e|\,, \tag{2.7}$$

where the operators $\hat{\sigma}_x, \hat{\sigma}_y, \hat{\sigma}_z$ can be represented by the Pauli matrices, defined as:

$$\sigma_x = \begin{pmatrix} 0 & 1 \\ 1 & 0 \end{pmatrix} \quad \sigma_y = \begin{pmatrix} 0 & -i \\ i & 0 \end{pmatrix} \quad \sigma_z = \begin{pmatrix} 1 & 0 \\ 0 & -1 \end{pmatrix}. \tag{2.8}$$

Note that there is a physical interpretation which can be attributed to these operators, even though not all of them are Hermitian and therefore do not necessarily correspond to physically measurable quantities. An example is the non-Hermitian $\hat{\sigma}_+$ operator, which generates a transition from the ground to the excited state and the operator $\hat{\sigma}_-$, which does the opposite. Conversely to these two, $\hat{\sigma}_z$ is a Hermitian operator, so its expectation value is an observable physical quantity. It is the difference between the probability of the excited state being occupied and the probability of the ground state being occupied, sometimes called the population inversion of the atom. Also the Hermitian $\hat{\sigma}_x$ operator has an intuitive interpretation - it acts as a flip operator, which changes one basis state into the other, since $\hat{\sigma}_x \ket{e} = \ket{g}$ and $\hat{\sigma}_x \ket{g} = \ket{e}$.

Using these fundamental operators as a basis, one can construct other operators which carry physical information about the system. The Hamiltonian is given by:

$$\hat{H}_{\mathrm{at}} = E_e \ket{e}\bra{e} + E_g \ket{g}\bra{g} = \begin{pmatrix} E_e & 0 \\ 0 & E_g \end{pmatrix}. \tag{2.9}$$

We can shift the energy scale as the only physically relevant information are the energy differences and not absolute energy values. This will be useful for later calculations.

$$\hat{H}_{\mathrm{at}} = \begin{pmatrix} E_e - E_g & 0 \\ 0 & E_g - E_g \end{pmatrix} = \begin{pmatrix} \hbar\omega_0 & 0 \\ 0 & 0 \end{pmatrix} = \hbar\omega_0 \sigma_+ \sigma_-, \tag{2.10}$$

where we introduced the resonant frequency of the atom ω_0, defined such that $E_e - E_g = \hbar\omega_0$ holds.

An electric dipole operator in the one-electron case is defined via the position operator $\hat{\mathbf{r}}$ as:

$$\hat{\mathbf{d}} = -q_e \hat{\mathbf{r}}, \tag{2.11}$$

where q_e is the elementary charge. The bold font highlights the fact that the elements of $\hat{\mathbf{d}}$ and $\hat{\mathbf{r}}$ are vectors in $\mathbb{R}^3$. The expectation value for the state 2.2 is given as:

$$\bra{\Psi} \hat{\mathbf{d}} \ket{\Psi} = -q_e \left(|c_e|^2 \bra{e} \hat{\mathbf{r}} \ket{e} + c_e c_g^* \bra{g} \hat{\mathbf{r}} \ket{e} + c_g c_e^* \bra{e} \hat{\mathbf{r}} \ket{g} + |c_g|^2 \bra{g} \hat{\mathbf{r}} \ket{g} \right). \tag{2.12}$$

We can use a simple parity argument to derive the form of the dipole operator in a spherically symmetric system. The parity operator $\hat{P}$ flips the sign of the position operator: $\hat{P}\hat{\mathbf{r}}\hat{P}^\dagger = -\hat{\mathbf{r}}$. Note that the parity operator is unitary and $\hat{P}^2 = \mathbb{1}$ and also that it anticommutes with the position operator. On the other hand, the parity operator commutes with an atomic Hamiltonian with a spherically symmetric potential, which has the form $\frac{p_e^2}{2m} - \frac{\alpha}{|\mathbf{r}|}$, therefore $\hat{P}$ and $\hat{H}$ have common eigenstates. Now let us consider a matrix element of the anticommutator $\left\{\hat{P}, \hat{\mathbf{r}}\right\}$ between energy eigenstates $|a\rangle$ and $|b\rangle$. Since these states are eigenstates of the Hamiltonian, they are also eigenstates of the parity operator, such that $\hat{P}|a\rangle = p_a|a\rangle$ and $\hat{P}|b\rangle = p_b|b\rangle$ hold. On one hand, as we already know, the anticommutator vanishes, so:

$$\langle a|\left\{\hat{P}, \hat{\mathbf{r}}\right\}|b\rangle = 0. \tag{2.13}$$

But since the states $|a\rangle$ and $|b\rangle$ are also eigenstates of the parity operator, the following holds as well:

$$\langle a|\left\{\hat{P}, \hat{\mathbf{r}}\right\}|b\rangle = \langle a|\left(\hat{P}\hat{\mathbf{r}} + \hat{\mathbf{r}}\hat{P}\right)|b\rangle = (p_a + p_b)\langle a|\hat{\mathbf{r}}|b\rangle. \tag{2.14}$$

Since $\hat{P}^2 = \mathbb{1}$, the possible eigenvalues of the parity operator are ± 1. For both Eq. 2.13 and Eq. 2.14 to hold, either $p_a + p_b = 0$ or $\langle a|\hat{\mathbf{r}}|b\rangle = 0$. If we take a look at the diagonal elements of the dipole moment operator - $\langle g|\hat{\mathbf{d}}|g\rangle$ and $\langle e|\hat{\mathbf{d}}|e\rangle$ - we can notice that it is impossible that $2p_e = 0$ or $2p_g = 0$ and therefore:

$$\langle g|\hat{\mathbf{d}}|g\rangle = \langle e|\hat{\mathbf{d}}|e\rangle = 0. \tag{2.15}$$

This means that an atom or any spherically symmetric system which is in an energy eigenstate has no permanent dipole moment.

Regarding the off-diagonal elements, it is reasonable to assume that $|g\rangle$ and $|e\rangle$ are levels of opposite parities, and therefore these elements do not vanish. An atom only exhibits a dipole moment if it is in a superposition of the basis states, i.e. $c_g c_e^* \neq 0$. Since the diagonal elements vanish, the expectation value becomes:

$$\langle\Psi|\hat{\mathbf{d}}|\Psi\rangle = -q_e\left(c_e c_g^*\langle g|\hat{\mathbf{r}}|e\rangle + c_g c_e^*\langle e|\hat{\mathbf{r}}|g\rangle\right) = \langle\Psi|\hat{\sigma}_-\mathbf{d_{eg}}^* + \hat{\sigma}_+\mathbf{d_{eg}}|\Psi\rangle, \tag{2.16}$$

where we have introduced the notation:

$$\mathbf{d_{eg}} = q_e\langle g|\hat{\mathbf{r}}|e\rangle. \tag{2.17}$$

And since this is true for an arbitrary state, the dipole moment can be represented as:

$$\hat{\mathbf{d}} = \hat{\sigma}_- \mathbf{d_{eg}}^* + \hat{\sigma}_+ \mathbf{d_{eg}} = \begin{pmatrix} 0 & \mathbf{d_{eg}} \\ \mathbf{d_{eg}}^* & 0 \end{pmatrix}. \tag{2.18}$$

If we choose the phase of the dipole matrix element $\mathbf{d_{eg}}$ such that it is real, we obtain the form:

$$\hat{\mathbf{d}} = \mathbf{d_{eg}}(\hat{\sigma}_- + \hat{\sigma}_+). \tag{2.19}$$

2.2   Light-matter interaction Hamiltonian

Now let us introduce a new element into the system - we add a monochromatic external field with angular frequency ω to model a laser field: $\mathbf{E} = \mathbf{E_0}\cos{(\omega t + \phi)}$. Note that we ignore the spatial dependence of the field, only considering the field at the location of the atom. This is appropriate in the long-wavelength approximation, where we assume that the wavelength of the illumination is much larger than the size of the atom, which is generally a reasonable assumption [56].

It is convenient to decompose the field into its positive- and negative-frequency components:

$$\mathbf{E}\left(t\right) = \mathbf{E}_0^{(+)}e^{-i\omega t} + \mathbf{E}_0^{(-)}e^{i\omega t} = \mathbf{E}^{(+)}\left(t\right) + \mathbf{E}^{(-)}\left(t\right), \tag{2.20}$$

where $\mathbf{E}^{(+)}$ and $\mathbf{E}^{(-)}$ are electric field amplitudes which fulfil the relation $(\mathbf{E}^{(+)})^\dagger = \mathbf{E}^{(-)}$. The interaction between the atom and the field $\hat{H}_{int}$ is given by:

$$\hat{H}_{int} = -\hat{\mathbf{d}}\mathbf{E}. \tag{2.21}$$

In this way the field induces the off-diagonal elements of the Hamiltonian, which is consistent with the experimentally known fact that laser illumination causes transitions between the eigenstates of an atom.

Just as we decomposed the electric field into positive- and negative-frequency parts, we can decompose the dipole operator as:

$$\hat{\mathbf{d}} = \mathbf{d_{eg}}(\hat{\sigma}_- + \hat{\sigma}_+) = \hat{\mathbf{d}}^{(+)} + \hat{\mathbf{d}}^{(-)}, \tag{2.22}$$

where for a monochromatic beam illumination the expectation values of the negative and positive components of the dipole moment operator depend on time as $\langle\hat{\mathbf{d}}^{(\pm)}\rangle \sim e^{\mp i\omega t}$.

The interaction Hamiltonian becomes:

$$\hat{H}_{int} = -\left(\hat{\mathbf{d}}^{(+)} + \hat{\mathbf{d}}^{(-)}\right) \cdot \left(\mathbf{E}^{(+)}(t) + \mathbf{E}^{(-)}(t)\right) =$$
$$= -\hat{\mathbf{d}}^{(+)} \cdot \mathbf{E}^{(+)} - \hat{\mathbf{d}}^{(-)} \cdot \mathbf{E}^{(-)} - \hat{\mathbf{d}}^{(+)} \cdot \mathbf{E}^{(-)} - \hat{\mathbf{d}}^{(-)} \cdot \mathbf{E}^{(+)}. \quad (2.23)$$

If we assume that the external field is weak or moderately strong, the atom's response is linear, meaning that a field with time dependence $|E| \propto e^{i\omega t}$ will result in the dipole moment oscillations with the same time dependence. Then, recalling that $\langle \hat{\mathbf{d}}^{(\pm)} \rangle \sim e^{\mp i\omega t}$ and $\mathbf{E}^{(\pm)} \sim e^{\mp i\omega t}$, we see that the expectation values of first two terms in Eq. 2.23 oscillate rapidly as $e^{\pm 2\omega t}$, while the last two terms depend on time very weakly. We can drop the first two terms, which are rapidly oscillating at optical frequencies and replace them by their zero average value, which amounts to a coarse-graining on femtosecond scale. This step is referred to as making the rotating-wave approximation (RWA). After performing the RWA, the atom-field Hamiltonian becomes:

$$\hat{H}_{AF} = -\hat{\mathbf{d}}^{(+)} \mathbf{E}^{(-)} - \hat{\mathbf{d}}^{(-)} \mathbf{E}^{(+)}. \quad (2.24)$$

Using the explicit time-dependence for the field and expression 2.22 for the dipole moment operator, we can write:

$$\hat{H}_{AF} = -\langle g| \hat{\mathbf{d}} |e\rangle \left(\mathbf{E_0}^{(-)} \sigma_- e^{i\omega t} + \mathbf{E_0}^{(+)} \sigma_+ e^{-i\omega t}\right) = \frac{\hbar\Omega}{2}\left(\sigma_- e^{i\omega t} + \sigma_+ e^{-i\omega t}\right), \quad (2.25)$$

where we assume $\mathbf{E_0}^{(+)}$ to be real and we have defined the Rabi frequency as:

$$\Omega := -\frac{2\langle g| \hat{\mathbf{d}} |e\rangle \mathbf{E_0}^{(+)}}{\hbar} = -\frac{\langle g| \hat{\mathbf{d}} |e\rangle \mathbf{E_0}}{\hbar}. \quad (2.26)$$

2.3   Rabi oscillations

In order to trace the dynamics of the system, we investigate the time-independent Schrödinger equation:

$$i\hbar \frac{d}{dt}|\Psi\rangle = \hat{H}|\Psi\rangle \quad (2.27)$$

and find its solutions. Our atomic state is a superposition of the two basis states:

$$|\Psi\rangle = c_g |g\rangle + c_e |e\rangle, \quad (2.28)$$

where c_e and c_g carry all the time-dependence of the state $|\Psi\rangle$. The Hamiltonian consists of two parts: the atomic part $\hat{H}_{\text{at}}$ (Eq. 2.10) and the atom-field interaction $\hat{H}_{AF}$ (Eq. 2.25):

$$\hat{H} = \hbar\omega_0\sigma_+\sigma_- + \frac{\hbar\Omega}{2}\left(\sigma_-e^{i\omega t} + \sigma_+e^{-i\omega t}\right). \tag{2.29}$$

Substituting these into Eq. 2.27 gives:

$$\frac{d}{dt}c_g\,|g\rangle + \frac{d}{dt}c_e\,|e\rangle = -i\omega_0 c_e\,|e\rangle - i\frac{\Omega}{2}e^{i\omega t}c_e\,|g\rangle - i\frac{\Omega}{2}e^{-i\omega t}c_g\,|e\rangle. \tag{2.30}$$

Projecting the equation onto the states $\langle g|$ and $\langle e|$ gives a pair of coupled differential equations:

$$\frac{d}{dt}c_g = -i\frac{\Omega}{2}c_e e^{i\omega t} \tag{2.31}$$
$$\frac{d}{dt}c_e = -i\omega_0 c_e - i\frac{\Omega}{2}c_g e^{-i\omega t}.$$

Without the time-dependent factor $e^{i\omega t}$ this set of equations would be easily solvable. Fortunately, we can remove this factor by a unitary transformation:

$$U = e^{i\omega t|e\rangle\langle e|}, \tag{2.32}$$

which transforms the state from Eq. 2.28 into:

$$|\tilde{\Psi}\rangle = U\,|\Psi\rangle = c_g\,|g\rangle + c_e e^{i\omega t}\,|e\rangle = c_g\,|g\rangle + \tilde{c}_e\,|e\rangle. \tag{2.33}$$

The Hamiltonian is transformed according to:

$$\tilde{H} = UHU^\dagger + i\hbar\left(\partial_t U\right)U^\dagger, \tag{2.34}$$

which results in the following atom-field interaction Hamiltonian in the new frame of reference:

$$\hat{H} = -\hbar\Delta\sigma_+\sigma_- + \hbar\Omega\left(\sigma_+ + \sigma_-\right), \tag{2.35}$$

where $\Delta = \omega - \omega_0$ is the detuning from resonance. Such a time-independent Hamiltonian is only possible in the rotating-wave approximation. The counter-rotating terms would still depend on time after the transformation given by Eq. 2.32. After the transformation, the Schrödinger equation gives the coupled equations:

$$\frac{d}{dt}c_g = -i\frac{\Omega}{2}\tilde{c}_e, \tag{2.36}$$
$$\frac{d}{dt}\tilde{c}_e = -i\Delta\tilde{c}_e - i\frac{\Omega}{2}c_g.$$

Solving them allows to trace the driven atomic dynamics. First, we look at the case of exact resonance ($\Delta = \omega - \omega_0 = 0$), where the set of equations reduces to:

$$\frac{d}{dt}c_g = -i\frac{\Omega}{2}\tilde{c}_e,$$
$$\frac{d}{dt}\tilde{c}_e = -i\frac{\Omega}{2}c_g. \tag{2.37}$$

These can be easily decoupled by differentiating each equation and substituting the derivatives in the original equations, which gives:

$$\frac{d^2}{dt^2}c_g = -\left(\frac{\Omega}{2}\right)^2 c_g,$$
$$\frac{d^2}{dt^2}\tilde{c}_e = -\left(\frac{\Omega}{2}\right)^2 \tilde{c}_e. \tag{2.38}$$

We can see that both equations have the form of an undamped harmonic oscillator of frequency $\frac{\Omega}{2}$ and therefore the general solutions for c_g and $\tilde{c}_e$ are linear combinations of trigonometric functions:

$$c_g(t) = c_g(0)\cos\left(\frac{\Omega}{2}t\right) - i\tilde{c}_e(0)\sin\left(\frac{\Omega}{2}t\right),$$
$$\tilde{c}_e(t) = \tilde{c}_e(0)\cos\left(\frac{\Omega}{2}t\right) - ic_g(0)\sin\left(\frac{\Omega}{2}t\right). \tag{2.39}$$

For an atom which is initially in the ground state, i.e. $c_g(0) = 1$, $\tilde{c}_e(0) = 0$, the probabilities of the ground and excited states being occupied are then:

$$P_g(t) = |c_g(t)|^2 = \cos^2\left(\frac{\Omega}{2}t\right) = \frac{1}{2}(1 + \cos(\Omega t)),$$
$$P_e(t) = |c_e(t)|^2 = |\tilde{c}_e(t)|^2 = \sin^2\left(\frac{\Omega}{2}t\right) = \frac{1}{2}(1 - \cos(\Omega t)). \tag{2.40}$$

Here, we explicitly see the meaning of the Rabi frequency. It is the frequency, at which the population in a two-level system oscillates between the ground state and the excited state, as shown in Fig. 2.2. In the case when $\Delta = \omega - \omega_0 \neq 0$ we speak about detuning from resonance. To find solutions of the set of Eqs. 2.36 we start again with differentiating the equations and eliminating appropriate variables, which yields:

$$\left(\frac{d^2}{dt^2} - i\Delta\frac{d}{dt} + \frac{\Omega^2}{4}\right)c_g = 0, \tag{2.41}$$

$$\left(\frac{d^2}{dt^2} - i\Delta\frac{d}{dt} + \frac{\Omega^2}{4}\right)\tilde{c}_e = 0.$$
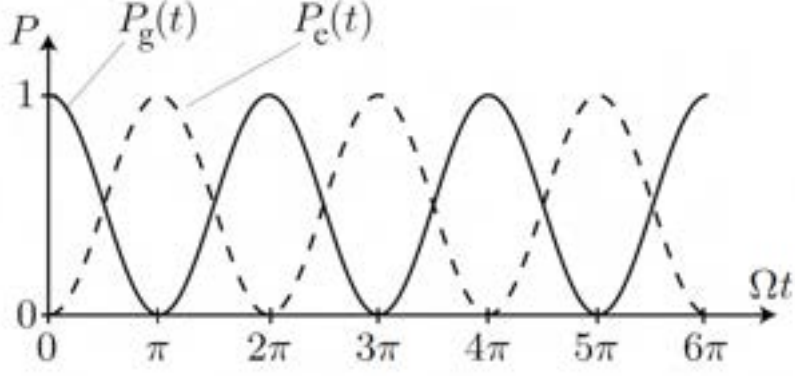
Figure 2.2: Rabi oscillations in a two-level system, which is subject to external illumination with a frequency perfectly resonant to the atomic transition, i.e. $\Delta = \omega - \omega_0 = 0$. The probability of the ground and excited states being occupied oscillates in time with frequency Ω. Figure from Ref. 55.

These can be rewritten in the form:

$$\left(\frac{d}{dt} - i\frac{\Delta}{2} + i\frac{\tilde{\Omega}}{2}\right)\left(\frac{d}{dt} - i\frac{\Delta}{2} - i\frac{\tilde{\Omega}}{2}\right) c_g = 0, \tag{2.42}$$

$$\left(\frac{d}{dt} - i\frac{\Delta}{2} + i\frac{\tilde{\Omega}}{2}\right)\left(\frac{d}{dt} - i\frac{\Delta}{2} - i\frac{\tilde{\Omega}}{2}\right) \tilde{c}_e = 0,$$

where we introduced the generalised Rabi frequency $\tilde{\Omega} = \sqrt{\Omega^2 + \Delta^2}$. Any function which causes either factor to vanish will solve the equation, therefore the solutions are linear combinations of functions of the form $e^{i\Delta t/2 \pm i\tilde{\Omega}t/2}$ and they read:

$$c_g(t) = e^{i\Delta t/2}\left\{c_g(0)\cos\left(\frac{\tilde{\Omega}}{2}t\right) - \frac{i}{\tilde{\Omega}}\left(\Delta\, c_g(0) + \Omega\tilde{c}_e(0)\right)\sin\left(\frac{\tilde{\Omega}}{2}t\right)\right\}, \tag{2.43}$$

$$\tilde{c}_e(t) = e^{i\Delta t/2}\left\{\tilde{c}_e(0)\cos\left(\frac{\tilde{\Omega}}{2}t\right) + \frac{i}{\tilde{\Omega}}\left(\Delta\, \tilde{c}_e(0) - \Omega c_g(0)\right)\sin\left(\frac{\tilde{\Omega}}{2}t\right)\right\}.$$

For an initially unexcited atom with $c_g(0) = 1$ and $\tilde{c}_e(0) = 0$ the solution becomes:

$$c_g(t) = e^{i\Delta t/2}\left\{\cos\left(\frac{\tilde{\Omega}}{2}t\right) - i\frac{\Delta}{\tilde{\Omega}}\sin\left(\frac{\tilde{\Omega}}{2}t\right)\right\}, \tag{2.44}$$

$$\tilde{c}_e(t) = -ie^{i\Delta t/2}\frac{\Omega}{\tilde{\Omega}}\sin\left(\frac{\tilde{\Omega}}{2}t\right).$$

The excited state population is given by:

$$P_e(t) = \frac{\Omega^2}{\tilde{\Omega}^2}\sin^2\left(\frac{\tilde{\Omega}t}{2}\right) = \frac{\Omega^2}{\tilde{\Omega}^2}\left(\frac{1}{2} - \frac{1}{2}\cos\left(\tilde{\Omega}t\right)\right). \tag{2.45}$$

29

As compared to the case without detuning, the detuned oscillations occur at a higher frequency (since $\tilde{\Omega} \geq \Omega$) and their amplitude is reduced, as shown in Fig. 2.3.
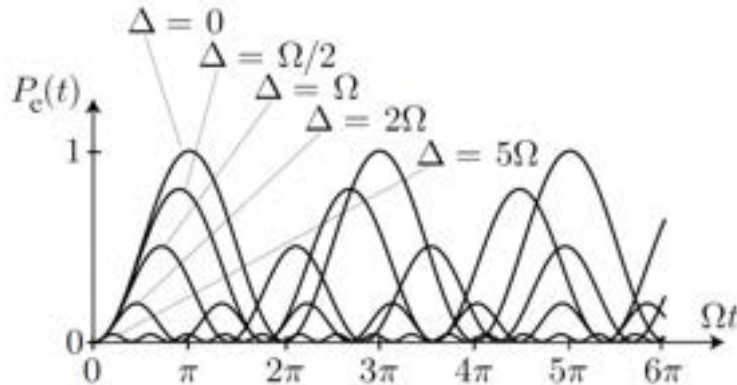

Figure 2.3: Oscillations of the excited state in a two-level system, which is subject to external illumination with a frequency nearly but not exactly resonant to the atomic transition, i.e. $\Delta = \omega - \omega_0 \neq 0$. The probability of excited state being occupied oscillates in time with higher frequency and a smaller amplitude than in the resonant case. Figure from Ref. 55.

2.4 Spontaneous emission

Spontaneous emission is a process in which a quantum system emits a photon, while simultaneously making a transition from an excited state to a lower energy state. According to quantum electrodynamics, spontaneous emission happens due the fluctuations of photonic vacuum, explained by the Heisenberg uncertainty principle [59]. In order to account for vacuum fluctuations, we employ the fully quantum-mechanical description, where both the field and the emitter are treated as quantum entities.

Our ultimate goal is to find the formula for the spontaneous emission rate from an emitter, which is located near a plasmonic nanostructure, in particular in the vicinity of a graphene nanoflake. To achieve this, the derived formulas will be expressed using the Green's tensor formalism. The first step will be to define the total Hamiltonian of the system, then we will find Heisenberg equations of motion for the atom and fields operators. For any operator $\hat{O}$:

$$\dot{\hat{O}} = -\frac{i}{\hbar} \left[\hat{O}, H \right]. \tag{2.46}$$

Afterwards, we will eliminate the field variables from atomic equations making use of the Markovian approximation. This will allow to identify two contributions in the atomic

equations - one which describes the exponential decay of the excited state (spontaneous emission) and another, which is responsible for its energy shift. If we insert into these equations the Green's function for vacuum, the first term gives us the same result as Weisskopf-Wigner theory of spontaneous emission [59].

The derivation in this section is performed within the electric-dipole approximation. The reasoning is based on the field quantisation in dispersive media scheme proposed in Ref. 60 followed by the spontaneous emission rate derivation by Dzsotjan *et al.* [61]. Please note that it can be generalised to include terms beyond the electric-dipole approximation, as done by the author of this thesis *et al.* in Ref. 62.

The field operator at a given position can be expressed as an integral over all frequencies [57]:

$$\mathbf{E}(\mathbf{r}) = \int_0^\infty \mathbf{E}(\mathbf{r}, \omega)\, d\omega. \qquad (2.47)$$

Note that in the Schrödinger picture the field operator is time-independent. The frequency components can be expressed via bosonic creation and annihilations operators which fulfil the commutation rules:

$$\left[\hat{a}_i\left(\mathbf{r}, \omega\right), \hat{a}_j^\dagger\left(\mathbf{r}', \omega'\right) \right] = \delta_{ij}\delta\left(\mathbf{r} - \mathbf{r}'\right)\delta\left(\omega - \omega'\right) \qquad (2.48)$$

$$\left[\hat{a}_i\left(\mathbf{r}, \omega\right), \hat{a}_j\left(\mathbf{r}', \omega'\right) \right] = 0. \qquad (2.49)$$

The indices i and j stand for the variables x, y, z and the operator $\hat{a}_i$ annihilates a photon of frequency ω polarised in the i direction at position $\mathbf{r}$. We also use vector notation $\hat{\mathbf{a}} = [\hat{a}_x, \hat{a}_y, \hat{a}_z]$.

The electric field $\mathbf{E}\left(\mathbf{r}, \omega\right)$ will be expressed *via* the electromagnetic Green's tensor $\mathbf{G}\left(\mathbf{r}, \mathbf{r}', \omega\right)$ and bosonic annihilation operators $\hat{a}_k$. The Green's tensor connects the source located at $\mathbf{r}'$ with the field at position $\mathbf{r}$. A detailed derivation of the relation is given in [57] and leads to the formula:

$$\mathbf{E}\left(\mathbf{r}, \omega\right) = i\sqrt{\frac{\hbar}{\pi\epsilon_0}}\frac{\omega^2}{c^2}\int d^3r' \sqrt{\mathrm{Im}\,\epsilon\left(\mathbf{r}', \omega\right)}\,\mathbf{G}\left(\mathbf{r}, \mathbf{r}', \omega\right)\hat{\mathbf{a}}\left(\mathbf{r}', \omega\right), \qquad (2.50)$$

where ϵ_0 is the vacuum permittivity, ϵ is the permittivity of the environment, c - speed of light. Now, let us by define the Hamiltonian of the total system, which consists of three parts - the Hamiltonian of the electromagnetic field, the atomic Hamiltonian and the Hamiltonian describing the light-matter interaction:

$$\hat{H} = \hat{H}_{\mathrm{field}} + \hat{H}_{\mathrm{at}} + \hat{H}_{\mathrm{AF}}. \qquad (2.51)$$

We also assume that the atom-field coupling is rather weak, so that we can work in the rotating-wave approximation, where $\hat{H}_{AF}$ takes the form

$$\hat{H}_{AF} = -\left[\sigma_+ \mathbf{d}_{eg}\mathbf{E}^{(+)}\left(\mathbf{r}_0\right) + \mathbf{d}_{eg}\mathbf{E}^{(-)}\left(\mathbf{r}_0\right)\sigma_-\right] \tag{2.52}$$

with

$$\mathbf{E}^{(+)}\left(\mathbf{r}\right) = \int_0^\infty d\omega\, \mathbf{E}\left(\mathbf{r},\omega\right), \tag{2.53}$$

$$\mathbf{E}^{(-)}\left(\mathbf{r}\right) = \int_0^\infty d\omega\, \mathbf{E}^\dagger\left(\mathbf{r},\omega\right). \tag{2.54}$$

Making use of Eq. 2.50 and the Heisenberg equation of motion (Eq. 2.46), we calculate the evolution of the annihilation operator $\hat{a}_k(\mathbf{r},\omega)$ and atomic operator σ_-. The evolution of the annihilation operator gives:

$$\dot{a}_j\left(\mathbf{r},\omega\right) = -\frac{i}{\hbar}\left[\hat{a}_j, \int d^3r \int_0^\infty d\omega\hbar\omega\hat{\mathbf{a}}^\dagger\left(\mathbf{r},\omega\right)\hat{\mathbf{a}}\left(\mathbf{r},\omega\right) - \sigma_+\mathbf{d}_{eg}\mathbf{E}^{(+)}\left(\mathbf{r}_0\right) - \mathbf{d}_{eg}\mathbf{E}^{(-)}\left(\mathbf{r}_0\right)\sigma_-\right] =$$

$$= -i\omega\hat{a}_j\left(\mathbf{r},\omega\right) + \frac{1}{\hbar}\sqrt{\frac{\hbar}{\pi\epsilon_0}}\frac{\omega^2}{c^2}\sqrt{\mathrm{Im}\varepsilon\left(\mathbf{r},\omega\right)}\mathbf{e}_j\mathbf{G}^\dagger\left(\mathbf{r}_0,\mathbf{r},\omega\right)\mathbf{d}_{eg}\sigma_-, \tag{2.55}$$

where we used the equal-time relations $[\sigma_-,\sigma_+] = -\sigma_z$, $[\sigma_-,\sigma_z] = 2\sigma_-$, $[\sigma_+,\sigma_z] = -2\sigma_+$ and commutation relations for annihilation and creation operators. Now we formally integrate the last equation over time:

$$\hat{a}_j\left(\mathbf{r},\omega\right) = \hat{a}_j^{\mathrm{free}}\left(\mathbf{r},\omega\right) + \sqrt{\frac{\mathrm{Im}\varepsilon\left(\mathbf{r},\omega\right)}{\hbar\pi\epsilon_0}}\frac{\omega^2}{c^2}\mathbf{e}_j\mathbf{G}^\dagger\left(\mathbf{r}_0,\mathbf{r},\omega\right)\mathbf{d}_{eg}e^{-i\omega t}\int_0^t dt'\sigma_-\left(t'\right)e^{i\omega t'}, \tag{2.56}$$

where $\hat{a}_j^{\mathrm{free}}\left(\mathbf{r},\omega\right)$ corresponds to the free evolution of the annihilation operator, i.e. the evolution due to free-field Hamiltonian H_{field}.

Now we can write the Heisenberg equation (Eq. 2.46) for the atomic operator σ_-:

$$\dot{\sigma}_- = -i\omega_0\sigma_- - \frac{i}{\hbar}\sigma_z\mathbf{d}_{eg}\mathbf{E}^{(+)}\left(\mathbf{r}_0\right)$$

$$= -i\omega_0\sigma_- - \frac{i}{\hbar}\sigma_z\mathbf{d}_{eg}\mathbf{E}_{\mathrm{free}}^{(+)}\left(\mathbf{r}_0\right)$$

$$+\frac{1}{\hbar\pi\epsilon_0}\int_0^\infty d\omega\int d^3r'\frac{\omega^4}{c^4}\mathrm{Im}\varepsilon\left(\mathbf{r}',\omega\right)\mathbf{d}_{eg}\mathbf{G}\left(\mathbf{r_0},\mathbf{r}',\omega\right)\mathbf{G}^\dagger\left(\mathbf{r}_0,\mathbf{r}',\omega\right)\mathbf{d}_{eg}\sigma_z\left(t\right)\int_0^t dt'\sigma_-\left(t'\right)e^{-i\omega(t-t')}, \tag{2.57}$$

where in the last line we used result 2.56 and $\mathbf{E}_{\mathrm{free}}^{(+)}$ denotes the electric field evolving freely due to the field Hamiltonian $\hat{H}_{\mathrm{field}}$:

$$\mathbf{E}_{\mathrm{free}}^{(+)} = \int_0^\infty d\omega\, i\sqrt{\frac{\hbar}{\pi\epsilon_0}}\frac{\omega^2}{c^2}\int d^3r'\sqrt{\mathrm{Im}\varepsilon\left(\mathbf{r}',\omega\right)}\mathbf{G}\left(\mathbf{r_0},\mathbf{r}',\omega\right)\hat{\mathbf{a}}^{\mathbf{free}}(\mathbf{r}',\omega). \tag{2.58}$$

To find the spontaneous emission rate, one has to deal with the integral over time, which appears in Eq. 2.57. This requires making several assumptions. First, please note that in the case of a free atom the operator oscillates freely in line with $\sigma_-(t) = \sigma_-(0)e^{-i\omega_0 t}$. If one assumes that the photonic environment introduces only relatively small modifications to this evolution, it is reasonable to see the influence of the environment as a certain envelope upon the free oscillations. Let us define $\tilde{\sigma}_-(t) = \sigma_-(t)e^{i\omega_0 t}$ which in this case can be assumed to change very little over the time interval where the rest of the integral is non-zero and which, therefore, can be taken out of the integral at a fixed time t. An interpretation of this step is that the evolution of the system is affected only by its present state (the system has no memory). This step is known as the Markovian approximation [63].

$$\int_0^t dt' \sigma_-(t') e^{-i\omega(t-t')} \approx e^{-i\omega_0 t} \int_0^t dt' \tilde{\sigma}_-(t') e^{-i(\omega-\omega_0)(t-t')} \approx \tilde{\sigma}_-(t) e^{-i\omega_0 t} \int_0^t dt' e^{-i(\omega-\omega_0)(t-t')} =$$

$$= \sigma_-(t) \int_0^t dt' e^{-i(\omega-\omega_0)(t-t')} = \sigma_-(t) \left[\pi\delta(\omega-\omega_0) + i\mathcal{P}\left(\frac{1}{\omega-\omega_0}\right) \right], \qquad (2.59)$$

where $\mathcal{P}$ denotes the principal value of an integral. Using the Sokhotski–Plemelj theorem we arrive at:

$$\int_0^\infty dt' e^{i(\omega-\omega_0)(t'-t)} = 2\pi\delta(\omega-\omega_0) + 2i\,\mathcal{P}\left(\frac{1}{\omega-\omega_0}\right). \qquad (2.60)$$

With respect to the integral in 2.59, the upper integration limit is modified from t to ∞. The delta function has a peak at $t = t'$, so we can assume that the correct result of the integral up to t is only a half of the integral value with the upper limit far above t [63]. Also, we assume that frequencies smaller than zero have no significant contribution to the integral and we go to $-\infty$ with the lower limit in the integral over frequencies in 2.57.

The final equation for evolution of operator σ_- reads:

$$\dot{\sigma}_- = - \left(i\omega_0 + i\delta\omega + \frac{1}{2}\Gamma \right) \sigma_- - \frac{i}{\hbar} \sigma_z \mathbf{d}_{eg} \mathbf{E}_{\text{free}}^{(+)}(\mathbf{r}, \omega),$$

where we introduced the Lamb shift $\delta\omega$ and the spontaneous emission rate Γ:

$$\delta\omega = \frac{1}{\hbar\pi\epsilon_0 c^2} \mathcal{P} \int_0^\infty d\omega \frac{\omega^2}{\omega-\omega_0} \mathbf{d}_{eg} \operatorname{Im} \mathbf{G}(\mathbf{r}_0, \mathbf{r}_0, \omega) \mathbf{d}_{eg},$$

$$\Gamma = \frac{2\omega_0^2}{\hbar\epsilon_0 c^2} \mathbf{d}_{eg} \operatorname{Im} \mathbf{G}(\mathbf{r}_0, \mathbf{r}_0, \omega_0) \mathbf{d}_{eg}. \qquad (2.61)$$

Using Eq. 2.61 with the Green's tensor for vacuum we get the familiar Weisskopf-Wigner spontaneous emission rate in free space:

$$\Gamma_{WW} = \frac{\omega^3 d_{eg}^2}{3\pi\epsilon_0 \hbar c^3}. \qquad (2.62)$$

However, please note that the expression 2.61 contains much more than just the free-space value of spontaneous emission, since it allows one to quantify the spontaneous emission in arbitrarily complicated environments, once their Green's tensor is known.

2.5   Density matrix

To study incoherent or dissipative processes it is necessary to switch to a statistical description. Instead of describing the state of the system with a wave function and the interaction of the atoms with the light field via the Schrödinger equation, one needs to use the density operator and the master equation.

For a state that can be represented by a state vector $|\Psi\rangle$, the density operator is defined as:

$$\rho = |\Psi\rangle \langle\Psi| . \tag{2.63}$$

Such a state is called a pure state and the information contained in the density matrix ρ is equivalent to the one in the state vector Ψ. However, the density operator can also represent an ensemble of identical systems described by statistical mixtures of states. A state that cannot be represented in the form of a pure state is called a mixed state and is described in the general form:

$$\rho = \sum_\alpha P_\alpha |\Psi_\alpha\rangle \langle\Psi_\alpha| , \tag{2.64}$$

which reflects the fact that we do not know which of the states $|\Psi_\alpha\rangle$ the system is in and we assign a probability (weight) P_α to each of the $|\Psi_\alpha\rangle$ states in the mixture. Note that $\sum_\alpha P_\alpha = 1$ for proper normalisation.

The physical content of the density operator is more apparent when we compute the elements $\rho_{\alpha\alpha'}$ of the corresponding density matrix with respect to a complete orthonormal basis. The density matrix elements are given by:

$$\rho_{\alpha\alpha'} = \langle\alpha| \rho |\alpha'\rangle . \tag{2.65}$$

The diagonal elements $\rho_{\alpha\alpha}$ are referred to as populations and they give the measurement probability of the system in the state $|\alpha\rangle$:

$$\rho_{\alpha,\alpha} = \langle\alpha| \rho |\alpha\rangle = |\langle\alpha|\Psi\rangle|^2 . \tag{2.66}$$

The off-diagonal elements $\rho_{\alpha\alpha'}$ $(\alpha \neq \alpha')$ are referred to as coherences, since they give information about the relative phase of different components of the superposition. If we write the state vector as a superposition with explicit phases:

$$|\Psi\rangle = \sum_\alpha |c_\alpha| e^{i\Phi_\alpha} |\alpha\rangle \,, \qquad (2.67)$$

then the coherences are:

$$\rho_{\alpha\alpha'} = |c_\alpha c_{\alpha'}| e^{i(\Phi_\alpha - \Phi_{\alpha'})}. \qquad (2.68)$$

2.6   Time-evolution of density operators

The time evolution of a density operator can be described with the Schrödinger-von Neumann equation:

$$\partial_t \rho = -\frac{i}{\hbar} [H, \rho] \,. \qquad (2.69)$$

However, the point of using density operators is to describe more general evolution processes than only those implied by state-vector dynamics. To achieve this, one can use the more general master equation:

$$\partial_t \rho = \mathcal{L}\rho, \qquad (2.70)$$

where $\mathcal{L}$ is called the Liouvillian superoperator, which acts on the Hilbert space of density matrices. The explicit form of the most general Liouvillian operator which preserves the properties of density matrices during the evolution reads:

$$\mathcal{L}\rho(t) = -i[H, \rho(t)] + \sum_i \left(L_i \rho(t) L_i^\dagger - \frac{1}{2} \left\{ L_i^\dagger L_i, \rho(t) \right\} \right), \qquad (2.71)$$

where H is a Hermitian Hamiltonian, which describes the reversible Schrödinger-like part of the evolution and L_i are so-called Lindblad operators. Inserting this superoperator into Eq. 2.70 we arrive at the Gorini-Kossakowski-Lindblad-Sudarshan (GKLS) equation:

$$\partial_t \rho(t) = -i[H, \rho(t)] + \sum_i \left(L_i \rho(t) L_i^\dagger - \frac{1}{2} \left\{ L_i^\dagger L_i, \rho(t) \right\} \right). \qquad (2.72)$$

A detailed derivation and discussion of the GKLS equation can be found in Ref. 64.

To fully describe dissipation processes occurring in two-level systems, commonly two types of Lindblad operator are used:

- jump operators $\sigma_{ij} = |i\rangle \langle j|$ describe population transfer from the eigenstate j to the eigenstate i at some corresponding rate; transfer from higher to lower energy states is called *decay* or *relaxation* and from lower to higher is often described as *pumping*,

- decoherence operators $\sigma_{ii} = |i\rangle \langle i|$ which lead to the decay of coherences (off-diagonal elements of the density matrix) without influencing the populations of the eigenstates.

Chapter 3

Properties of graphene nanoflakes

3.1 Hamiltonian of pristine graphene nanoflakes

In this Section, we proceed to present the components of the framework, which we use for modelling graphene nanoflakes. In this Chapter we do not include any adatoms but instead we start with the description of pristine graphene nanoflakes. The adatoms will be added to the system in Chapter 4 . Here, we use the second-quantisation Hamiltonian (Eq. 1.5) in the simpler single-particle form:

$$H_{TB} = -t \sum_{\langle l, l' \rangle} \left(|l\rangle \langle l'| + |l'\rangle \langle l| \right), \tag{3.1}$$

where the Hilbert space spans over sites $|l\rangle$ which can be occupied by an electron. The Hamiltonian is constructed within the tight-binding approximation, where each carbon atom corresponds to one site associated with a p_z orbital. We assume that an electron can be exchanged between nearest carbon-atom neighbours with the rate t, and $\langle l, l' \rangle$ means summation over nearest neighbour atomic sites l and l'. Again, we use $t = 2.66 \, \text{eV}$.

Having constructed the Hamiltonian, we can diagonalise it, which gives us the energies E_j and eigenvectors $|\phi_j\rangle$ of the system. This already provides a lot of information about a nanoflake - the eigenvalues of equation 3.1 determine its resonant frequencies. The eigenvectors let one construct the ground-state density matrix ρ^{Aufbau} of a flake filled with a given number of electrons N_e according to the Aufbau principle:

$$\rho^{\text{Aufbau}} = \frac{2}{N_e} \sum_j f_j \left(N_e \right) |\phi_j\rangle \langle \phi_j|, \tag{3.2}$$

where $f_j(N_e) \in [0,1]$ is the Fermi-Dirac distribution, which determines how many electrons per spin occupy the state $|\phi_j\rangle$. Thus defined density matrix is normalised as $\mathrm{Tr}\rho = 1$.

Please note that from now on we can operate in two different bases, in which we can describe our system. On one hand, we speak about the real-space basis of sites $|l\rangle$, in which we construct the tight-binding Hamiltonian. On the other hand, we have the basis of eigenstates $|\phi_j\rangle$ obtained from the diagonalisation of the Hamiltonian, which we will also call the energy basis. The two bases are related via a linear transformation with coefficients a_{jl}:

$$|\phi_j\rangle = \sum a_{jl} |l\rangle . \tag{3.3}$$

The coefficients a_{jl} explain how much of a given eigenstate in energy basis can be attributed to charge located on a given site in real space.

The Hamiltonian in Eq. 3.1 describes connections between the carbon atoms and in this way contains information about the shape of the graphene flake and its edges. Now we can investigate how the edge type of a graphene nanoflake can influence its energy spectrum, which will lead to some interesting conclusions. We focus on triangular flakes, since they can have a homogenous edge of both entirely armchair or entirely zigzag character (Fig. 3.1). Other flake shapes such as a hexagon or a circle always cause the flake to have mixed character of the edges (see Fig. 3.2). A short overview of possible triangular flake geometries is shown in table 3.1. The energy spectra are presented in Figs. 3.3 and 3.4. The energy levels in both cases originate from the quantisation of the graphene spectrum and thus are contained within $\pm 3t \approx \pm 8$ eV. In the case of armchair-edged flakes there is always a gap around the zero energy. The gap decreases with the size of the flake but nonetheless it is always present. In zigzag-edged flakes the opposite is true - there are always some energy levels present at the zero energy, hence there is no gap around the Fermi level.
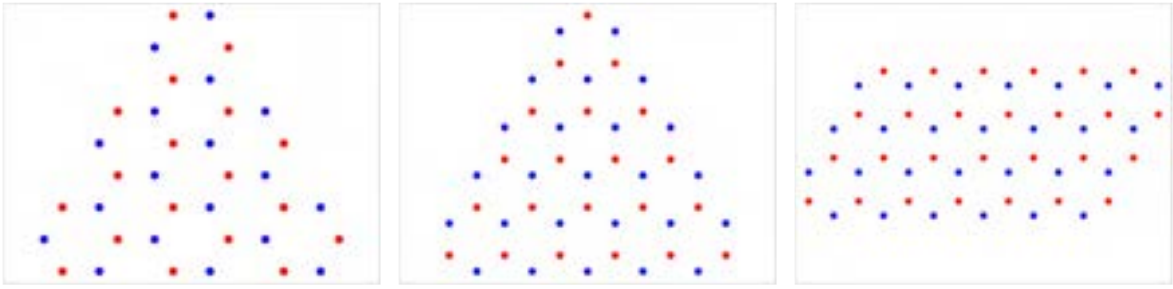
Figure 3.1: Graphene nanoflakes that have edges of only one type - purely armchair (left panel) or purely zigzag (middle and right panels).
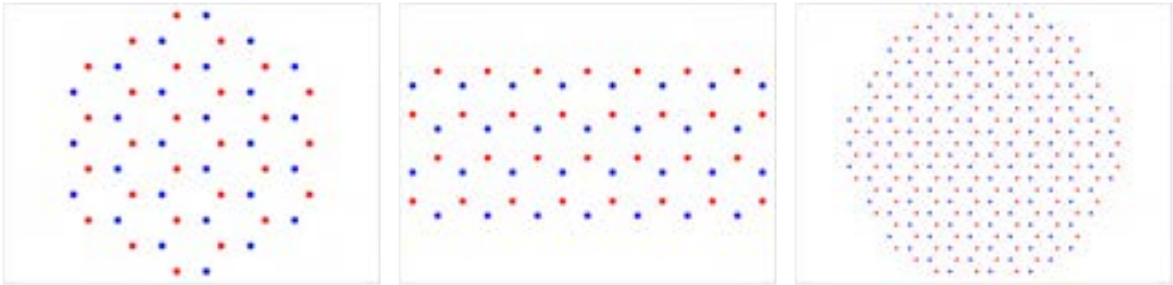

Figure 3.2: Graphene nanoflakes that have edges of mixed type. An arbitrary flake shape most likely has mixed-type edges.
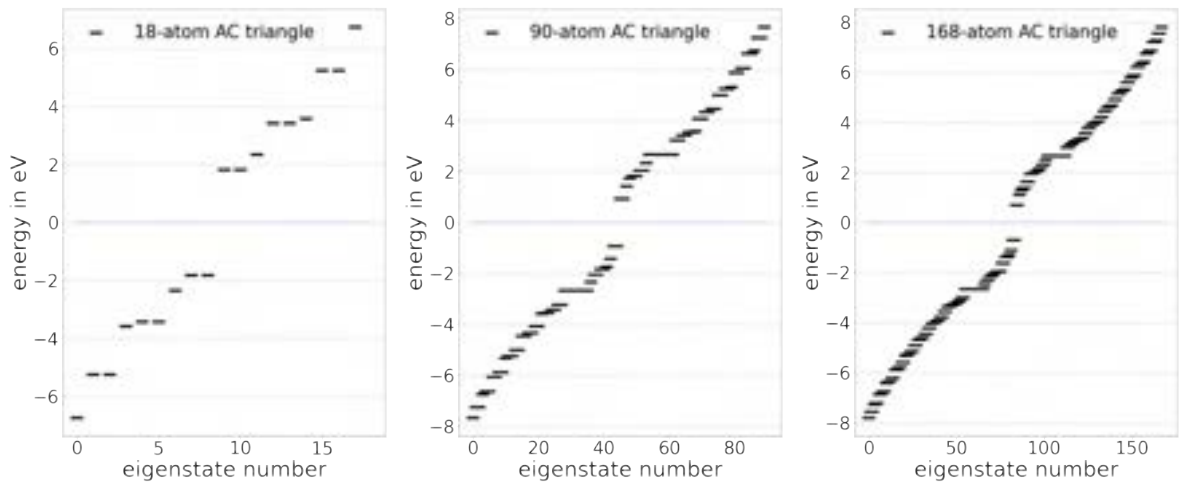

Figure 3.3: Energies of three armchair-edged triangular graphene nanoflakes of various sizes. Note that there is always a gap around the Fermi energy, which decreases with the size of the flake. The energy values are contained in the range between -8 and 8 eV.

Armchair edge		
Number of hexagons on side	Number of atoms in flake	Side length (nm)
2	18	0.71
3	36	1.14
4	60	1.56
5	90	1.99
6	126	2.41
7	168	2.84
8	216	3.27
9	270	3.69
10	330	4.12
n	$3n(n+1)$	$0.426\,n - 0.142$
Zigzag edge		
Number of hexagons on side	Number of atoms in flake	Side length (nm)
2	13	0.49
3	22	0.74
4	33	0.98
5	46	1.23
6	61	1.48
7	78	1.72
8	97	1.97
9	118	2.21
10	141	2.46
n	$n^2 + 4n + 1$	$0.246\,n$

Table 3.1: Possible sizes and numbers of atoms in armchair and zigzag edge triangular graphene nanoflakes.
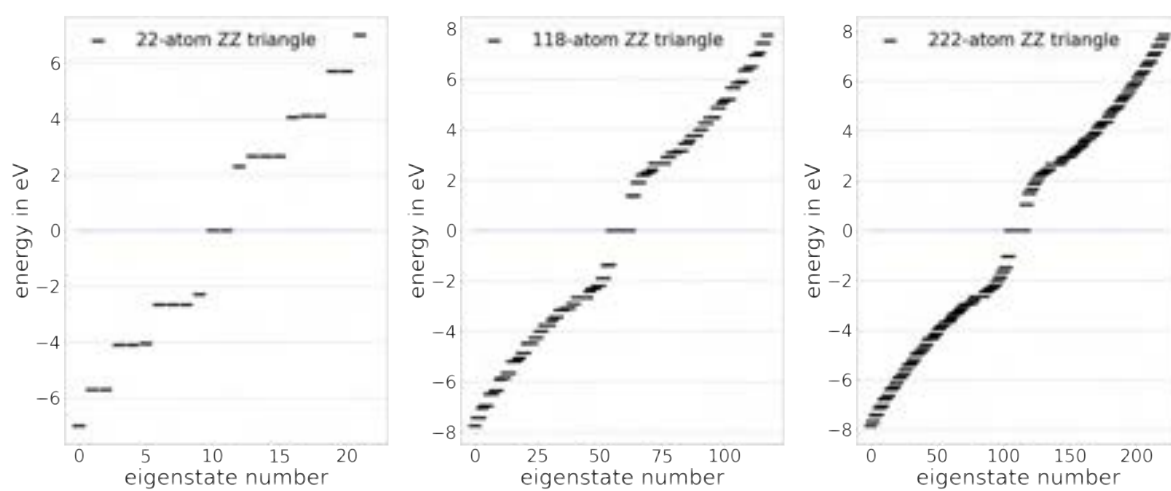
Figure 3.4: Energies of three zigzag-edged triangular graphene nanoflakes of various sizes. Note the presence of states located at the Fermi energy.

3.2 Coulomb interaction in the flake

Knowing the eigenvalues obtained from the diagonalisation of equation 3.1 allows us to construct the density matrix of a flake filled with a given number of electrons according to Eq. 3.2. For a bare nanoflake without doping or adatoms, the resulting ground state in zero temperature gives a uniform charge distribution across the flake $(\rho^{\text{uniform}})_{kl} = \frac{\delta_{kl}}{N}$, where N is the number of sites. In this case, the number of electrons in the system is equal to the number of sites: $N_e = N$. Note that this does not hold in general - we may consider electron or hole doping, and later the adatom may introduce a different number of orbitals and electrons.

The ground state exhibits a uniform charge distribution across the flake only in pristine graphene flakes. If we add doping electrons, the ground state charge distribution that follows from the ground state density matrix calculated from the tight-binding states is no longer uniform. In this case, we expect some Coulomb repulsion in the initially prepared state, pushing the electrons towards a uniform distribution. On the other hand, the uniform distribution does not necessarily need to be the lowest-energy state. The equilibrium state of the system is a result of a trade-off between the two effects, such that the energy minimisation in the non-interacting system and the Coulomb repulsion balance each other. This equilibrium state can be found iteratively in a self-consistency procedure. The procedure described below additionally provides a new basis set, which is dressed in the Coulomb interaction. It consists of the following steps [65]:

1. For a given graphene flake, diagonalise the free Hamiltonian (3.1).

2. With the specified number of electrons N_e (equal to the sum of the number of atoms in flake and the number of doping electrons), calculate the density matrix ρ^{Aufbau} according to the Aufbau principle (Eq. 3.2). For an undoped flake at adatom absence and at zero temperature, the density matrix calculated in this way corresponds to a uniform distribution of electrons among all N sites with, in general, non-zero off-diagonal elements.

3. Calculate the potential induced by the non-uniformity of charge distribution on the l-th site:

$$(\Phi_{\text{charge}})_{ll'} = -eN_e\delta_{ll'} \sum_k v_{lk} \left(\rho^{\text{Aufbau},kk} - \rho^{\text{uniform},kk} \right)$$

Here, indices k, l, l' correspond to different sites (i.e. carbon sites or later adatom orbitals). The symbol v_{lk} stands for the Coulomb interaction matrix element between sites l and k. For carbon-carbon interactions we employ the values evaluated in Ref. 66.

4. Construct a Hamiltonian including the induced charge $H = H_{TB} - e\Phi_{\text{charge}}$. In practice, to ensure the convergence of the procedure, at each iteration we only include a fraction of the new induced potential and combine it with the induced potential from the previous iteration, i.e.: $H^{(n+1)} = H_{TB} - e(1 - p_{\text{mix}})\Phi_{\text{charge}}^{(n-1)} - ep_{\text{mix}}\Phi_{\text{charge}}^{(n)}$, where $p_{\text{mix}} \in [0, 1]$. Usually a good choice for p_{mix} is in the range $0.1 - 0.5$.

Steps 1-4 can now be repeated with the new Hamiltonian from step 4, and a new ρ^{Aufbau} built based on the new Hamiltonian eigenstates. The procedure should be repeated until self-consistency is reached, i.e. the evaluated charge-nonuniformity induced potential Φ_{charge} and the equilibrium density matrix ρ^{sc} from steps 2 and 3 are stable. The "sc" superscript stands here for "self-consistency".

For flakes which are doped with additional electrons, the energies obtained by using the above-mentioned procedure differ from the energies of the pure tight-binding Hamiltonian given by Eq. 3.1, however the difference is very small (Fig. 3.5). A slight impact of the self-consistency procedure can also be seen in the real-space charge distribution (Fig. 3.6).

3.3 Including external illumination

The external electric field is coupled to the nanoflake using the following coupling scheme:

$$H\left(\rho(t), t\right) = H_{\text{TB}} - e\Phi_{\text{charge}} - e\Phi(t) = H_{\text{TB}} - e\Phi_{\text{charge}} + \left[e\Phi^{\text{ext}}(t) - e\Phi^{\text{ind}}\left(\rho(t)\right)\right]. \quad (3.4)$$

Here,

$$\Phi^{\text{ext}}(t) = -\sum_l \mathbf{r}_l \cdot \mathbf{E}(\mathbf{r}_l, t) \, |l\rangle \langle l| \quad (3.5)$$

is the energy of the external field that arises due to the illumination $\mathbf{E}(\mathbf{r}, t)$ polarised in the plane of the graphene flake. In the case of a laser illumination we can use the quasistatic limit and neglect the spatial dependence of the external field. The summation goes over all carbon sites l. The Hamiltonian in Eq. 3.4 depends explicitly on the density
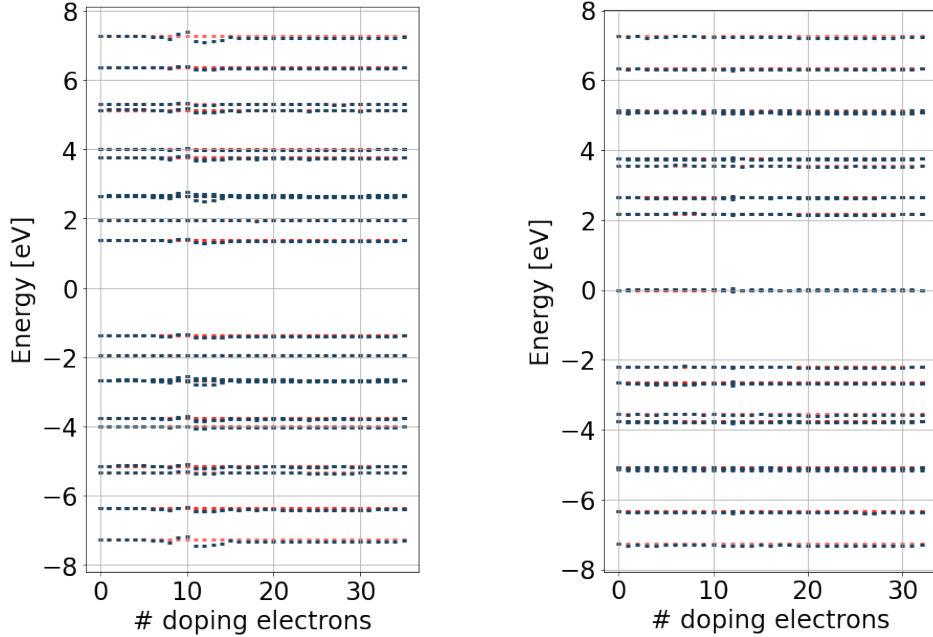
Figure 3.5: Left: Energy spectrum of a 36-atom (1.14 nm) armchair-edged triangular graphene flake doped with an increasing number of electrons. Right: Energy spectrum of a 33-atom (0.98 nm) zigzag-edged triangular graphene flake doped with an increasing number of electrons. The navy lines present the energies after the self-consistency procedure. The red dashed lines in the background correspond to the undoped case and serve for comparison. In flakes of both edge types, the self-consistency procedure shifts the states' energies slightly with respect to the undoped case.

matrix ρ. Usually in quantum mechanics we deal with Hamiltonians that do not depend on ρ and their evolution equation is linear. The non-linearity in our case is the price which we pay for including the Coulomb interactions and at the same time keeping a single-particle Hilbert-space dimension. This allows us to investigate much larger systems than we would be able to using a many-particle approach with a much larger Hilbert space size.

As the electric field moves the electrons away from their equilibrium positions, Coulomb interactions arise, which are accounted for by the field-induced potential:

$$\Phi^{ind}(t) = -eN_e\delta_{kl} \sum_{l'} v_{ll'} \left(\rho_{l'l'}(t) - \rho_{l'l'}^{\mathrm{sc}} \right), \tag{3.6}$$

where the summation goes over the all carbon sites l'. The induced potential is between one and two orders of magnitude smaller than the external one and has an opposite sign.
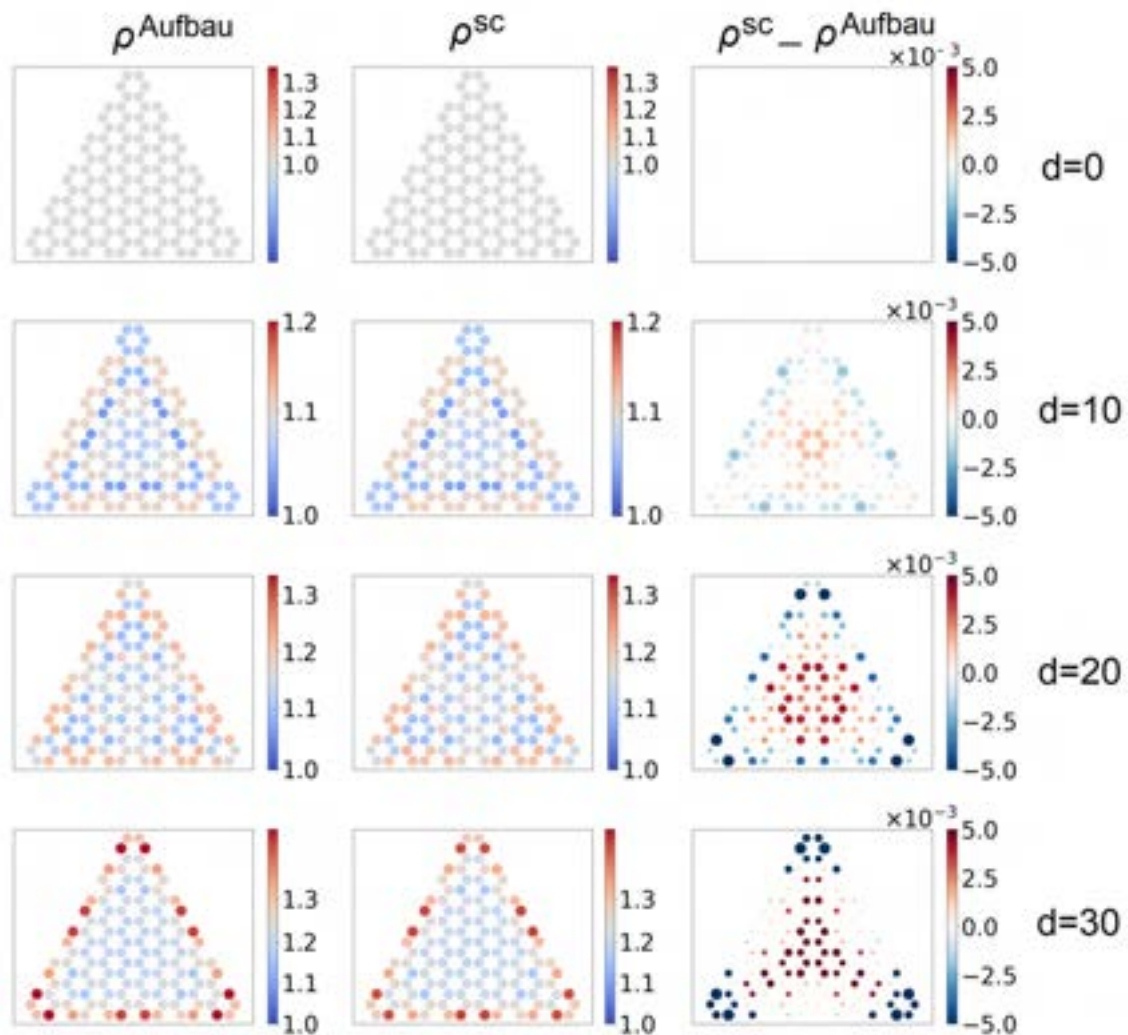
44

Figure 3.6: Real-space charge distribution in triangular graphene flake of size 2.41 nm doped with 0, 10, 20, 30 electrons: before the self-consistency ρ^{Aufbau} (left), after the self-consistency ρ^{sc} (middle) and the difference $\rho^{sc} - \rho^{\text{Aufbau}}$ (right). Naturally, when there is no doping, the distribution is uniform and the self-consistent procedure has no effect on the charge distribution.

3.4 Time evolution and dissipative processes

The dynamics of the system is described via the single-electron master equation

$$\frac{\partial}{\partial t}\rho(t) = -\frac{i}{\hbar}\left[H\left(\rho(t),t\right),\rho(t)\right] - \mathcal{D}\left[\rho(t)\right]. \qquad (3.7)$$

The Hermitian Hamiltonian described in previous sections accounts for the reversible processes in the system, with the non-linearity related to the inclusion of the Coulomb interactions. Dissipation effects can be taken into account in the term $\mathcal{D}\left[\rho(t)\right]$, which we consider in one of the two forms described below and refer to as *phenomenological* and *Lindblad-based* approaches. In the following, we discuss their form, underlying approxi-

45

mations and compare their advantages and drawbacks.

3.4.1   Phenomenological approach

The phenomenological damping term has a relatively simple form and interpretation [67]:

$$\mathcal{D}\left[\rho(t)\right] = \frac{1}{2\tau}\left(\rho(t) - \rho^{sc}\right). \tag{3.8}$$

The model characterises the whole dissipative process with one parameter only: the decoherence lifetime τ, where the advantage of simplicity comes for the price of several approximations. Its value can be found from the relation $\hbar\tau^{-1} = 10\,\text{meV}$, which is known from experiments in bulk graphene, being a very good approximation for large flakes [67]. An important advantage of the phenomenological approach is that it forces the system back into its equilibrium state. By construction, that state includes the information on the many-electron character of the system: ρ^{sc} is built according to the Aufbau principle which takes the Pauli principle into account so that no more than two electrons are put in one state.

However, this approach does not indicate how to modify the damping rates for small flakes of graphene, where the bulk value of τ does not necessarily have to be the correct one. Moreover, the stationary state of perturbed dissipative quantum systems results from a trade off between the excitation strength (here, proportional to the electric field) and the loss rates. For strong perturbations, saturation effects occur [68]. The field influence on the equilibrium state is beyond the scope of this approach, which is a good approximation for strongly dissipative systems, in particular for large flakes, as well as in the case of moderately strong illumination in the form of pulses shorter than the relaxation time τ. Another drawback of the phenomenological approach is the fact that it describes a very specific situation of all transition and decoherence rates being equal, even for transitions which should be forbidden in flakes with inversion symmetry. Later, when we include the adatom, this approach will not allow us to modify the dissipation on the adatom, therefore being a rather coarse description from the atomic perspective and for weak atom-flake coupling rates $t_{e,g}$.

3.4.2 Lindblad-based formalism

A fully quantum-mechanical description of dissipative processes can be achieved through the use of the GKLS equation (Eq. 2.72) which involves the superoperator in the form:

$$\mathcal{D}\left[\rho(t)\right] = \sum_{k=1}^{N^2-1} \gamma_k \left(L_k \tilde{\rho}(t) L_k^\dagger - \frac{1}{2} \left\{ L_k^\dagger L_k, \tilde{\rho}(t) \right\} \right). \tag{3.9}$$

L_k are Lindblad operators and to fully describe dissipation in a system of several energy levels two types of these operators are used: $N(N-1)$ jump operators $\sigma_{ij} = |i\rangle \langle j|$ and $N-1$ independent decoherence operators $\sigma_{ii} = |i\rangle \langle i|$. In this work we usually consider transfer from higher to lower energy states and disregard incoherent pumping effects. Note that each of these dissipation channels is described with an independent rate γ_k, that provides us with the possibility to assign different rates to different processes, in particular to treat the adatom individually, to turn selected channels off, or even to include pumping with $L_k \to \sigma_{ij} = |i\rangle \langle j|$ for $i > j$. For multilevel systems it was shown that there are additional, nontrivial constraints on the pure dephasing rates, which can be found in Ref. 69.

However, there is a strong drawback of the rigorous approach. In the proper quantum-mechanical form of Eq. (3.9) we simply have $\tilde{\rho} = \rho$. The equation could then describe a many-body problem under the condition that it is described in a many-body Hilbert space. Here, we approach the problem with the single-particle formalism, which has the great advantage of ability to approximately tackle relatively large systems with hundreds of electrons. The price to pay is that the Pauli principle is not accounted for in the master equation. The extreme manifestation of this fact is that the dissipation term (3.9) without optical pumping pushes all electrons into the lowest-energy eigenstate of the system, severely breaking the Pauli principle, as shown in the left panel in Fig. 3.7. To overcome this problem, we have tried several correction methods, which are presented in detail in Appendix A. Finally, we decided to set $\tilde{\rho} = \rho - \rho^{sc}$. This choice leads to a similar type of dissipation as the phenomenological approach described in the previous subsection but it has some advantages. With the new approach we can separately modify transition rates between pairs of eigenstates, in particular for the adatom. In practice, we can set them to the values obtained from dipole moment calculations with the Weisskopf-Wigner formula. We have tested this method numerically for a great deal of flakes of different shapes and sizes for various initial states in presence of weak and moderate electric fields,

i.e. up to 10^{10} V/m and have not encountered any example breaking the Pauli exclusion principle or cause any problems with the normalisation or positive-definiteness of the density matrix.
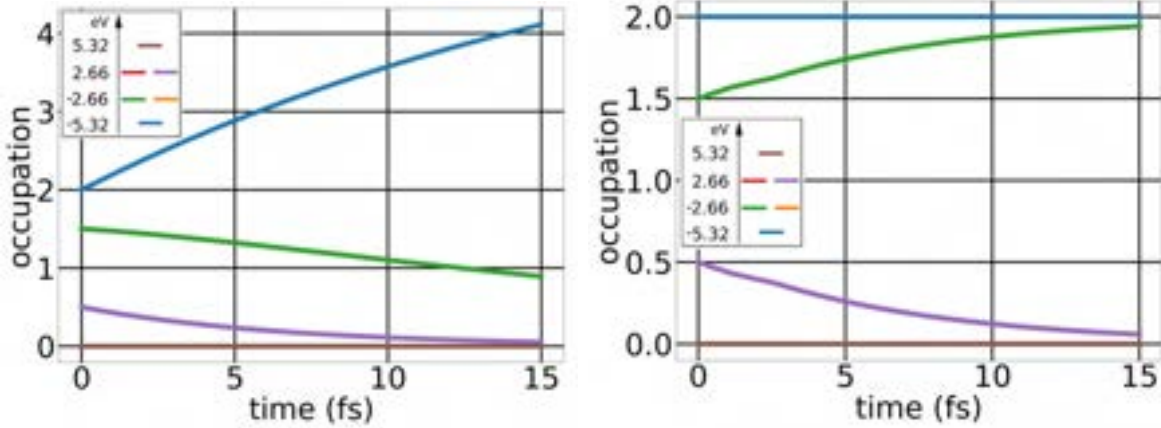

Figure 3.7: Comparison of the dissipation in a benzene ring (6 atoms) which initially has the HOMO-LUMO transition excited using the a) uncorrected Lindblad method ($\tilde{\rho} = \rho$) and b) the corrected Lindblad method ($\tilde{\rho} = \rho - \rho^{sc}$). The energy levels of the benzene ring are labelled with colours, as shown in the small plot in the upper-left corner of the subfigures. There is no external field nor doping.

3.4.3 Dissipation rates in small systems

Using the large decoherence rate of bulk graphene is justified for large flakes. However, in general the decoherence rate scales with the size of a quantum system and we expect it should be reduced for small flakes to prevent unphysically large damping. In this subsection, we investigate conditions in which the two approaches described in the previous subsections converge to the same dynamics, both on the analytical and numerical grounds. This will help us to understand how the decoherence rate τ^{-1}, which is known from bulk graphene, should be modified for small flakes of graphene.

The phenomenological approach describes a specific situation in which all transition and decoherence rates are equal. The second approach is more complex, as the model contains many more adjustable parameters. We compare just the dissipative part and omit the Hamiltonian-evolution term which is equal in both methods. The first approach, given by Eq. 3.8, is very straightforward to analyse and yields:

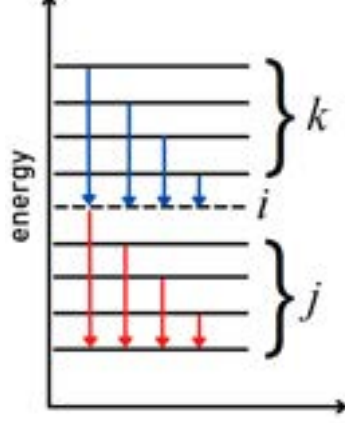$$\dot{\rho}_{ij} = \frac{1}{2\tau} \tilde{\rho}_{ij}. \tag{3.10}$$

Figure 3.8: A graphical demonstration of transitions which will be modelled in a system of several energy levels. We only include transitions from higher energy levels to lower energy levels, which are driven by jump operators $|i\rangle\langle k|$ and $|j\rangle\langle i|$.

In the second case, let us first consider only jump operators:

$$
\begin{aligned}
\dot{\rho}_{ii} &= \langle i| \left[\sum_{j,k}^{N_e} \gamma_{jk} \left(|j\rangle\langle k| \tilde{\rho} |k\rangle\langle j| - \frac{1}{2} |k\rangle\langle k| \tilde{\rho} - \frac{1}{2} \tilde{\rho} |k\rangle\langle k| \right) \right] |i\rangle = \\
&= \sum_{j,k} \gamma_{jk} \left[\delta_{ij} \langle k| \tilde{\rho} |k\rangle - \frac{1}{2}\delta_{ik} \langle k| \tilde{\rho} |i\rangle - \frac{1}{2} \langle i| \tilde{\rho} |k\rangle \delta_{ki} \right] = \\
&= \sum_k \gamma_{ik} \langle k| \tilde{\rho} |k\rangle - \frac{1}{2} \sum_j \gamma_{ji} \langle i| \tilde{\rho} |i\rangle - \frac{1}{2} \sum_j \gamma_{ji} \langle i| \tilde{\rho} |i\rangle = \\
&= \sum_{k>i} \gamma_{ik}\tilde{\rho}_{kk} - \sum_{j<i} \gamma_{ji}\tilde{\rho}_{ii}.
\end{aligned}
\tag{3.11}
$$

If we assume that all emission rates in the equations above are equal, i.e. $\gamma_{kl} = \gamma$ for any pair of states $|k\rangle$ and $|l\rangle$ where $E_k > E_l$ (for spontaneous emission we only include transitions from higher energy states to lower energy states as shown in Fig. 3.8), this result can be written in the form:

$$
\dot{\rho}_{ii} = -\gamma(i-1)\tilde{\rho}_{ii} + \gamma \sum_{k=i+1}^{N} \tilde{\rho}_{kk}.
\tag{3.12}
$$

Similarly, one can obtain evolution equations for the off-diagonal density matrix terms:

$$
\dot{\rho}_{ij} = -\frac{\gamma}{2}(i+j-2)\tilde{\rho}_{ij}.
\tag{3.13}
$$

An analogous calculation for the decoherence operators shows that they do not influence the diagonal elements of the density matrix:

$$
\dot{\rho}_{ii} = 0
\tag{3.14}
$$

49

and the off-diagonal terms are modified similarly as in the case of spontaneous emission:

$$\dot{\rho_{ij}} = -\frac{\gamma}{2}(i+j-2)\tilde{\rho}_{ij}. \tag{3.15}$$

If we restrict ourselves to the case of undoped or weakly doped flakes, we can assume that the majority of the dynamics happens around the HOMO-LUMO gap, hence the important case is $i, j \approx \frac{N}{2}$. If the flake is sufficiently large we have $i, j \gg 1$ and therefore $i + j - 2 \approx i + j \approx N$. The diagonal elements above the LUMO state are most likely not occupied. Then, we can approximate Eq. 3.12 with:

$$\dot{\rho_{ii}} = -\frac{N\gamma}{2}\tilde{\rho}_{ii} \tag{3.16}$$

and Eq. 3.13 gives approximately:

$$\dot{\rho_{ij}} = -\frac{N\gamma}{2}\tilde{\rho}_{ij}. \tag{3.17}$$

From the comparison of Eqs. 3.10 and 3.16 one can then find the relation between τ and γ:

$$\tau = \frac{1}{N\gamma}. \tag{3.18}$$

In general, we expect similar evolution from the phenomenological and Lindblad approaches if we set the rates τ and γ, such that they satisfy Eq. 3.18.

Note that the number N is limited by the coherence length l_{coh} in graphene. In low temperatures, $l_{\text{coh}} \sim 1\mu\text{m}$ [70, 71]. Only atoms which are located in the area πl_{coh}^2 contribute here, such that the number of atoms contributing to the emission $N_{\text{coh}} \propto \pi l_{\text{coh}}^2$. Assuming that the transition rate in bulk is a sum of the contributions on particular atoms, we get that the emission rate on one atom $\gamma_{\text{at}} = \gamma/N_{\text{coh}}$. These single atom contributions sum up to the collective decoherence rate γ in bulk. In smaller flakes with sizes below πl_{coh}^2, where $N \ll N_{\text{coh}}$, the value of τ should be then rescaled linearly with the number of atoms N/N_{coh}.

Now we will verify formula 3.18 for small flakes prepared in a state with the HOMO-LUMO transition excited (i.e. one electron transferred from HOMO to LUMO as compared to the ground state). We investigate the spontaneous emission and decoherence by changing corresponding γ values. The decoherence rate is given relatively to the

spontaneous emission rate. In Fig. 3.9 the results obtained numerically from the phenomenological dissipation method are compared to results obtained using the adjusted Lindblad dissipation. The difference between two evolutions was estimated using the following formula:

$$\Delta = \frac{1}{T} \sum_{t_m} \sum_i |\rho_{ii,Lindblad}(t_m) - \rho_{ii,phenom.}(t_m)| \cdot (t_{m+1} - t_m), \quad (3.19)$$
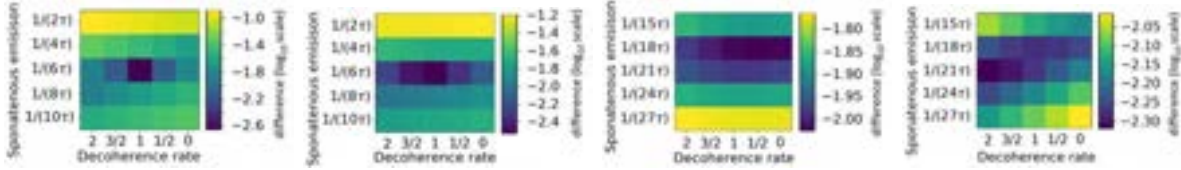
where t_m denotes the m-th time step and T the total propagation time.

Figure 3.9: The plots show the difference between the phenomenological dissipation and the Lindblad dissipation calculated from the occupations in the energy basis (left panel) and in the site basis (right panel). In subfigures a) and b) the results are shown for a 6-atom flake - benzene ring. In subfigures c) and d) the results are shown for a 18-atom flake. The decoherence rate is given relative to the chosen spontaneous emission rate (so decoherence rate = 1 means decoherence rate is the same as the spontaneous emission rate).

One can see that the best γ value to reproduce the phenomenological evolution for a benzene ring lies around $\frac{1}{6\tau}$ (Fig. 3.9), which would agree with the prediction in Eq. 3.18. Similarly, for the flake which contains 18 atoms, the optimal γ seems to lie in the range $\frac{1}{18\tau}$ - $\frac{1}{21\tau}$. This relation does not depend on the choice of τ. In this way we have verified that formula 3.18 provides a fair estimate of the relation between γ and τ also for small flakes. The assessments made in this section confirm the intuitions that decoherence rates are smaller in smaller systems and gives an idea about their orders of magnitude.

3.5 Absorption spectra

At this stage we are able to calculate absorption spectra of graphene nanoflakes. This is of high importance, since the absorption spectrum is a quantity which can be directly measured in experiments. There are two ways in which we can calculate the absorption spectrum of a graphene nanoflake:

1. Based on the possible transitions between eigenstates [72, 73]:

$$\sigma^{\text{nonint}}(\omega) \propto \sum_{if} (E_f - E_i) \, |\, \langle f| \, \mathbf{r} \, |i\rangle \,|^2 \, \delta \left(E_f - E_i - \hbar\omega \right), \qquad (3.20)$$

where $(E_f - E_i) \,|\, \langle f| \, \mathbf{r} \, |i\rangle \,|^2$ is the oscillator strength of the transition from state $|i\rangle$ to $|f\rangle$ and the summation goes over indices $i \in [1, \#\text{HOMO}]$ and $f \in [\#\text{LUMO}, N]$. This method neglects the Coulomb interactions in the system, therefore σ^{nonint} is also called the *non-interacting* absorption cross-section.

2. By illuminating the structure with a short spectrally broad pulse $\mathbf{E}(t) = E(t)\hat{e}_i$ ($i \in [x, y]$). In the extreme case of $\mathbf{E}(t) \sim \delta(t)$ this corresponds to exciting the nanoflake with all possible frequencies simultaneously. Then one can record the resulting dipole moment $\mathbf{P}(t)$ and after taking the Fourier transform of $\mathbf{E}(t)$ and $\mathbf{P}(t)$ calculate the frequency-dependent polarizabilities $\alpha_{i,j}(\omega)$ according to [74]:

$$\alpha_{i,j}(\omega) = \frac{P_i(\omega)}{E_j(\omega)}, \qquad (3.21)$$

where $i, j \in [x, y]$. The absorption cross-section is then proportional to:

$$\sigma_j^{\text{int}}(\omega) \propto \omega \operatorname{Im} \left(\alpha_{x,j}(\omega) + \alpha_{y,j}(\omega) \right). \qquad (3.22)$$

The numerical implementation of these equations has been performed by our co-workers from the Institute of Theoretical Solid State Physics at Karlsruhe Institute of Technology (special thanks to prof. Carsten Rockstuhl and to Marvin Müller). The analysis of absorption spectra has proven to be an important tool for classifying resonances in nanostructures. The framework which is presented in this section has been used to explore the problem of distinguishing between plasmonic (or more generally interaction-mediated) and single-particle-like resonances in graphene nanostructures. It has been an important tool in the creation of the energy-based plasmonicity index, which is one of the measures for resonance classification in nanostructures. More details on this subject can be found in Refs. 40, 75.

Figure 3.10 presents the absorption spectra for triangular graphene nanoflakes of varying size. Both for armchair- and zigzag-edged flake we observe that as the size of the nanoflake grows, the energies of its resonant absorption peaks decrease and their intensity increases. This result is in agreement with the energy plots presented in Figs. 3.3 and 3.4.
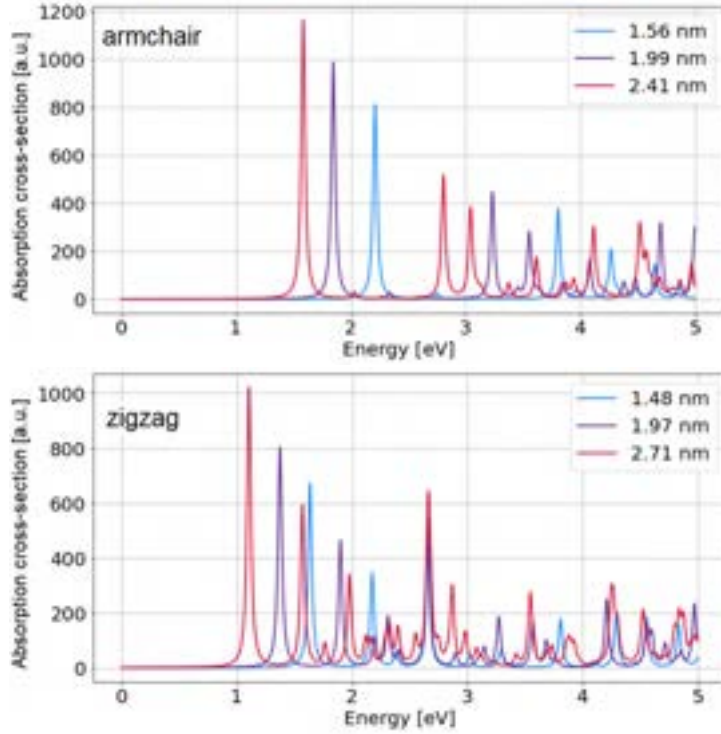
Figure 3.10: Exemplary non-interacting absorption spectra for triangular graphene nanoflakes of various sizes and edge-type character. Upper panel: armchair-edged nanoflakes. Lower panel: zigzag-edged nanoflakes.

In the non-interacting approach, the absorption peaks correspond to transitions between pairs of eigenstates, therefore the decreasing energy gap around the Fermi level directly leads to lower resonant energies in larger flakes. Figure 3.11 presents a comparison of the interacting and non-interacting spectrum for a triangular armchair-edge graphene nanoflake with 18 atoms (size 0.71 nm). The left subfigure shows the interacting spectrum, which takes into account Coulomb interactions in the system, and the non-interacting spectrum, in which the Coulomb interaction is neglected. The relation between these two spectra is explained in the right subfigure. It shows how the absorption spectra vary as the Coulomb interaction strength in the system is gradually scaled by a factor in the range from 0 to 1. This reveals a continuous transition from the non-interacting (scaling factor = 0) to the interacting (scaling factor = 1) case.
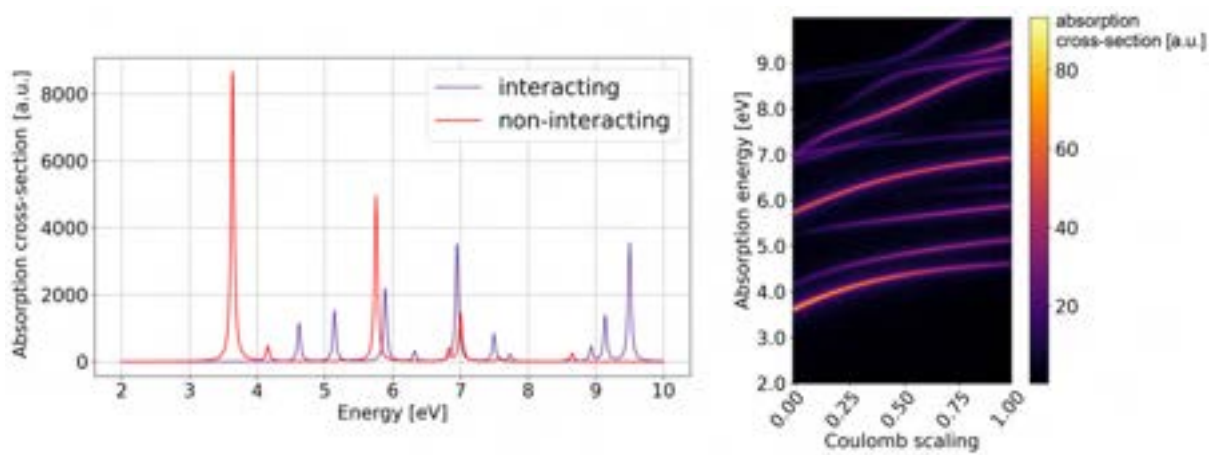
Figure 3.11: Absorption spectra for an 18-atom triangular graphene nanoflake. Left: Comparison of interacting and non-interacting absorption spectrum. Right: Absorption spectra in the function of Coulomb interaction strength in the system. The Coulomb interaction here is continuously scaled from 0 (which corresponds to a non-interacting spectrum) to 1 (interacting spectrum).

Chapter 4

Properties of graphene nanoflakes with adatoms

The most general form of our model describes the dynamics of a graphene nanoflake with an adatom, illuminated with external electromagnetic field. In this Section, we will follow a similar path as in Chapter 3, this time concentrating on how to incorporate the adatom (modelled as a two-level system) into our framework. We start with the tight-binding Hamiltonian of the hybrid system consisting of the flake and the adatom. The adatom introduces charge inhomogeneity and modifies Coulomb forces in the system, which proves the self-consistency procedure especially useful in this case. After including the external illumination in the Hamiltonian, we look closely at the time evolution, exploring both processes in the two-level system, such as Rabi oscillations and spontaneous emission, and properties of the entire system, like absorption spectra and their dependence on the adatom position.

4.1   Hamiltonian of graphene nanoflakes with adatoms

The field-independent part of the Hamiltonian

$$H_{TB} = -t \sum_{\langle l,l' \rangle} \left(|l\rangle \langle l'| + |l'\rangle \langle l| \right) + \sum_{\alpha} E_{\alpha} |\alpha\rangle \langle \alpha| + \sum_{\alpha,l} t_{\alpha,l} \left(|l\rangle \langle \alpha| + |\alpha\rangle \langle l| \right) \qquad (4.1)$$

is constructed in the tight-binding approximation, similarly as in Chapter 3 for stand-alone graphene nanoflakes. Again, we assume that an electron can be exchanged between nearest carbon-atom neighbours with the rate t and $\langle l, l' \rangle$ means summation over nearest

neighbour atomic sites l and l'. The adatom introduces several orbitals labelled by α, whose energies E_α are evaluated with respect to the on-site energy in graphene, e.g., by comparison of ionisation energies in graphene and of a given atom orbital. Electrons can be exchanged between the adatom orbitals and selected flake sites, and the corresponding hopping rate is denoted as $t_{\alpha,l}$. We keep $t = 2.66\,\text{eV}$ as the hopping parameter between the neighbouring sites in graphene. We consider adatoms bonded to graphene in the *top* position, as shown in Fig. 1.8.

The hopping rates between the adatom orbitals and carbon sites $t_{\alpha,l}$ generally depend on the adatom parameters. We leave these parameters unspecified in order to keep the approach general and characterise the scope of possible physical effects achievable within the model, rather than investigate specific adatoms. However, in the next section we investigate the relation of the hopping rates with the distance to the coupling site, to provide intuitions about the orders of magnitude for relevant distances. Adatom - flake hopping rates set to zero $t_{\alpha,l} = 0$ correspond to an infinite distance and the absence of coupling.

4.2   Relation of model parameters and adatom distance

Throughout this thesis, we do not specify the adatom type exactly but rather study the scaling of effects with the hopping parameters between its energy levels and the graphene flake. Here, we provide an estimate of adatom distances to the coupling site of the graphene flake that correspond to given hopping rates.

If we take pristine graphene and shift one particular carbon atom by some distance, we can model the hopping rate value as following a quadratic relation of the form: $t' = t \cdot (a_{cc}/l)^2$, where t' is the hopping rate between the shifted atom and its nearest neighbour, a_{cc} is the carbon-carbon distance in graphene (which is related to the lattice constant as $a_{cc} = \dfrac{a}{\sqrt{3}} \approx 1.42\text{Å}$) and l is the distance from the shifted atom to the nearest carbon atom in the modified lattice [76].

We assume that the hopping rates between the graphene sites and the adatom states follow a similar relation which is a good approximation for small distances. This allows
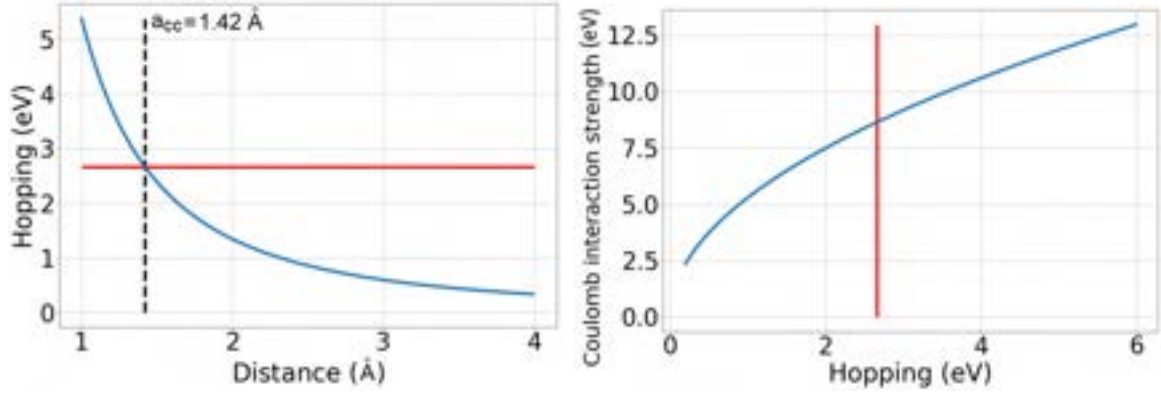
Figure 4.1: Left: Hopping rate t_α between the adatom and the nearest graphene site as a function of the distance between them. Right: Coulomb interaction between the adatom and the nearest graphene site as a function of the hopping rate. The black dashed line is located at the distance between nearest atoms in graphene (at $a_{cc} = 2.46\,\text{Å}/\sqrt{3} \approx 1.42\,\text{Å}$). The red lines are located at the hopping rate for pristine graphene: $t = 2.66\,\text{eV}$. Here, we assume the adatom has carbon-type orbitals, i.e. $\beta = 1$ and $a = a_{cc}$.

us to estimate the distance between the adatom and flake based on the hopping value:

$$l = \beta a \sqrt{\frac{t}{t_\alpha}}, \tag{4.2}$$

where a is the distance, at which the hopping parameter $t_\alpha = t$ for a carbon atom and β is a constant, which accounts for the choice of a different adatom type than carbon, in particular with a different orbital type than p_z. For carbon $\beta = 1$. The left panel in Fig. 4.1 shows the relation of the distance l to the hopping parameter t_α for an adatom with carbon-like orbitals, such that $\beta = 1$ and $a = a_{cc}$.

4.3 Coulomb interaction on the adatom

Since the Coulomb interaction is inversely proportional to distance, it depends on the hopping rate t_α in the following way: $v \propto \frac{1}{a_{cc}}\sqrt{\frac{t_\alpha}{t}}$. We include the Coulomb interaction modification in the matrix v by scaling the elements corresponding to the adatom sites by a coupling-dependent term:

$$v_{\alpha l} = \frac{v_{nn}}{\beta}\sqrt{\frac{t_\alpha}{t}}, \tag{4.3}$$

where $e^2 v_{nn} = 8.64\,\text{eV}$ denotes the equilibrium Coulomb interaction value for nearest neighbours in graphene [66]. The resulting relation of the coupling constant t_α on distance

57

and its relation with the Coulomb interaction strength is shown in the right panel of Fig. 4.1.

Another noteworthy fact is that the adatom introduces two sites at the exact same location. So the *on-site* influence on these sites should arise from both of them, contrary to the situation on the rest of the flake where the *on-site* element only arises from one site. Therefore, on the diagonal of v, we impose the *on-site* value $e^2 v_{\mathrm{os}} = 16.52\,\mathrm{eV}$ [66] on the entire 2×2 part which corresponds to the adatom sites, s.t. $v_{gg} = v_{ee} = v_{eg} = v_{ge} = v_{\mathrm{os}}$.

Note that the proposed scaling guarantees that the Coulomb interaction between the adatom and a graphene flake disappears as the flake is moved to infinity (i.e. when $t_\alpha \longrightarrow 0$).

4.4   Energy spectra of nanoflakes with adatoms

In this section, we look at the possible energies of graphene nanoflakes with adatoms. We also investigate how the energy spectra change while the flake and the adatom are coupled to each other with increasing coupling strength. We focus on armchair-edged triangular nanoflakes and adatoms with two energy levels: an excited state with energy $E_e = 0.5\,\mathrm{eV}$ and a ground state with energy $E_g = -0.5\,\mathrm{eV}$.

Knowing the Coulomb interaction between the adatom and the flake, we can now proceed to perform the self-consistent procedure described in 3.2, which gives us a new dressed basis set, that includes the initial Coulomb interaction. Note that the Coulomb interaction values on the adatom need to be modified accordingly, as described in the previous section. The resulting energy spectra and real-space charge distributions are shown in Figs. 4.2, 4.4 and 4.5. In Fig. 4.2 we present the dependence of the energy spectra on the hopping parameters t_e, t_g (here assumed to be equal) for two different nanoflakes. As expected, we can explicitly see that the eigenstates of the nanoflake which mix with the adatom eigenstates most strongly are also the ones which change their energies the most when we increasingly couple the adatom to the nanoflake. Moreover, the same figure shows that the presence of a strongly coupled adatom can produce states that have energies outside of the $[-8, 8]$ eV range. Shifting up or down the excited and ground adatom levels breaks the electron-hole symmetry in the energy spectrum of the system, as shown in Fig. 4.3. In particular, the energy differences between the energy

levels are not symmetric around the zero energy anymore. This causes a splitting of the originally degenerate peaks in the optical absorption spectrum, leading to a more complex optical response. For the zig-zag triangle and an adatom with symmetrical energy levels ± 0.5 eV, there are two degenerate eigenstates corresponding to the energy 0 eV that do not move with increasing t_e and t_g. One of these states, however, couples to the adatom, whereas the other does not, hence the multi-coloured line at 0 eV. When the adatom energies are not symmetrical around zero, the degeneracy of these states is lifted. Then, one of the zero-energy states lowers its energy with increasing coupling to the adatom and the other remains in place.

In Fig 4.4 we can see that a pristine graphene flake has uniform charge distribution. As expected, when the coupling between the graphene flake and adatom is increased, a higher fraction of the charge becomes exchanged between the two subsystems. The biggest perturbation is located in the vicinity of the adatom and the influence on the carbon atom located further than 1 nm away from the adatom is negligible.

In Fig. 4.5 we present energy spectra of a nanoflake with an adatom and doping. Again, the adatom has a dominant impact on atoms which are located near it. However, now the perturbation is extended across the entire nanoflake, which can be clearly seen in the case of 30 doping electrons. Although the adatom adds only one new electron into the system, the symmetry breaking is enough to affect the charge distribution in the entire nanoflake.
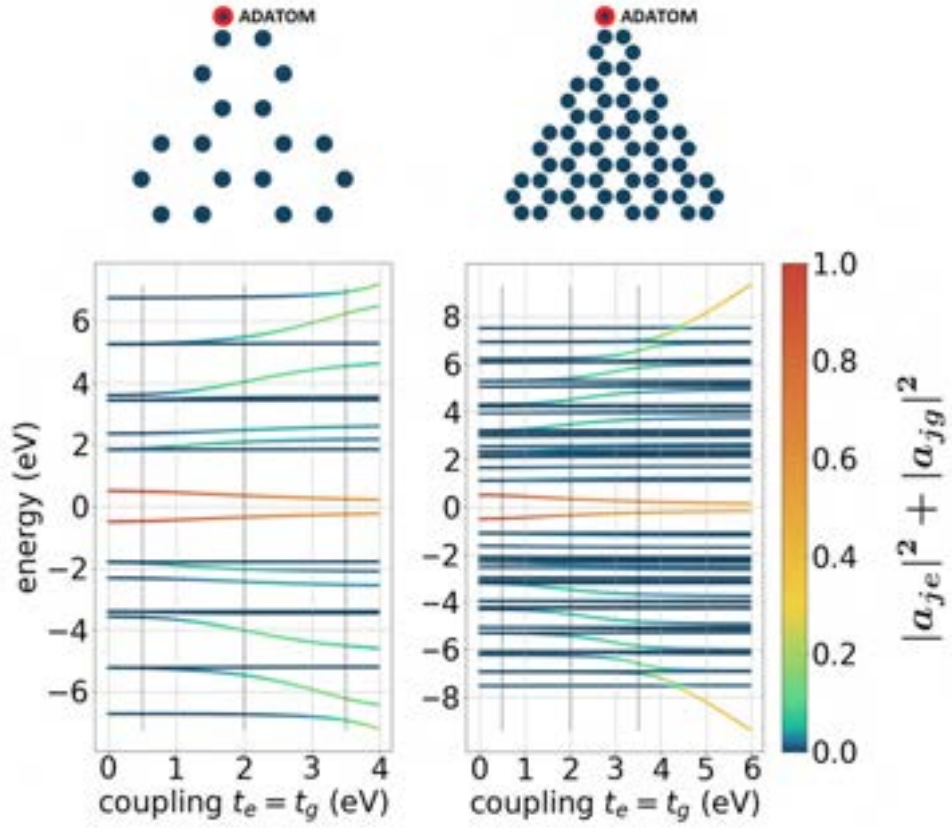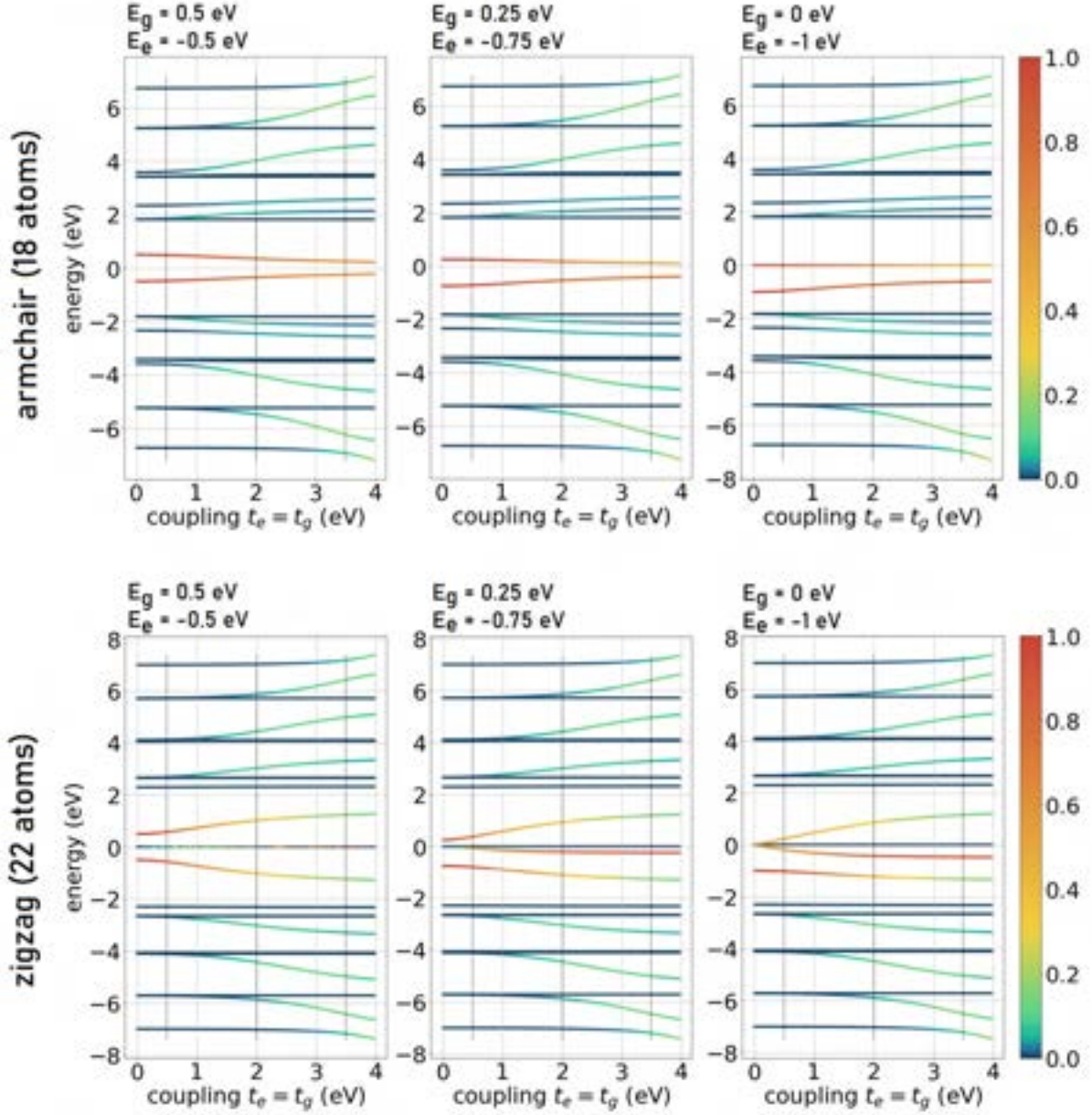
Figure 4.2: Dependence of the energy spectra on the hopping parameter $t_e = t_g$ of two graphene nanoflakes, each with an adatom attached at the left top-most atom of the flake. Left: 18-atom flake (size 0.71 nm), right: 60-atom flake (1.56 nm). The adatom has levels $\pm 0.5\,\text{eV}$. The line colour indicates the population of a given eigenstate localised on the adatom in real space: $C_j = |a_{je}|^2 + |a_{jg}|^2$, where e and g denote the excited and ground adatom sites, and a_{jl} is defined *via* Eq. 3.3.

Figure 4.3: Dependence of the energy spectra on the hopping parameter $t_e = t_g$ of two graphene nanoflakes, each with an adatom attached at the left top-most atom of the flake. Upper row: 18-atom armchair-edge flake (size 0.71 nm), lower row: 22-atom zigzag-edge flake (0.74 nm). The adatom level energies are given in the top left corner of each subfigure. The line colour indicates the population of a given eigenstate localised on the adatom in real space: $C_j = |a_{je}|^2 + |a_{jg}|^2$, where e and g denote the excited and ground adatom sites, and a_{jl} is defined *via* Eq. 3.3.
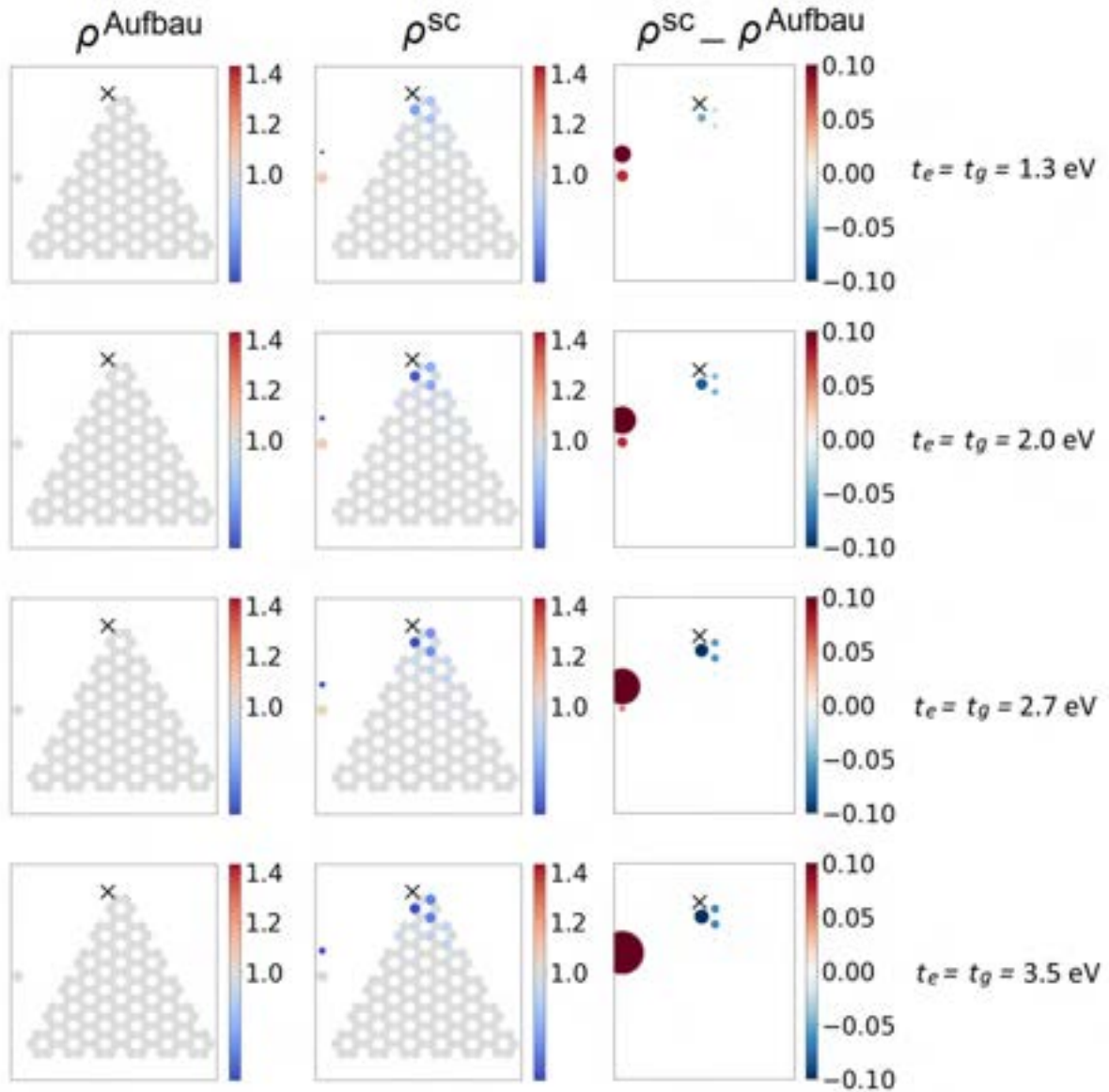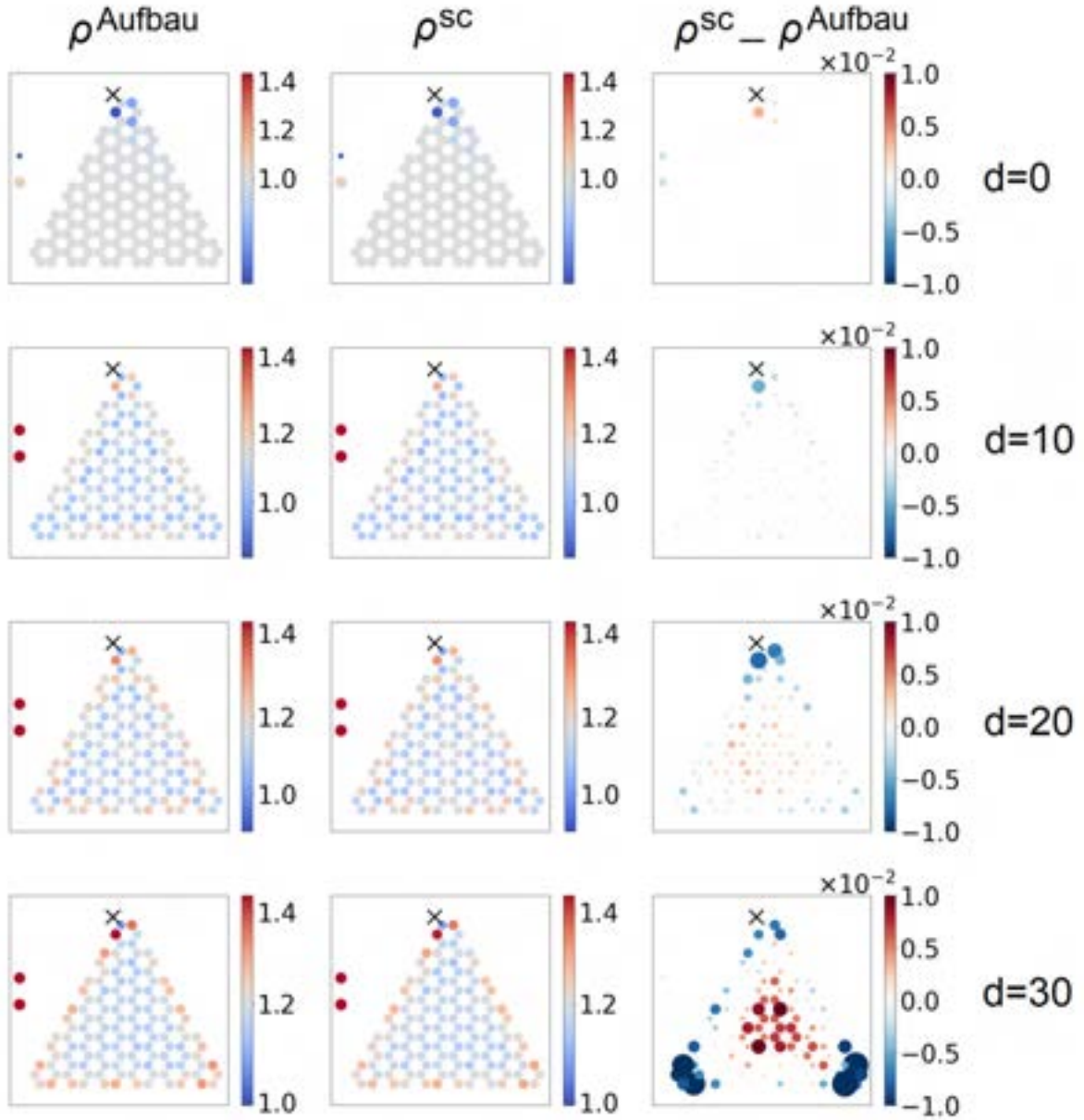
Figure 4.4: Real-space charge distribution in a triangular graphene flake of size 2.41 nm with an adatom attached at the top of the flake and coupled with increasing strength: before the self-consistency (left), after the self-consistency (middle) and the difference $\rho^{\mathrm{sc}} - \rho^{\mathrm{Aufbau}}$ (right). The charge on the adatom is presented on the left side next to the flake: the lower dot denotes the charge in the ground state, upper dot - in the excited state.

Figure 4.5: Real-space charge distribution in a triangular graphene flake of size 2.41 nm with an adatom attached at the top of the flake coupled with $t_e = t_g = 2$ eV and with additional doping of $d = 0, 10, 20, 30$ electrons: before the self-consistency (left), after the self-consistency (middle) and the difference $\rho^{\text{sc}} - \rho^{\text{Aufbau}}$ (right). The charge on the adatom is presented on the left side next to the flake: the lower dot denotes the charge in the ground state, upper dot - in the excited state.

4.5 Eigenstate symmetry breaking due to the adatom

The real-space distribution of eigenstates of a free triangular armchair-edged flake consisting of 60 atoms (1.56 nm) is presented in Fig. 4.6. Each subfigure presents one particular eigenstate ϕ_j with the energy E_j indicated in the upper-left corner. The quantity which is shown for each eigenstate ϕ_j is the absolute value of the amplitude $|a_{jl}|$ as defined in Eq. 3.3. In general, states with energies $\pm E_j$ have the same probability distribution $|a_{jl}^2|$ but the exact amplitudes a_{jl} can vary by a phase factor. In Figs. 4.6 to 4.8 the phase factor is omitted for the sake of clarity. Figures which contain the full information about the amplitude, including the sign, can be found in Appendix B (Figs. B.4- B.6).

First, let us look at eigenstates of the 60-atom nanoflake without the adatom attached. It is worth noting that not all eigenstates have threefold symmetry. Even though it might seem wrong at the first glance, it is not a problem. In fact, after a careful examination one can see that only states that correspond to degenerate energy levels do not manifest this symmetry. For any chosen energy value a superposition of corresponding eigenstates can be constructed which is symmetric with respect to 120° rotations and, therefore, no particular direction is preferred in the real world.

Locating the adatom near the flake causes a perturbation in the symmetry of the system and leads to symmetry breaking in the eigenstates. The distribution of charge in the eigenstates in real space for triangular graphene nanoflakes with a coupled adatom is shown in Figs. 4.7 and 4.8.

The adatom introduces two new eigenstates, namely the states which appear at $\pm 0.34\,\text{eV}$ for $t_e = t_g = 2\,\text{eV}$ and at $\pm 0.18\,\text{eV}$ for $t_e = t_g = 5\,\text{eV}$. These states origin at the ground and excited adatom states with energies $\pm 0.5\,\text{eV}$ at the absence of coupling and gradually hybridise with flake states as t_e and t_g increase, which correspondingly shifts their energies. These states become the new HOMO and LUMO of the system and therefore are crucial for the optical properties of the system. The states which are located directly below HOMO ($-1.11\,\text{eV}$) and directly above LUMO ($1.11\,\text{eV}$) do not couple to the adatom states and consequently, their energies remain unchanged when the adatom is present. Here, we only present visually the results for a 1.56 nm nanoflake, since the number of eigenstates is not too large and it is convenient to analyse with the bare eye. This finding, however, is a general observation which is true for HOMO-1 and LUMO+1 states in graphene nanoflakes of various sizes and shapes.
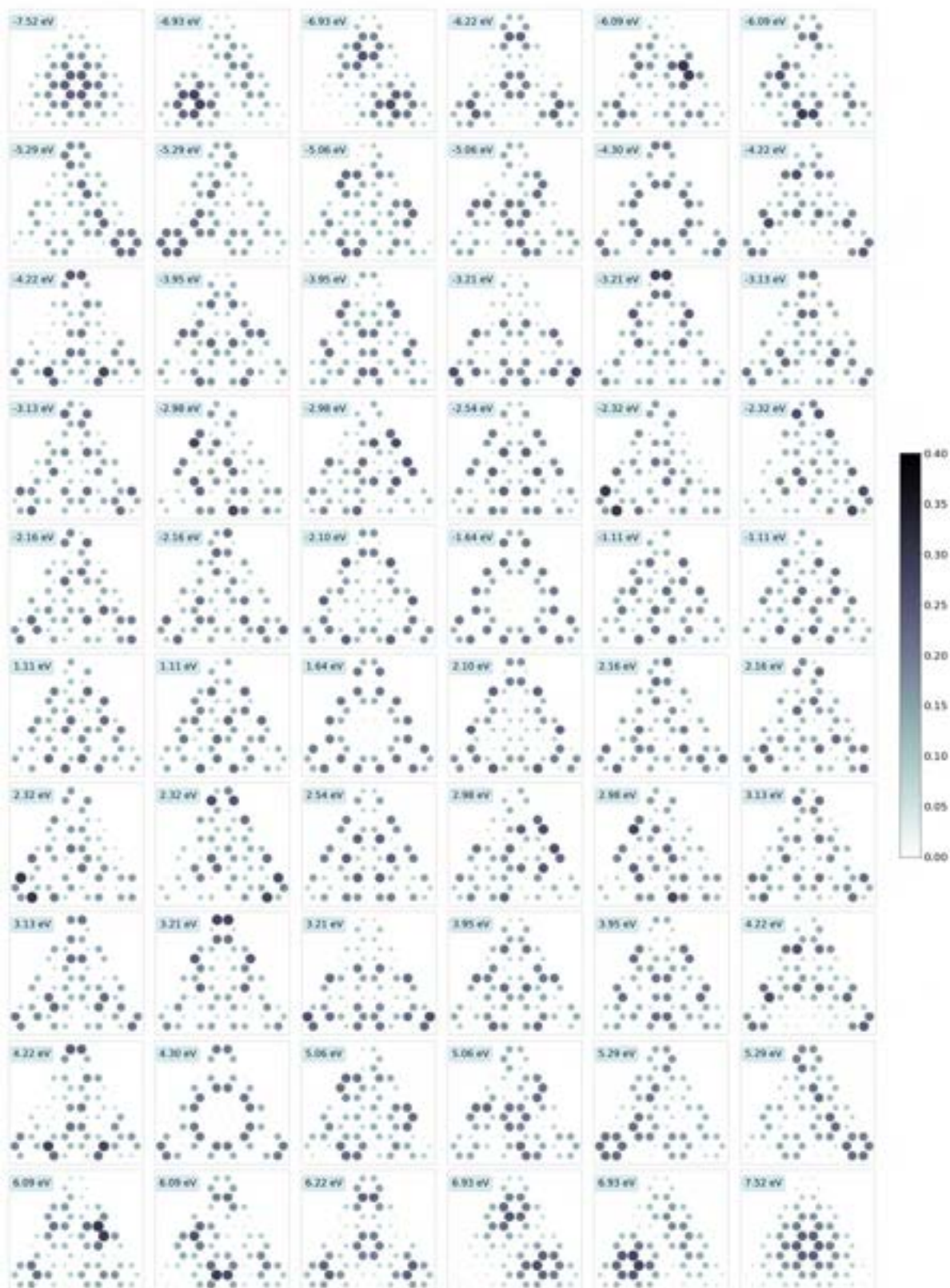
64

Figure 4.6: Distribution on sites in real space of eigenstates of a solo 60-atom (1.56 nm) triangular graphene nanoflake.
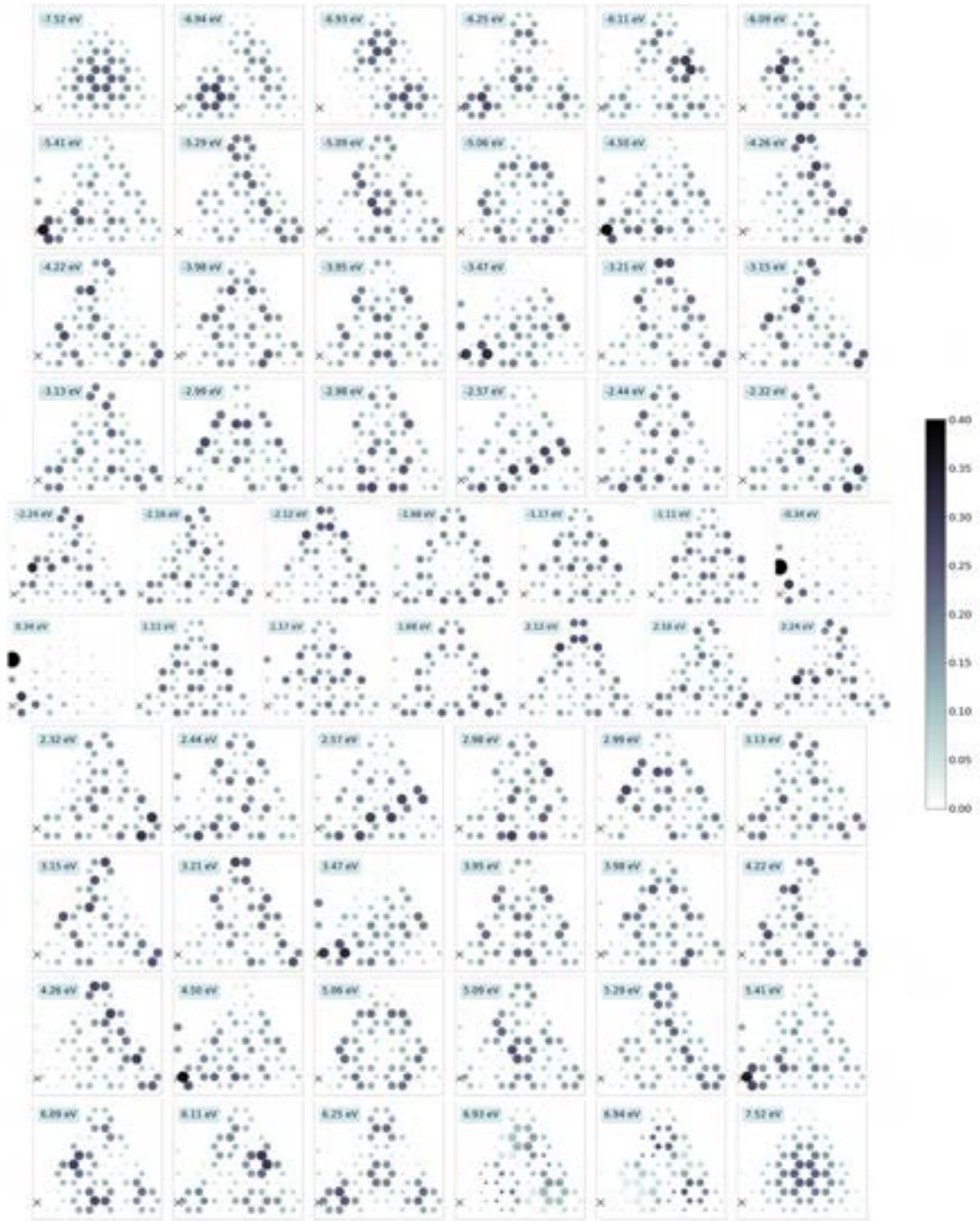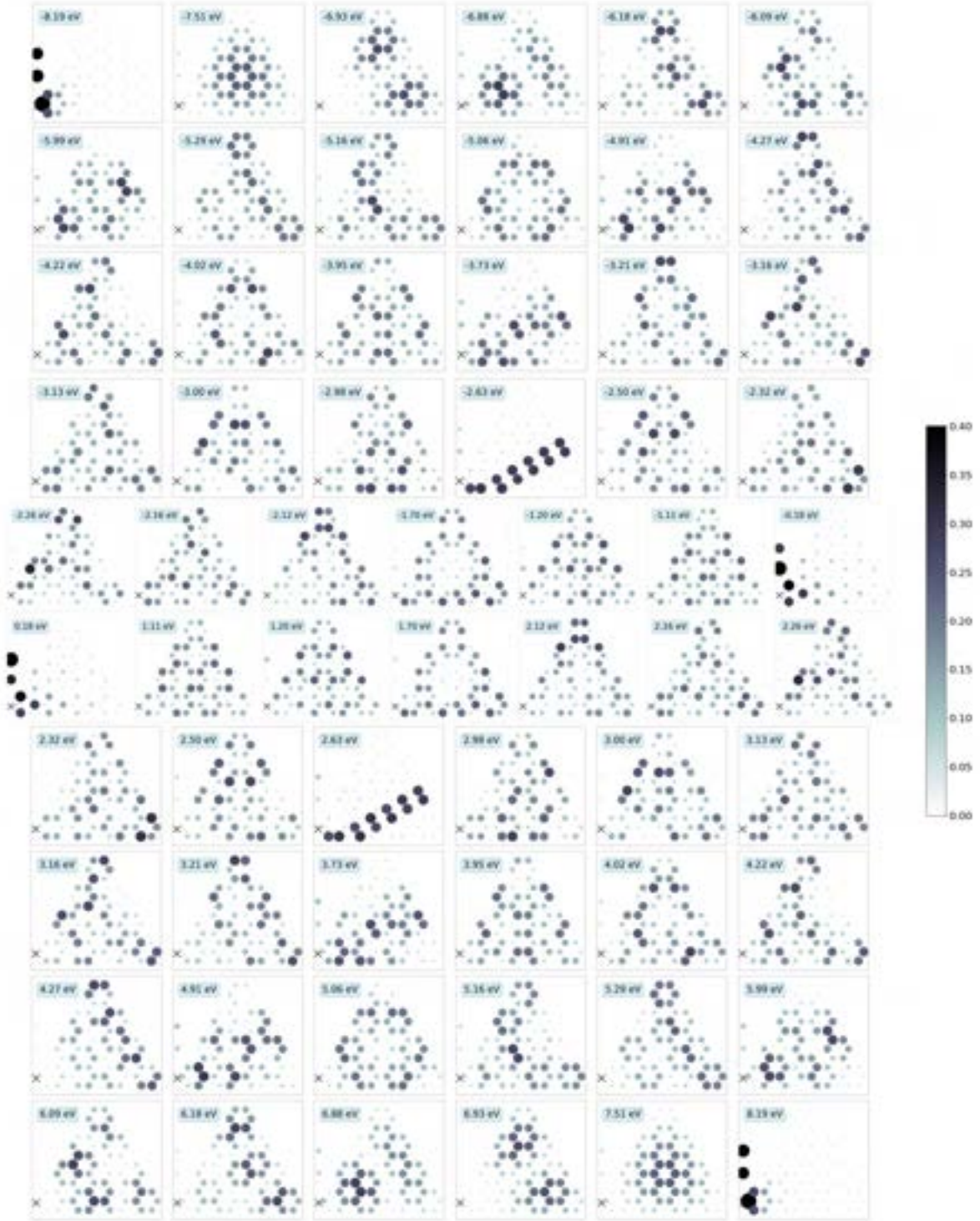
Figure 4.7: Distribution on sites in real space of eigenstates of a 60-atom (1.56 nm) armchair-edged triangular graphene nanoflake with an adatom attached in the lower-left corner of the nanoflake (location denoted with an X mark) with coupling strengths $t_e = t_g = 2\,\text{eV}$. The phase factor is neglected for clarity.

Figure 4.8: Distribution on sites in real space of eigenstates of a 60-atom (1.56 nm) armchair-edged triangular graphene nanoflake with an adatom attached in the lower-left corner of the nanoflake (location denoted with an X mark) with coupling strengths $t_e = t_g = 5$ eV. The phase factor is neglected for clarity.

We can also note that in the states which are initially degenerate attaching the adatom

causes one state of the pair to couple to the adatom states and change its energy, while the other state remains unaffected. Hence, attaching the adatom lifts the degeneracy of states. States which in the solo graphene flake correspond to degenerate energy values and can be combined to form three-fold symmetric states with the adatom become non-degenerate states with approximate two-fold symmetry, e.g. for the case of the coupling strength $t_e = t_g = 2\,\mathrm{eV}$ the states at $\pm 5.41\,\mathrm{eV}$, $\pm 5.29\,\mathrm{eV}$ and $\pm 2.32\,\mathrm{eV}$. This finding is also true in zigzag-edged nanoflakes. Moreover, the investigation of zigzag-edged flakes suggests that when there are multiply degenerate states (more than two eigenstates per energy), still only one eigenstate couples to the adatom states and the other states remain unchanged (see Figs. B.1, B.2 and B.3 in Appendix B).

4.6   Including external illumination

The external electric field is coupled to the nanoflake, similarly as in Chapter 3:

$$H\left(\rho(t),t\right) = H_{\mathrm{TB}} - e\Phi_{\mathrm{charge}} - e\Phi(t) = H_{\mathrm{TB}} - e\Phi_{\mathrm{charge}} + \left[H^{\mathrm{ext}}(t) - e\Phi^{\mathrm{ind}}(t)\right]. \quad (4.4)$$

Here,

$$H^{\mathrm{ext}}(t) = -\sum_{L} e\,\mathbf{r}_L \cdot \mathbf{E}(\mathbf{r},t)\,|L\rangle\langle L| - \mathbf{d}_{eg} \cdot \mathbf{E}(\mathbf{r},t)\left(|e\rangle\langle g| + |g\rangle\langle e|\right) \quad (4.5)$$

is the energy of the external field that arises due to the illumination with an electric field $\mathbf{E}(\mathbf{r},t)$ assumed to be polarised in the plane of the graphene flake. The capital letter L denotes a joint summation index $L = \{l, \alpha\}$ going over the carbon sites l and over the adatom orbitals α. The graphene flake and the adatom are treated at the same level of approximation. We explicitly take the flake's spatial structure into account through the summation over the sites. Each carbon atom site is, however, approximated as a point, and so is the adatom. The internal structure of the adatom is taken into account through the transition dipole moment operator $\mathbf{d}_{eg}$. The last Hamiltonian term describes transitions induced by the external field between the ground and excited states of the adatom.

As the electric field moves the electrons away from their equilibrium positions, Coulomb interactions arise which are accounted for by the field-induced potential:

$$\Phi^{\mathrm{ind}}_{KL}(t) = -eN_e\delta_{KL}\sum_{L}v_{LL'}\left(\rho_{L'L'}(t) - \rho^{\mathrm{sc}}_{L'L'}\right), \quad (4.6)$$

x-polarized external illumination
$\log_{10}(|E_{\text{ind},x}|/|E_0|)$ $\log_{10}(|E_{\text{ind},y}|/|E_0|)$

y-polarized external illumination
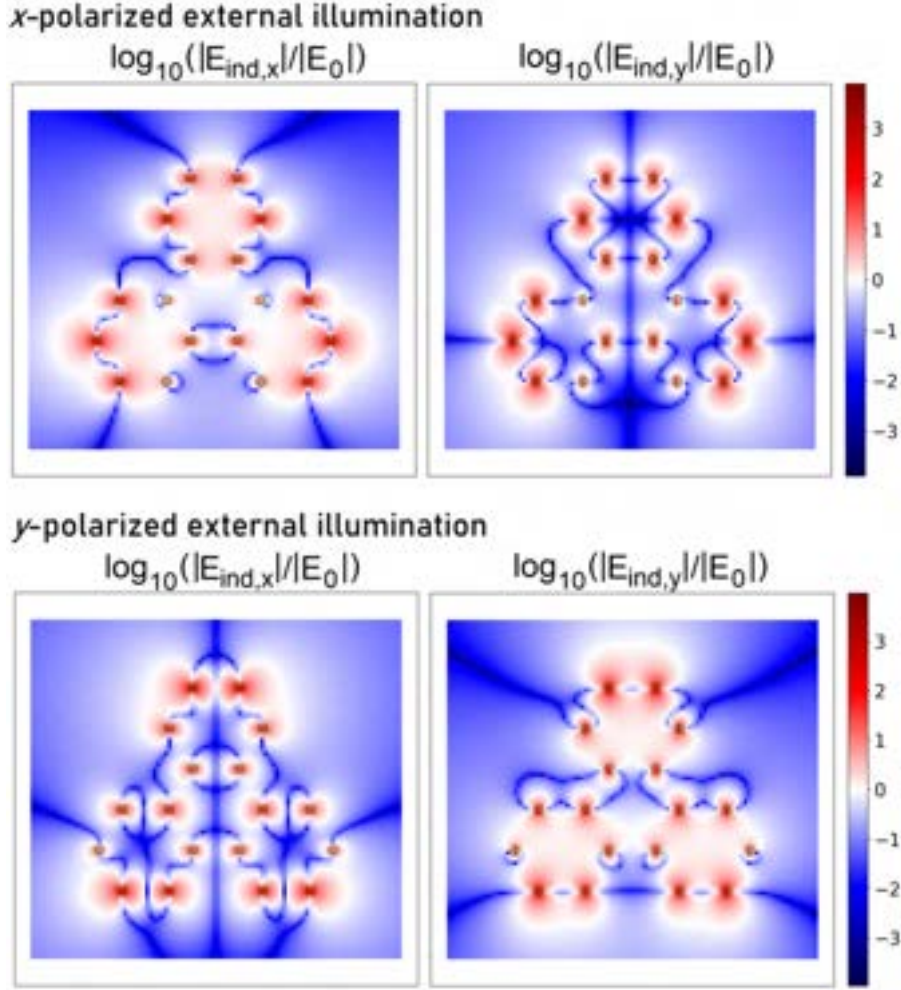$\log_{10}(|E_{\text{ind},x}|/|E_0|)$ $\log_{10}(|E_{\text{ind},y}|/|E_0|)$

Figure 4.9: Distribution of the x-components (left) and y-components (right) of the electric field that is induced around an 18-atom graphene nanoflake due to an external illumination polarised either in x-direction (upper panels) or in y-direction (lower panels). The locations of graphene sites are marked in the figures as thin green circles.

where the summation goes over the all carbon and adatom sites $L = \{l, \alpha\}$.

Finally, we add to our Hamiltonian a term coming from the fact that when the external electromagnetic field excites the electronic charge density, the electrons respond by oscillating and thus generate an induced electric field [77]:

$$\mathbf{E}_{\text{ind}}(t, \mathbf{r}) = \frac{1}{4\pi\epsilon_0} \sum_{l \in \text{flake}} \frac{Q_l(t)(\mathbf{r}_l - \mathbf{r})}{|\mathbf{r}_l - \mathbf{r}|^3}, \tag{4.7}$$

where $Q_l(t) = N_e \left(\rho_{ll}(t) - \rho_{ll}^{\text{sc}} \right)$ is the charge induced on the l-th site at time t. This field is added to the illumination in the Hamiltonian.

Depending on the location of the adatom with respect to the flake, the induced field can either enhance the effect of the external field or be opposite in phase and reduce

its impact. The distributions of the induced fields for an 18-atom graphene nanoflake illuminated at the frequency 1 eV are shown in Fig. 4.9. The colorbar is centred such that white colour indicates spots where the induced field is equal in amplitude to the external field, and blue regions show where the induced field is weaker than the external one. The induced field dominates the external field in the red and pink regions, i.e. at distances up to 3 Å from the flake. The dominant component of the induced field is always the one whose orientation is in agreement with the external field orientation. However, since we show the near field, also the perpendicular component of the induced field is present.

4.7   Time evolution

The local enhancement of the electromagnetic field around nanostructures, such as graphene nanoflakes, produces extremely strong light-matter interactions, on the order of hundreds of THz. Because of this, placing a two-level system near a graphene nanoflake will greatly enhance the intensity of its spontaneous emission. This is an optical channel for the interaction of the graphene flake with an adatom. On the other hand, the extreme electromagnetic fields are strongly localised and the emitter has to be located at a very small distance from the nanoflake to experience the effects of its presence. At distances below 0.5 nm the tunnelling effects become important [78], meaning the hopping of electrons t_α between subsystems has to be taken into account. In this Section, we explore the impact of the electron hopping effect between the adatom and the nanoflake on coherent (Rabi oscillations) and incoherent (spontaneous emission) processes in the two-level system, and compare it to the influence of the optical mechanism.

4.7.1   Modification of Rabi oscillations

We will apply the formalism presented above to the case of a single two-level adatom coupled to a selected site of a graphene flake, illuminated with an external laser beam. First, we study how the coherent Rabi oscillations between the adatom eigenstates are modified by the presence of the carbon flake. The time evolution of the density matrix is again described via the master equation 3.7 similarly as in Section 3.4. In this section, we focus only on reversible Hamiltonian dynamics, assuming that there is no dissipation,

i.e. $\mathcal{D}\left[\rho(t)\right] = 0$.

One of the canonical systems discussed in quantum optics is an atomic two-level system subject to external illumination. Its population undergoes sinusoidal Rabi oscillations between the ground and excited states, as described in Chapter 2. The population oscillation amplitude is equal to 1 in the case of resonance, and the oscillation frequency (called Rabi frequency) reads as $\Omega = \dfrac{1}{\hbar}\mathbf{E} \cdot \mathbf{d}_{eg}$, where $\mathbf{E}$ is the external and induced field amplitude at the position of the two-level system and $\mathbf{d}_{eg}$ is the transition dipole moment between the ground and excited adatom states. Below we study how the generic Rabi oscillations are modified for different coupling strengths between the adatom and the flake. We focus on armchair-edged triangular nanoflakes of sizes 0.71 nm and 2.41 nm, respectively with 18 and 126 carbon atoms. The adatom is a two-level system with energy states 0.5 eV and -0.5 eV and a dipole moment of 7.5 D. The value of the dipole moment has been chosen such that for moderately strong fields we can observe the Rabi oscillations happening on a similar time-scale as the dissipation in bulk graphene (which happens with a lifetime $\tau = 100\ \hbar/\mathrm{eV}$). We assume for simplicity that both adatom levels are coupled to the graphene flake equally strongly, i.e. $t_e = t_g$ for all simulations presented in this section. The investigated hopping parameters t_e and t_g are in the range from 0 to 5 eV, which corresponds to distances starting from 1 Å according to the selected model (see Fig. 4.1). The external field has an amplitude of $0.05\ \frac{\mathrm{V}}{\text{Å}}$ and is vertically polarised.

Dipole moment change due to state mixing

At first, we neglect the electron-electron Coulomb interactions in the system for the sake of clarity. This allows us to see the basic effect happening in the adatom as it is coupled to the flake with increasing strength - the change of frequency of the Rabi oscillations between the HOMO and LUMO states.

For the parameters given above, we find that the stronger we couple the adatom to the graphene flake, the lower frequency of Rabi oscillations it exhibits when illuminated resonantly (Fig. 4.11). This can be explained by the fact that the dipole moment of the adatom has been set to a relatively large value. In the graphene flake, the transitions between its eigenstates have lower dipole moments, up to 5 Debye or none at all. When we move the adatom closer to the graphene flake, the eigenstates of both systems mix and the dipole moment between HOMO and LUMO states is decreased with respect to the original

dipole moment in the adatom. In Fig. 4.10 we present the change of the transition dipole moment between the HOMO and LUMO states in an 18-atom armchair-edged triangular nanoflake due to the coupling of an adatom with increasing strength. Since the Rabi frequency of oscillations depends on the transition dipole moment between the states which exchange population, it will also decrease with increasing coupling of the adatom. This is presented in Fig. 4.11. The energies of the HOMO and LUMO states in the hybrid system consisting of a nanoflake and an adatom change with increasing coupling of the adatom, as was shown in Fig. 4.2. We chose the right illumination frequency for each value of t_e and t_g, so that it is resonant to the HOMO-LUMO transition.
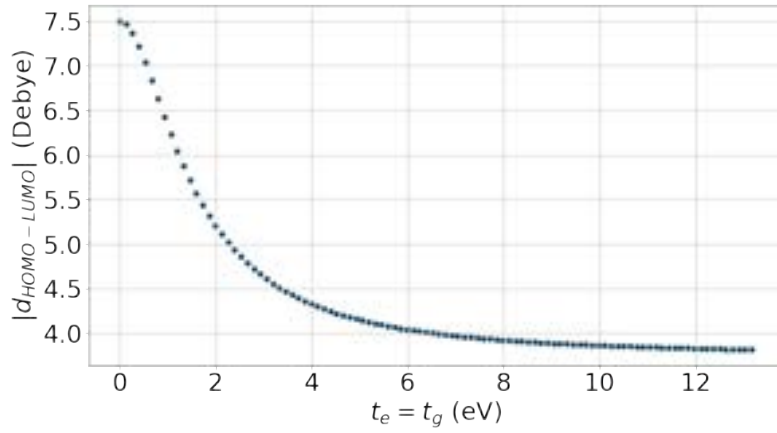
Figure 4.10: Change of the dipole moment in an 18-atom armchair-edged triangular nanoflake due to the coupling of an adatom with increasing strength $t_e = t_g$ and the resulting eigenstate mixing of both subsystems.
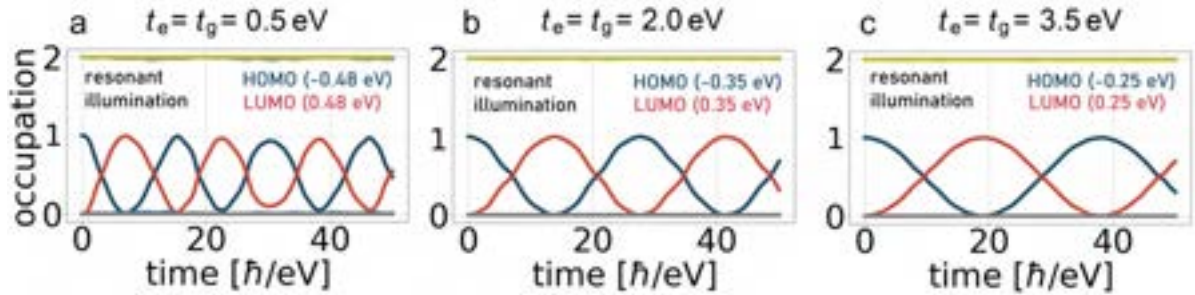

Figure 4.11: Rabi oscillations. Occupations in energy basis in an 18-atom flake with an adatom coupled with a) $t_e = t_g = 0.5\,\mathrm{eV}$ b) $t_e = t_g = 2.0\,\mathrm{eV}$ c) $t_e = t_g = 3.5\,\mathrm{eV}$. The HOMO and LUMO states exchange population. The population of other states remains nearly constant in time. Here, the Coulomb interaction is neglected. The illumination frequency is always resonant to the HOMO-LUMO transition frequency.

Now, let us fix the illumination frequency to be constant and equal to the energy difference between the ground and excited level of an uncoupled two-level system. As the adatom is increasingly coupled to the flake, the energy structure of the system is modified but the illumination frequency does not adjust to it, so that in this case detuned behaviour is expected. In fact, we observe increased Rabi frequency and lowered amplitude of oscillations, as shown in Fig. 4.12.
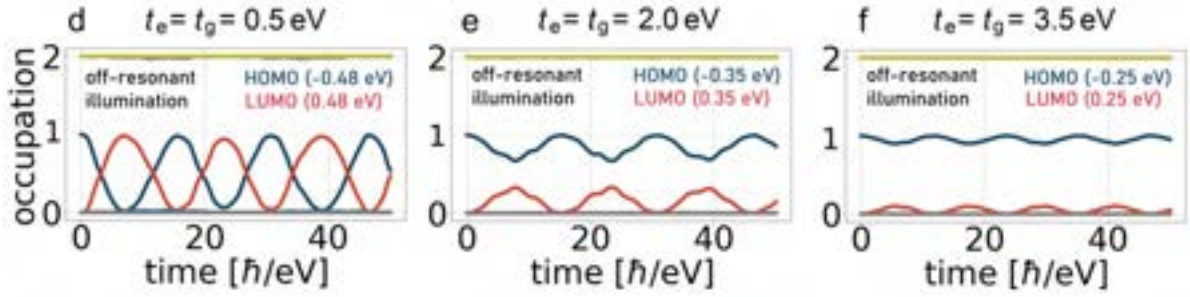

Figure 4.12: Rabi oscillations. Occupations in the energy basis in time for a 18-atom flake with an adatom coupled with a) $t_e = t_g = 0.5\,\text{eV}$ b) $t_e = t_g = 2.0\,\text{eV}$ c) $t_e = t_g = 3.5\,\text{eV}$. Here, the Coulomb interaction is neglected. The illumination frequency is fixed and equal 1 eV in each case.

Finally, we include the electron-electron interaction and look again at the time evolution of the hybrid system consisting of the triangular armchair graphene flake and the two-level adatom. The Coulomb interactions depend on time and modify the Hamiltonian differently at each timestep. Therefore, the energy levels change accordingly in time and there is no particular illumination frequency, which would be resonant to the HOMO-LUMO transition at all times. We thus expect a detuned and more irregular behaviour than without the Coulomb interactions. However, we are still able to reproduce Rabi oscillations when illuminating the system with a frequency which corresponds to the HOMO-LUMO transition in the system without any external illumination. As compared to the previous cases, these oscillations are modified by the Coulomb interaction, especially in the case of stronger coupling of the adatom (Fig. 4.13).

Change of field amplitude due to the field induced by the flake

Under external illumination, the electric charge in the flake oscillates and generates an additional induced electric field, which should be included in the time evolution. Since
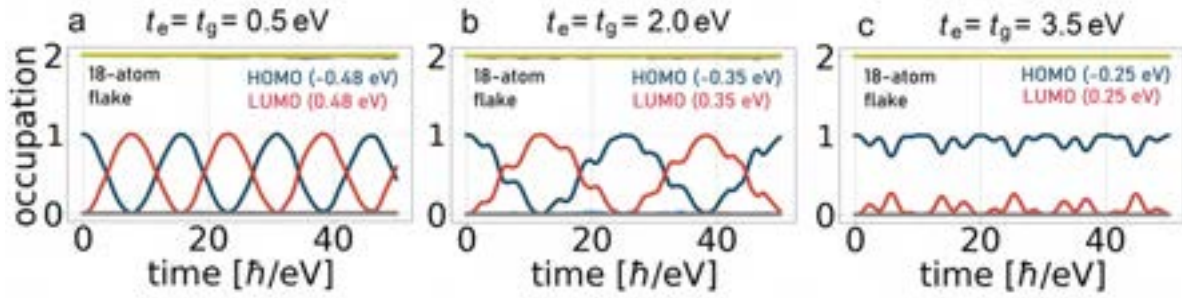
Figure 4.13: Rabi oscillations. Occupations in the energy basis in time of an 18-atom flake a) $t_e = t_g = 0.5\,\text{eV}$ b) $t_e = t_g = 2.0\,\text{eV}$ c) $t_e = t_g = 3.5\,\text{eV}$. The illumination frequency is resonant to the transition frequency between HOMO and LUMO states of the system before illumination.

the Rabi frequency depends on the field amplitude, it will change due to the change of the field amplitude by the flake. Depending on the sign of the induced field, it can either increase or decrease the Rabi frequency. For the chosen position of the adatom, the optical effect (induced field impact) is negligible compared to the effect of the electron exchange between the flake and the adatom. The effect would be stronger if one positioned the adatom in regions where the induced field is equally strong or stronger than the external field (like in the reddish regions in Fig. 4.9). However, then the evolution becomes erratic and a much smaller integration step is required to perform calculations.

Evolution in larger flakes

In general, the shift of Rabi frequency with increasing adatom coupling strength looks similarly in larger flakes. First, we look at two adatom positions - near the centre of the flake and near one corner of the flake - and find in both cases that the Rabi oscillations are distorted in a similar manner as for the 18-atom case. The dynamics in energy basis for both adatom locations and HOMO state distributions are presented in Figs. 4.14, 4.15 and 4.16.

Even though the details of the evolution are different, the three distinct cases are similar as for the smaller flakes. For small values of t_e and t_g we can see slightly modified Rabi oscillations, large values of t_e and t_g cause detuning and the evolution in the intermediate regime is irregular.

A natural question which arises in larger flakes is whether the position of the adatom affects the behaviour of the system. To investigate this, twelve different adatom coupling sites were chosen along two axes and labelled with letters A-L, as shown in Fig. 4.17.
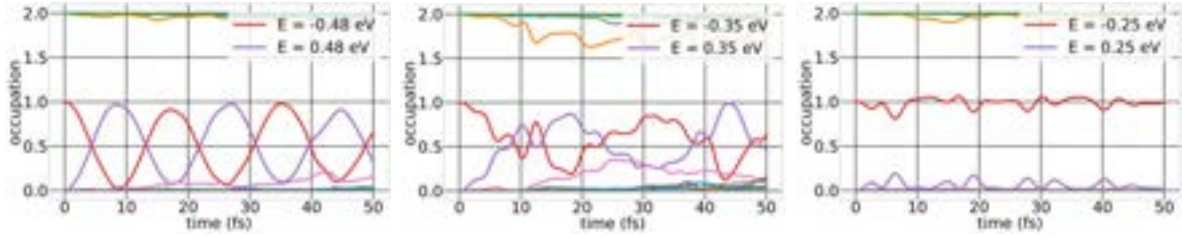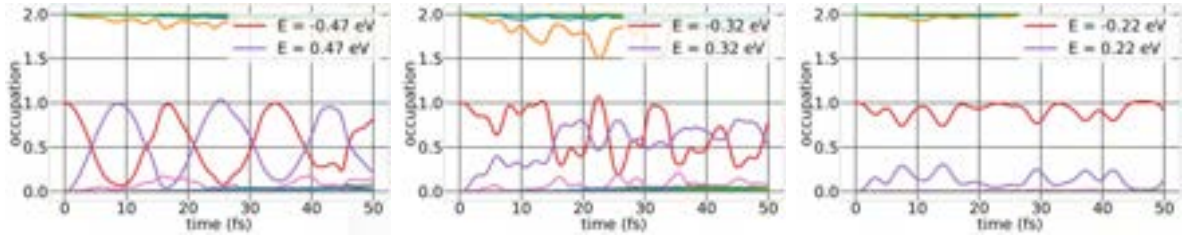
Figure 4.14: Rabi oscillations in a 126-atom flake with the adatom attached near the edge of the flake with a coupling strength of a) $t_e = t_g = 0.5\,\mathrm{eV}$ b) $t_e = t_g = 2.0\,\mathrm{eV}$ c) $t_e = t_g = 3.5\,\mathrm{eV}$.

Figure 4.15: Rabi oscillations in a 126-atom flake with the adatom attached near the centre of the flake with a coupling strength of a) $t_e = t_g = 0.5\,\mathrm{eV}$ b) $t_e = t_g = 2.0\,\mathrm{eV}$ c) $t_e = t_g = 3.5\,\mathrm{eV}$.
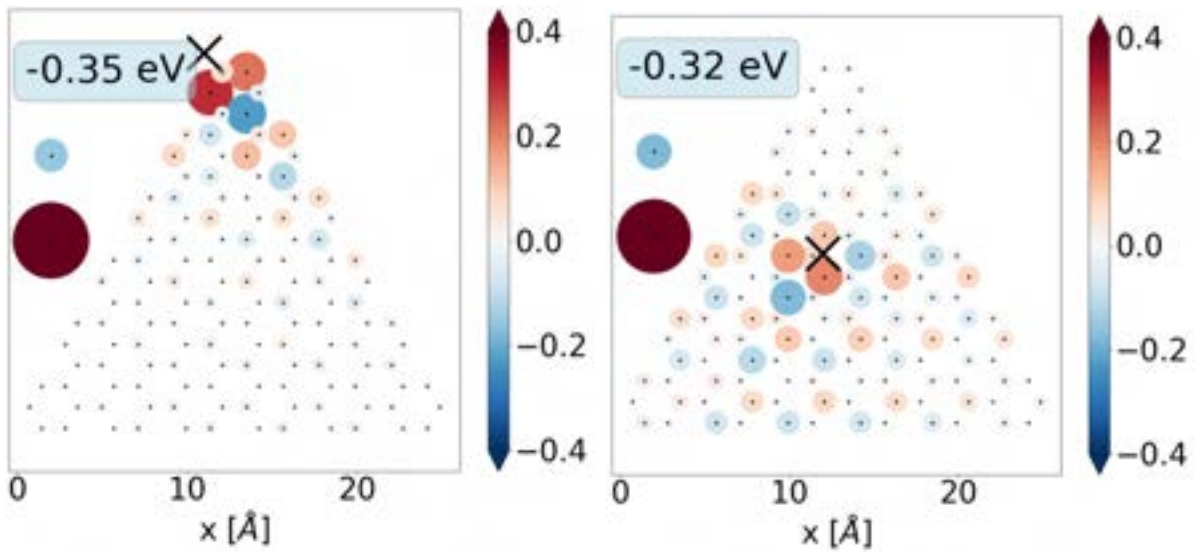

Figure 4.16: Real-space distribution of the HOMO state in a 126-atom flake with the adatom attached with a coupling strength of $t_e = t_g = 2.0\,\mathrm{eV}$ a) near the edge of the flake, b) near the centre of the flake. The occupation on adatom sites is marked by the two dots on the left (upper dot - excited state, lower dot - ground state). The location of the adatom is denoted by the black X mark.

We focus on the case of $t_e = t_g = 2\,\mathrm{eV}$, since this is a coupling strength which lies in the intermediate regime between the resonant and detuned Rabi oscillations. The energy basis dynamics is presented in Figs. 4.18. One can note that the time evolution depends
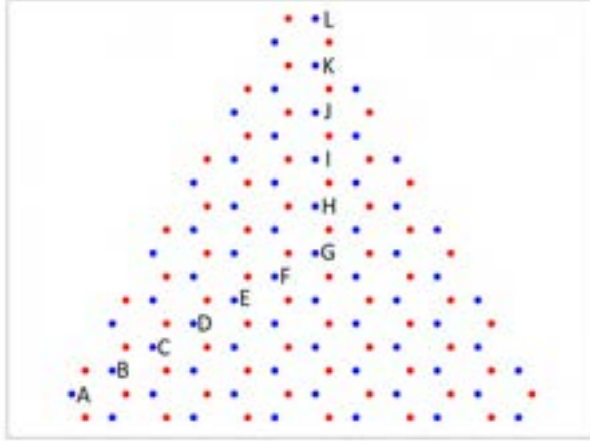
Figure 4.17: Atom labelling.

to some extent on the adatom's position but further research is required to precisely determine the impact of the adatom's location on the evolution of the system.

4.7.2 Spontaneous emission

An excited atomic system can spontaneously decay from an excited state into a lower-energy state, while simultaneously releasing energy into the surrounding environment. The rate of this emission depends on the properties of the environment. The enhancement of spontaneous emission rates of atoms upon coupling to environment was discovered by Edward Purcell and is hence called the Purcell effect [79]. A strong Purcell effect can be observed in atoms in weakly coupled cavities and in emitters located near plasmonic nanostructures, which are able to confine the electromagnetic field into very small volumes [80]. In this section, we investigate how the graphene nanoflakes influence the emission rates in adatoms which they are coupled to.

We exploit the Green's tensor formalism, with the decay rate given by Eq. 2.61. The Green's tensor can be decomposed into the homogeneous part G_0 and the scattered part G_s: $G = G_0 + G_s$, which in turn allow us to rewrite the decay rate as a sum of two corresponding contributions $\Gamma = \Gamma_0 + \Gamma_s$, involving either G_0 or G_s in Eq. 2.61. In free space, the scattered part of the Greens tensor vanishes and so does the scattered emission rate. The homogeneous part of the tensor leads to the Weisskopf-Wigner formula 2.62, describing the spontaneous decay of a system with a given transition frequency and dipole moment. Below, we investigate the influence of electronic interactions between the adatom and the flake on the homogenous spontaneous emission rate which occurs due
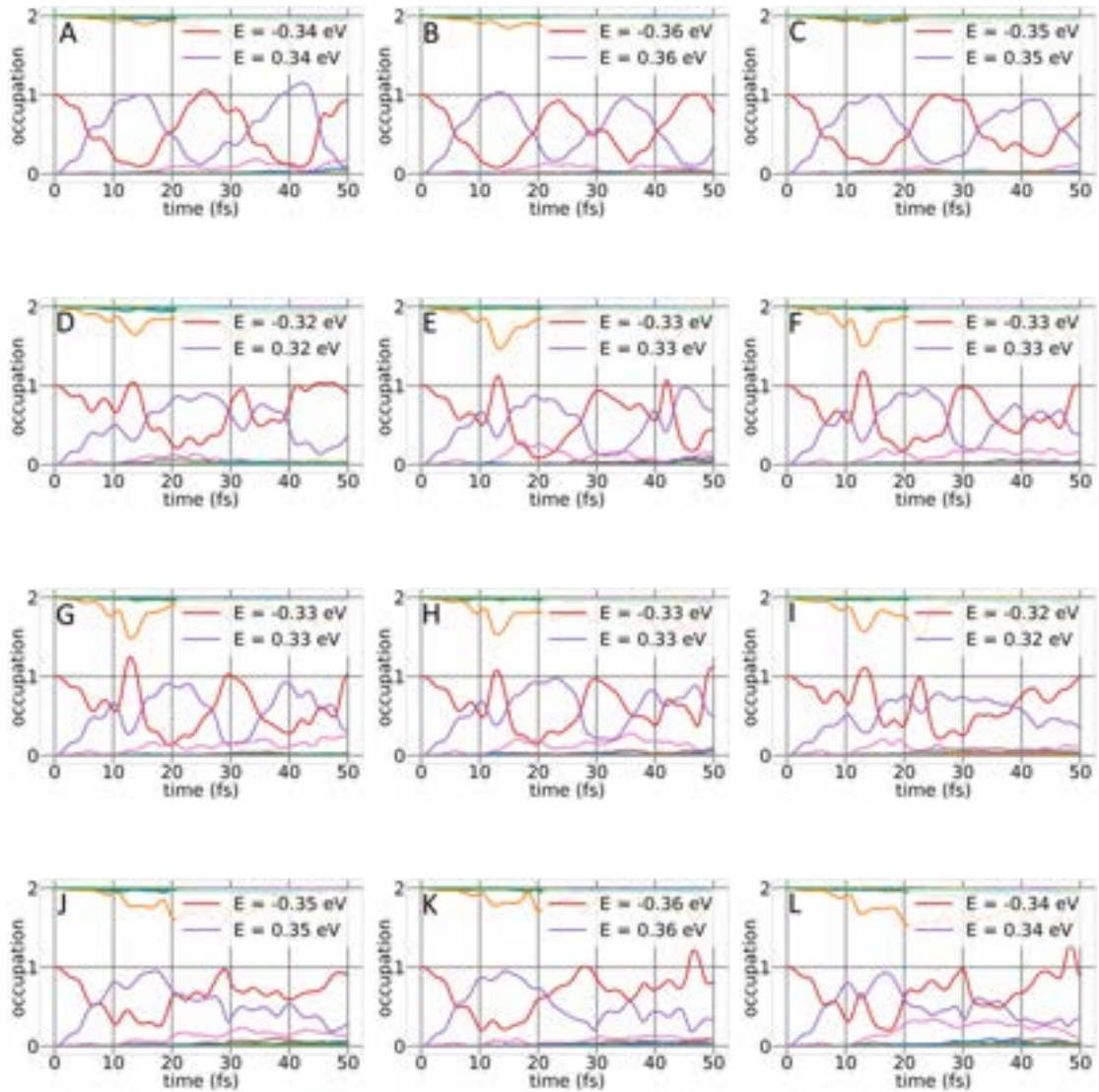
76

Figure 4.18: Occupation of energy states in time in a 126-atom graphene nanoflake with the adatom attached at sites A-L (see Fig. 4.17).

to modification of these two parameters, as ω_{eg} is replaced by ω_{LH} being the frequency difference between the LUMO and HOMO states, and similarly as the dipole moment d_{eg} is replaced by the gradually modified d_{LH}.

On top of that, the field of our dipole emitter, to a good approximation localised at the adatom position, is scattered by the flake giving rise to the scattered Green's tensor component G_s and the corresponding emission rate component Γ_s.

Below, we analyse these effects one by one. First, we investigate the electronic mechanism by first attaching the adatom to the nanoflake and calculating new eigenstates of the combined system, whose energies are changed with respect to the energies in a pristine graphene nanoflake without adatoms (conf. Fig 4.2) due to the exchange of electrons between the two subsystems. The next step is the evaluation of transition dipole moments and frequencies between pairs of eigenstates in the system and then using the Weisskopf-Wigner formula for spontaneous emission.

The *optical* enhancement of emission rates can be calculated based on the evaluation of the scattered Green's tensor arising in the dipole illumination scheme. We perform this calculation twice. First, we neglect the effects of electronic coupling by setting $t_e = t_g = 0$ and keeping the adatom dipole moment and frequency unmodified regardless of the distance to the flake. Please note that this calculation reflects the classical approach widely used in plasmonics, where the Purcell enhancement is quantified via the scattered field intensity at the emitter's position.

The final calculation extends this approach and includes both the optical and the electronic effects: the scattered Green's tensor is evaluated for a system with the modified transition dipole d_{LH} and frequency ω_{LH}. This step-by-step method allows us to compare different contributions and estimate their impact for different adatom-flake distances.

Electronic influence on the spontaneous emission rate

To calculate the spontaneous emission rate modification caused by the *electronic* mechanism we start by evaluating transition dipole moments between energy states from the formula:

$$\mathbf{d}_{ij} = \langle \phi_i | \, \mathbf{r} \, | \phi_j \rangle . \tag{4.8}$$

Putting Eq. 3.3 into Eq. 4.8 we obtain:

$$\mathbf{d}_{ij} = \left(\sum_l a_{il}^* \langle l|\right) e\mathbf{r} \left(\sum_k a_{jk} |k\rangle\right) = \sum_{l,k} a_{il}^* a_{jk} \langle l| e\mathbf{r} |k\rangle = \sum_{l,k} e a_{il}^* a_{jk} \delta_{kl} = \sum_l a_{il}^* a_{jl}. \tag{4.9}$$

As before, the resonant frequency ω_{ij} is evaluated by diagonalisation of the tight-binding Hamiltonian which describes the adatom and flake. Now we have all the quantities which are necessary to evaluate the spontaneous emission rate in the system with the use of the Weisskopf-Wigner formula 2.62:

$$\Gamma\left(\phi_j \to \phi_i\right) = \frac{\omega_{ij}^3 d_{ij}^2}{3\pi\epsilon_0 \hbar c^3}, \tag{4.10}$$

where $\Gamma\left(\phi_j \to \phi_i\right)$ is the transition rate from state $|\phi_j\rangle$ to $|\phi_i\rangle$. The dependence of the spontaneous emission rate on the distance between the nanoflake and adatom is shown for two triangular nanoflakes in Fig. 4.19. The coupling strengths t_e and t_g have been evaluated based on the distance using Eq. 4.2 with $\beta = 1$.
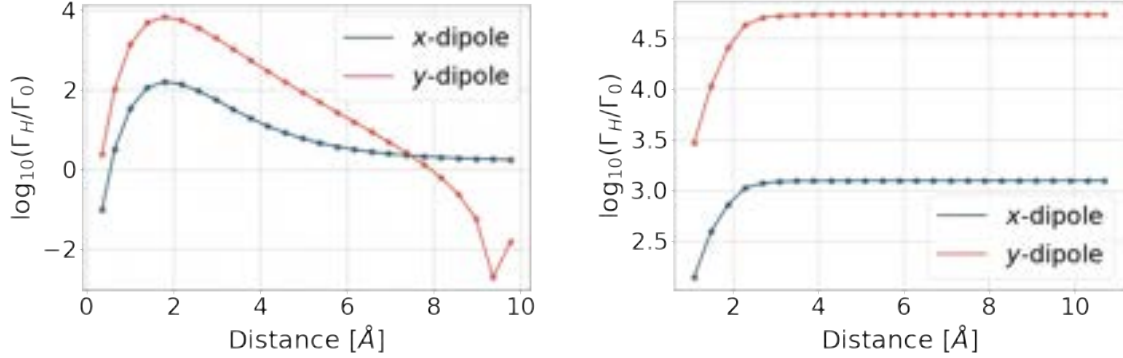

Figure 4.19: Dependence of the spontaneous emission on the distance from two triangular armchair-edged graphene nanoflakes consisting of 36 atoms (left panel) and 126 atoms (right panel) computed from the transition dipole moment and frequency modification of the HOMO-LUMO transition due to the electronic coupling of the adatom with the flake. The dipole moment in the uncoupled adatom was set to $d_{eg} = 0.01\,e\text{Å} \approx 0.05D$.

Optical influence on the spontaneous emission rate

To evaluate the spontaneous emission rate arising from the *optical* mechanism, we illuminate the nanostructure with a dipole field source of a given orientation located at the position of the adatom $\mathbf{r}_{\text{ad}}$ and propagate the entire system in time. Next, we calculate

the scattered part of the field which is induced from the nanoflake at the position of the adatom using formula 4.7. We continue by performing a Fourier transform of the induced field:

$$\mathbf{E}_{\text{ind}}(\mathbf{r}_{\text{ad}}, t) \longrightarrow \mathbf{E}_{\text{ind}}(\mathbf{r}_{\text{ad}}, \omega). \tag{4.11}$$

Next, we construct the scattered part of the Green's tensor of the graphene nanoflake as defined by the following relation:

$$\mathbf{G}_s\left(\mathbf{r}_{\text{ad}}, \mathbf{r}_{\text{ad}}, \omega\right) \mathbf{d} = \frac{1}{\omega^2 \mu_0} \mathbf{E}_{\text{ind}}\left(\mathbf{r}_{\text{ad}}, \omega\right), \tag{4.12}$$

Finally, the spontaneous emission rate can be evaluated from the expression:

$$\Gamma_s = \frac{2\omega_0^2}{\hbar \epsilon_0 c^2} \mathbf{d} \, \text{Im} \, \mathbf{G}_s\left(\mathbf{r}_{ad}, \mathbf{r}_{ad}, \omega_0\right) \mathbf{d}, \tag{4.13}$$

where $\mathbf{d} = [d_x, d_y, d_z]$ describes the dipole moment of the adatom and ω_0 is its resonant frequency. To obtain a more accurate prediction of the spontaneous emission rate, one might go beyond the dipole approximation and add further multipolar terms in equation 4.13, as we have described in Ref. 62.

The dependence of the spontaneous emission rate on the distance between the nanoflake and adatom is shown for two adatom dipole orientations in Fig. 4.20. We observe that for small distances the optical mechanism dominates the electronic influence by several orders of magnitude. However, when we go far away from the flake, the spontaneous emission rate evaluated with the Green's tensor goes to zero, whereas the electronic part remains constant on the order of 10^6 Hz.

4.8   Absorption spectra with adatom

Here, we investigate the influence of the adatom's position on the absorption spectra of the nanoflakes with adatoms (Fig. 4.21). Generally, in hybrid systems consisting of a nanoflake and adatom increasing the coupling strength t_e and t_g causes a splitting of resonances. When the adatom is attached to sites near the centre of a flake (D, E, F, G, H, I), the resonances of the hybrid system get more affected than resonances in systems with an adatom located near the edge of the flake.

The influence of the adatom is seen strongest in small nanoflakes, especially in the armchair-edges ones (Fig. 4.22). The most pronounced resonance (at 2.84 eV in the
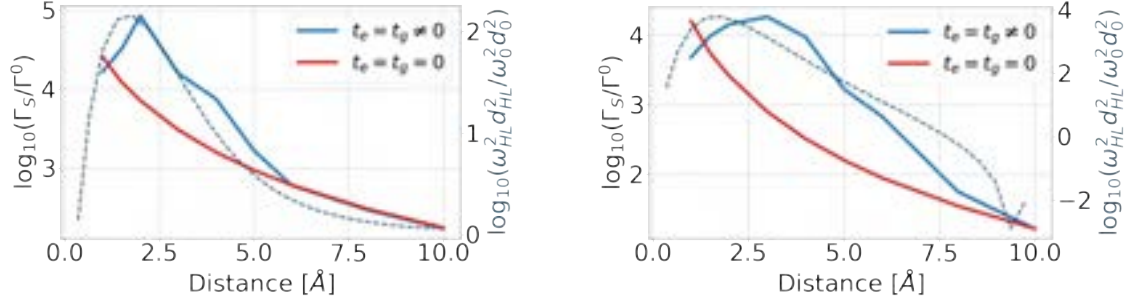
80

Figure 4.20: Dependence of the spontaneous emission rate on the distance from the flake. Left: For x-orientation of the adatom dipole moment. Right: For y-orientation of the adatom dipole moment. Here, the emission rate is computed from the scattered part of the Green's tensor of the structure and plotted relatively to the free-space emission value. Figure from Ref. 62.
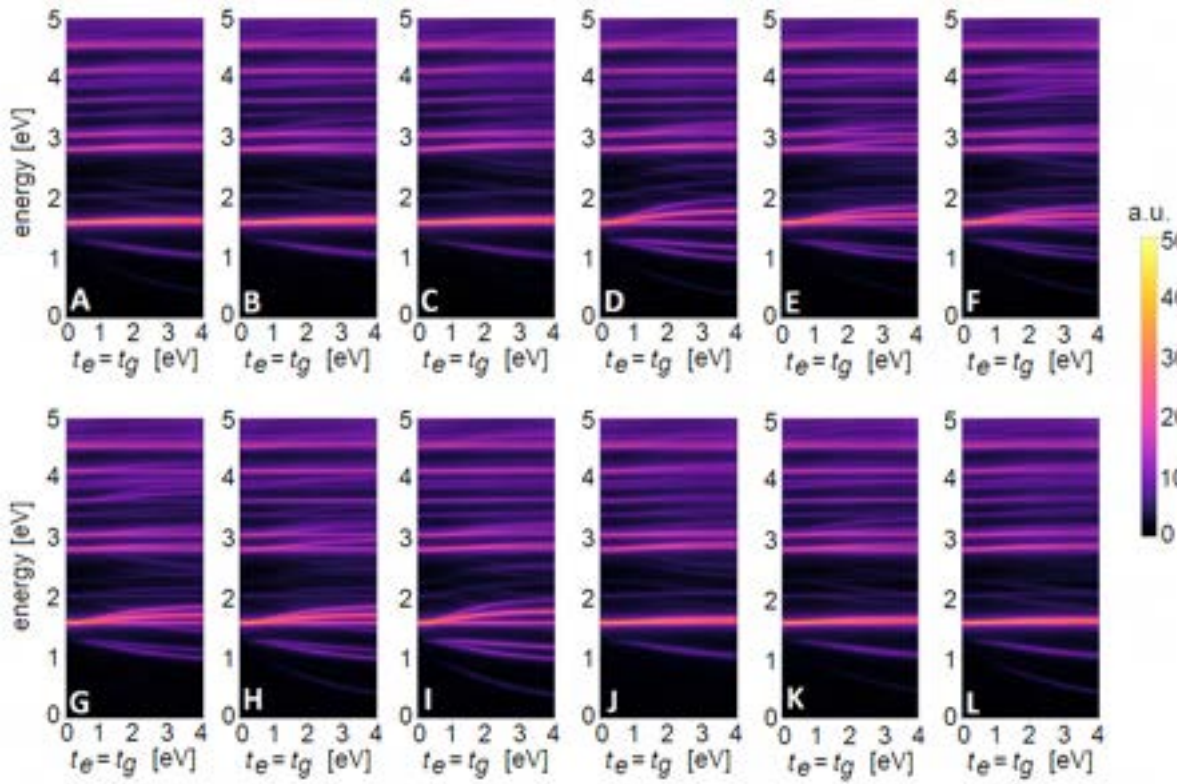

Figure 4.21: Non-interacting absorption spectra and their dependence on the adatom coupling strength $t_e = t_g$ for a triangular nanoflake with 126 atoms and an adatom attached at positions A-L, as labelled in Fig 4.17. The spectra are shown in arbitrary units.

smallest armchair triangle) corresponds to the HOMO-LUMO transition in the pristine nanoflake. With the adatom, new HOMO and LUMO states arise which consist mostly of adatom levels. The resonance corresponding to there states is the one with the lowest
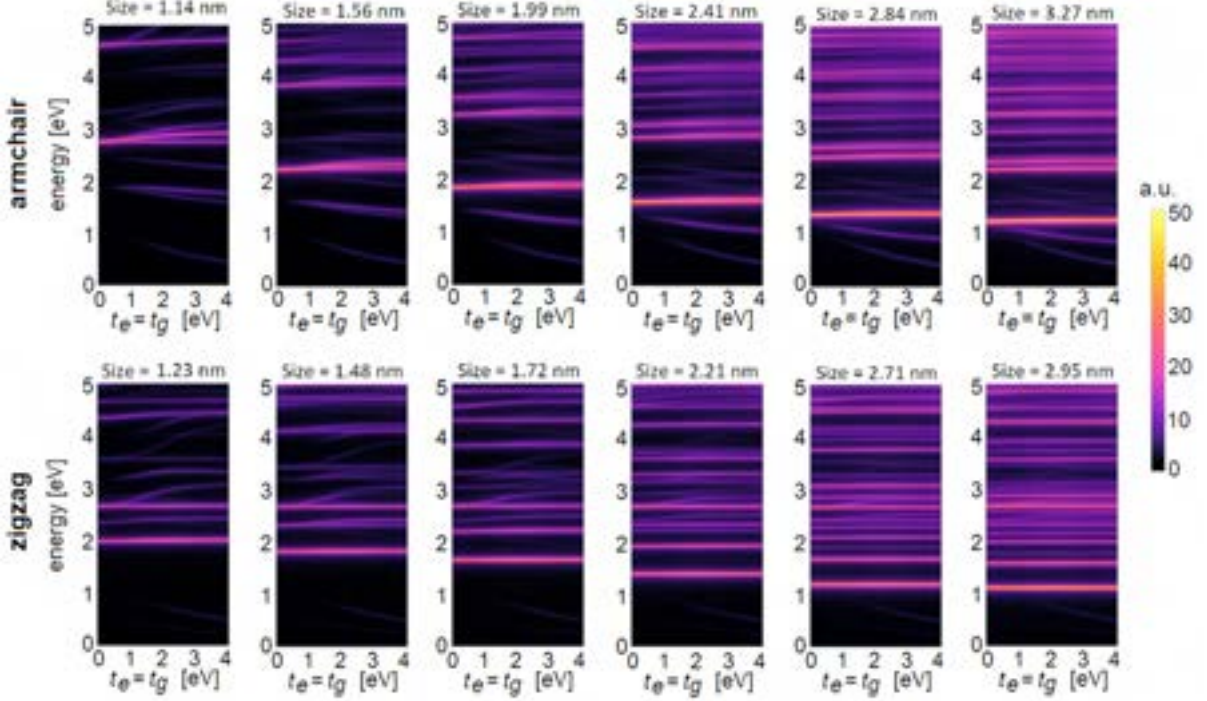
Figure 4.22: Non-interacting absorption spectra and their dependence on the adatom coupling strength $t_e = t_g$ for triangles of various sizes with an adatom attached at the coordinates [0, 1]Å (next to the lower-left corner of the flake). Upper row: armchair edged. Lower row: zigzag-edged.

energy (at 1 eV for $t_e = t_g = 0$). The intensity of this resonance grows with t_e and t_g, since for this calculation we assumed the transition dipole moment element in the adatom d_{eg} to be equal zero. The energy of this resonance decreases with growing t_e and t_g since the adatom levels shift their energies closer to the zero-point energy, as shown in Fig. 4.3. The influence of the adatom is more pronounced in armchair-edge flakes.

In Fig. 4.23 we present absorption spectra for a triangular armchair-edge graphene flake with 18 atoms (side length 0.71 nm) with an adatom attached near its tip (at the coordinates [3, 7.5]Å). On the left we show the dependence of the non-interacting absorption spectrum on the hopping rate t_e and t_g, on the right - the same but for the interacting absorption spectrum, and in the middle panel we show the continuous transition from one case to the other for a fixed value of the hopping rate $t_e = t_g = 2$ eV by scaling the Coulomb interaction strength in the system.
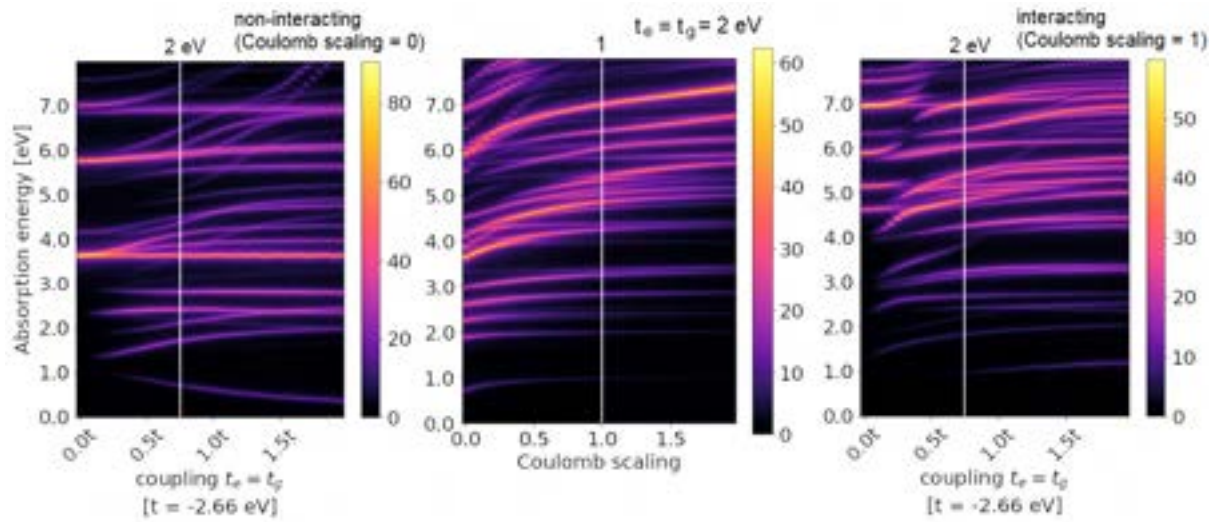
Figure 4.23: Absorption spectra for an 18-atom triangular graphene nanoflake with an adatom attached at the coordinates [3, 7.5]Å. Left: Non-interacting absorption spectrum dependence on the flake-adatom hopping rate $t_e = t_g$. Middle: Absorption spectrum for fixed hopping rates $t_e = t_g = 2t$ in the function of Coulomb interaction strength in the system. The Coulomb interaction is scaled by a factor continuously changing from 0 (which corresponds to a non-interacting spectrum) to 2. Right: Interacting absorption spectrum dependence on the flake-adatom hopping rate $t_e = t_g$.

Final remarks

The thesis introduces tools for describing and predicting the behaviour of graphene nanoflakes coupled to two-level atoms subject to illumination with electromagnetic fields. The presented framework combines concepts from solid-state physics, like the tight-binding approximation, with methods from quantum optics and quantum dynamics, such as the master equation. This required a consolidation of various distinct ways to describe the same phenomena, e.g. different ways of modelling a dipole moment, either calculated from the charge distribution or seen just as a parameter.

The proposed method allows to describe many-body systems with hundreds of electrons using a simple one-electron Hamiltonian, which gives a large computational advantage. The many-body character of the problem is included as a non-linearity in the Hamiltonian. A similar approach has been used before to pristine graphene nanoflakes but in this thesis it has been extended to systems with adatoms. In dissipative systems, this kind of description leads to problems with the Pauli exclusion principle. A solution that allows to overcome this problem has also been proposed in the thesis.

The entire framework has been implemented numerically in Python and the thesis presents a large number of results obtained using this code. In particular, we show for various hybrid systems consisting of nanoflakes with adatoms: their energy levels, charge distribution of eigenstates, symmetry breaking due to the adatom presence, absorption spectra, change of time evolution caused by increasing the adatom-flake interaction strength, spontaneous emission in the adatom and its dependence on the flake-adatom distance. The implemented model has also been used to explore subjects which are not contained in the thesis, such as the investigation of the resonance character in graphene nanostructures [40].

The presented framework is quite general and contains many tunable parameters to characterize both the flake and the adatom. In the thesis, the phenomena were presented

only for specific systems and many of them require a more systematic investigation. A potential area for further research is the examination of the influence of the adatom position on the optical properties of the nanoflakes. This would allow to define optimal locations for attaching the adatom such that it affects the measurable quantities in a controlled way. Another topic worth studying would be a systematic study of how the properties of the nanoflakes affect spontaneous emission in the adatoms which they are coupled to.

There are many ways in which this work can be extended to further investigate similar systems. Using only the equations and methods presented in this thesis, one could proceed by adding multiple adatoms in the system to find if and how they can interact with each other via the graphene nanoflake. The next step could be to replace the graphene by a different type of 2-D material, e.g. hBN or transition metal dichalcogenides. This would require several changes in the model but can still be achieved relatively easily by adjusting the hopping parameters, onsite energies and geometrical properties of the 2D material. Finally, throughout the thesis we focused only on systems that do not exhibit magnetic properties, therefore it was rather superfluous to include this kind of effects in the description. However, to make the tool even more general and applicable to any arbitrary nanoflake shape and adatom type, magnetic effects could be included. This would probably require a significant amount of work, since it demands adding new components to the system and consequently modifying nearly all presented equations.

Bibliography

[1] M. I. Katsnelson. Zitterbewegung, chirality, and minimal conductivity in graphene. *Eur. Phys. J. B*, 51(2):157–160, 2006.

[2] F. Liu, Q. Li, R. Wang, J. Xu, J. Hu, W. Li, G. Yufen, Y. Qian, W. Deng, Z. Ullah, Z. Zeng, and L. Liu. Low resistivity of graphene nanoribbons with zigzag-dominated edge fabricated by hydrogen plasma etching combined with Zn/HCl pretreatment. *Appl. Phys. Lett.*, 111:203102, 11 2017.

[3] M. I. Katsnelson, K. S. Novoselov, and A. K. Geim. Chiral tunnelling and the Klein paradox in graphene. *Nat. Phys.*, 2(9):620–625, Sep 2006.

[4] Ke Cao, Shizhe Feng, Ying Han, Libo Gao, Thuc Hue Ly, Zhiping Xu, and Yang Lu. Elastic straining of free-standing monolayer graphene. *Nat. Commun.*, 11(1):284–284, Jan 2020.

[5] M. Sang, J. Shin, K. Kim, and K. J. Yu. Electronic and thermal properties of graphene and recent advances in graphene based electronics applications. *Nanomaterials*, 9(3):374, Mar 2019.

[6] P. Z. Sun, Q. Yang, W. J. Kuang, Y. V. Stebunov, W. Q. Xiong, J. Yu, R. R. Nair, M. I. Katsnelson, S. J. Yuan, I. V. Grigorieva, M. Lozada-Hidalgo, F. C. Wang, and A. K. Geim. Limits on gas impermeability of graphene. *Nature*, 579(7798):229–232, Mar 2020.

[7] H. Geng, D. Yuan, Z. Yang, Z. Tang, X. Zhang, K. Yang, and Y. Su. Graphene van der Waals heterostructures for high-performance photodetectors. *J. Mater. Chem. C*, 7:11056–11067, 2019.

[8] K. S. Novoselov, A. K. Geim, S. V. Morozov, D. Jiang, Y. Zhang, S. V. Dubonos, I. V. Grigorieva, and A. A. Firsov. Electric field effect in atomically thin carbon films. *Science*, 306(5696):666–669, 2004.

[9] N. D. Mermin. Crystalline order in two dimensions. *Phys. Rev.*, 176:250–254, Dec 1968.

[10] M. Yi and Z. Shen. A review on mechanical exfoliation for the scalable production of graphene. *J. Mater. Chem. A*, 3:11700–11715, 2015.

[11] J. M. Tour. Scaling up exfoliation. *Nat. Mater.*, 13(6):545–546, Jun 2014.

[12] P. W. Sutter, J.-I. Flege, and E. A. Sutter. Epitaxial graphene on ruthenium. *Nat. Mater.*, 7(5):406–411, May 2008.

[13] J. Lin, Z. Peng, Y. Liu, F. Ruiz-Zepeda, R. Ye, E. L. G. Samuel, M. J. Yacaman, B. I. Yakobson, and J. M. Tour. Laser-induced porous graphene films from commercial polymers. *Nat. Commun.*, 5(1):5714, Dec 2014.

[14] D. V. Kosynkin, A. L. Higginbotham, A. Sinitskii, J. R. Lomeda, A. Dimiev, B. K. Price, and J. M. Tour. Longitudinal unzipping of carbon nanotubes to form graphene nanoribbons. *Nature*, 458(7240):872–876, Apr 2009.

[15] L. Tang, X. Li, R. Ji, K. S. Teng, G. Tai, J. Ye, C. Wei, and S. P. Lau. Bottom-up synthesis of large-scale graphene oxide nanosheets. *J. Mater. Chem.*, 22:5676–5683, 2012.

[16] L. Lin, H. Peng, and Z. Liu. Synthesis challenges for graphene industry. *Nat. Mater.*, 18(6):520–524, Jun 2019.

[17] Jeff Cruzan. Orbital hybridization. https://xaktly.com/OrbitalHybridization.html, 2012.

[18] A. H. Castro Neto, F. Guinea, N. M. R. Peres, K. S. Novoselov, and A. K. Geim. The electronic properties of graphene. *Rev. Mod. Phys.*, 81:109–162, Jan 2009.

[19] P. R. Wallace. The band theory of graphite. *Phys. Rev.*, 71:622–634, May 1947.

[20] A. Ayuela, W. Jaskólski, H. Santos, and L. Chico. Electronic properties of graphene grain boundaries. *New J. Phys.*, 16(8):083018, aug 2014.

[21] N. Lindvall. Towards graphene-based devices: Fabrication and characterization. licenciate of engineering, 2012.

[22] A. K. Geim and K. S. Novoselov. The rise of graphene. *Nat. Mater.*, 6(3):183–191, Mar 2007.

[23] K. S. Novoselov, D. Jiang, F. Schedin, T. J. Booth, V. V. Khotkevich, S. V. Morozov, and A. K. Geim. Two-dimensional atomic crystals. *Proc. Natl. Acad. Sci.*, 102(30):10451–10453, 2005.

[24] R. Mintae, L. Paengro, K. Jingul, P. Heemin, and C. Jinwook. Band gap engineering for single-layer graphene by using slow li+ ions. *Nanotechnology*, 27(31):31LT03, jun 2016.

[25] T. Ohta, A. Bostwick, T. Seyller, K. Horn, and E. Rotenberg. Controlling the electronic structure of bilayer graphene. *Science*, 313(5789):951–954, 2006.

[26] W. Zhang, C. Lin, K. Liu, T. Tite, C.-Y. Su, C.-H. Chang, Y.-H. Lee, C.-W. Chu, K.-H. Wei, J.-L. Kuo, and L.-J. Li. Opening an electrical band gap of bilayer graphene with molecular doping. *ACS Nano*, 5(9):7517–7524, Sep 2011.

[27] N. Savage and E. Cooper. Graphene makes transistors tunable. https://spectrum.ieee.org/semiconductors/materials/graphene-makes-transistors-tunable, 8 2009.

[28] T. W. Ebbesen, H. J. Lezec, H. F. Ghaemi, T. Thio, and P. A. Wolff. Extraordinary optical transmission through sub-wavelength hole arrays. *Nature*, 391(6668):667–669, Feb 1998.

[29] L. Martín-Moreno, F. J. García-Vidal, H. J. Lezec, K. M. Pellerin, T. Thio, J. B. Pendry, and T. W. Ebbesen. Theory of extraordinary optical transmission through subwavelength hole arrays. *Phys. Rev. Lett.*, 86:1114–1117, Feb 2001.

[30] P. A. D. Gonçalves and N. M. R. Peres. *An Introduction to Graphene Plasmonics*. World Scientific, 2016.

[31] L. Ju, B. Geng, J. Horng, C. Girit, M. Martin, Z. Hao, H. A. Bechtel, X. Liang, A. Zettl, Y. R. Shen, and F. Wang. Graphene plasmonics for tunable terahertz metamaterials. *Nat. Nanotechnol.*, 6(10):630–634, Oct 2011.

[32] A. N. Grigorenko, M. Polini, and K. S. Novoselov. Graphene plasmonics. *Nat. Photon.*, 6(11):749–758, Nov 2012.

[33] F. J. García de Abajo. Graphene plasmonics: Challenges and opportunities. *ACS Photonics*, 1(3):135–152, Mar 2014.

[34] F. H. L. Koppens, D. E. Chang, and F. J. García de Abajo. Graphene plasmonics: A platform for strong light–matter interactions. *Nano Lett.*, 11(8):3370–3377, Aug 2011.

[35] M. Jablan, H. Buljan, and M. Soljačić. Plasmonics in graphene at infrared frequencies. *Phys. Rev. B*, 80:245435, Dec 2009.

[36] Y. V. Bludov, A. Ferreira, N. M. R. Peres, and M. I. Vasilevskiy. A primer on surface plasmon-polaritons in graphene. *Int. J. Mod. Phys.*, 27(10):1341001, Apr 2013.

[37] H. Yan, T. Low, W. Zhu, Y. Wu, M. Freitag, X. Li, F. Guinea, P. Avouris, and F. Xia. Damping pathways of mid-infrared plasmons in graphene nanostructures. *Nat. Photon.*, 7(5):394–399, May 2013.

[38] S. Thongrattanasiri, I. Silveiro, and F. J. García de Abajo. Plasmons in electrostatically doped graphene. *Appl. Phys. Lett.*, 100(20):201105, 2012.

[39] A. Manjavacas, R. Thongrattanasiri, and F.J. García de Abajo. Plasmons driven by single electrons in graphene nanoislands. *Nanophotonics*, 2(2):139–151, 2013.

[40] M. M. Müller, M. Kosik, M. Pelc, G. W. Bryant, A. Ayuela, C. Rockstuhl, and K. Słowik. From single-particle-like to interaction-mediated plasmonic resonances in graphene nanoantennas. *J. Appl. Phys.*, 129(9):093103, 2021.

[41] R. Yu, V. Pruneri, and F. J. García de Abajo. Active modulation of visible light with graphene-loaded ultrathin metal plasmonic antennas. *Sci. Rep.*, 6(1):32144, Aug 2016.

[42] E. Townsend and G. W. Bryant. Which resonances in small metallic nanoparticles are plasmonic? *J. Opt.*, 16(11):114022, nov 2014.

[43] C. M. Krauter, S. Bernadotte, C. R. Jacob, M. Pernpointner, and A. Dreuw. Identification of plasmons in molecules with scaled ab initio approaches. *J. Phys. Chem. C*, 119(43):24564–24573, Oct 2015.

[44] R. Zhang, L. Bursi, J. D. Cox, Y. Cui, C. M. Krauter, A. Alabastri, A. Manjavacas, A. Calzolari, S. Corni, E. Molinari, E. A. Carter, F. J. García de Abajo, H. Zhang, and P. Nordlander. How to identify plasmons from the optical response of nanostructures. *ACS Nano*, 11(7):7321–7335, Jul 2017.

[45] K. Wakabayashi. Electronic transport properties of nanographite ribbon junctions. *Phys. Rev. B*, 64:125428, Sep 2001.

[46] S. Ihnatsenka and G. Kirczenow. Dirac point resonances due to atoms and molecules adsorbed on graphene and transport gaps and conductance quantization in graphene nanoribbons with covalently bonded adsorbates. *Phys. Rev. B*, 83:245442, Jun 2011.

[47] E. J. Duplock, M. Scheffler, and P. J. D. Lindan. Hallmark of perfect graphene. *Phys. Rev. Lett.*, 92:225502, Jun 2004.

[48] D. C. Elias, R. R. Nair, T. M. G. Mohiuddin, S. V. Morozov, P. Blake, M. P. Halsall, A. C. Ferrari, D. W. Boukhvalov, M. I. Katsnelson, A. K. Geim, and K. S. Novoselov. Control of graphene's properties by reversible hydrogenation: Evidence for graphane. *Science*, 323(5914):610–613, 2009.

[49] Jannik C. Meyer, C. O. Girit, M. F. Crommie, and A. Zettl. Imaging and dynamics of light atoms and molecules on graphene. *Nature*, 454(7202):319–322, Jul 2008.

[50] A.H. Castro Neto, V.N. Kotov, J. Nilsson, V.M. Pereira, N.M.R. Peres, and B. Uchoa. Adatoms in graphene. *Solid State Commun.*, 149(27):1094–1100, 2009. Recent Progress in Graphene Studies.

[51] S. Y. Davydov. Model of adsorption on amorphous graphene. *Semiconductors*, 50(3):377–383, Mar 2016.

[52] S. Irmer, D. Kochan, J. Lee, and J. Fabian. Resonant scattering due to adatoms in graphene: Top, bridge, and hollow positions. *Phys. Rev. B*, 97:075417, Feb 2018.

[53] F. Wu, E. Kan, H. Xiang, S.-H. Wei, M.-H. Whangbo, and J. Yang. Magnetic states of zigzag graphene nanoribbons from first principles. *Appl. Phys. Lett.*, 94(22):223105, 2009.

[54] J. Li, S. Sanz, J. Castro-Esteban, M. Vilas-Varela, N. Friedrich, T. Frederiksen, D. Peña, and J. I. Pascual. Uncovering the triplet ground state of triangular graphene nanoflakes engineered with atomic precision on a metal surface. *Phys. Rev. Lett.*, 124:177201, Apr 2020.

[55] D. A. Steck. Quantum and atom optics. https://atomoptics-nas.uoregon.edu/ dsteck/teaching/quantum-optics/, 2007. (revision 0.13.4, 24 September 2020).

[56] M. Fox. *Quantum optics: an introduction*. Oxford master series in atomic, optical, and laser physics. Oxford Univ. Press, Oxford, 2006.

[57] W. Vogel and D.-G. Welsch. *Quantum Optics*. John Wiley and Sons, 2006.

[58] S. Haroche and J. M. Raimond. *Exploring the Quantum: Atoms, Cavities, and Photons*. Oxford Univ. Press, Oxford, 2006.

[59] M. O. Scully and M. S. Zubairy. *Quantum Optics*. Cambridge University Press, 1997.

[60] H. T. Dung, L. Knöll, and D.-G. Welsch. Three-dimensional quantization of the electromagnetic field in dispersive and absorbing inhomogeneous dielectrics. *Phys. Rev. A*, 57:3931–3942, May 1998.

[61] D. Dzsotjan, A. S. Sørensen, and M. Fleischhauer. Quantum emitters coupled to surface plasmons of a nanowire: A Green's function approach. *Phys. Rev. B*, 82:075427, Aug 2010.

[62] M. Kosik, O. Burlayenko, C. Rockstuhl, I. Fernandez-Corbaton, and K. Słowik. Interaction of atomic systems with quantum vacuum beyond electric dipole approximation. *Sci. Rep.*, 10(1):5879, Apr 2020.

[63] Claude Cohen-Tannoudji, Bernard. Diu, Franck Laloë, and Susan R. Hemley. *Quantum mechanics Vol.2 Vol.2*. 1977.

[64] D. Manzano. A short introduction to the Lindblad master equation. *AIP Advances*, 10(2):025106, 2020.

[65] M. Kosik, M. M. Müller, M. Pelc, G. W. Bryant, A. Ayuela, C. Rockstuhl, and K. Słowik. Revising quantum optical phenomena in adatoms coupled to graphene nanoantennas. *under review*, 2022.

[66] P. Potasz, A. D. Güçlü, and P. Hawrylak. Spin and electronic correlations in gated graphene quantum rings. *Phys. Rev. B*, 82:075425, Aug 2010.

[67] J. D. Cox and F. J. García de Abajo. Electrically tunable nonlinear plasmonics in graphene nanoislands. *Nat. Commun.*, 5(1):5725, Dec 2014.

[68] R. Loudon. *The quantum theory of light*. Oxford University Press, 2000.

[69] S. G. Schirmer and A. I. Solomon. Constraints on relaxation rates for n-level quantum systems. *Phys. Rev. A*, 70:022107, Aug 2004.

[70] S. V. Morozov, K. S. Novoselov, M. I. Katsnelson, F. Schedin, L. A. Ponomarenko, D. Jiang, and A. K. Geim. Strong suppression of weak localization in graphene. *Phys. Rev. Lett.*, 97:016801, Jul 2006.

[71] K. Kechedzhi, D. W. Horsell, F. V. Tikhonenko, A. K. Savchenko, R. V. Gorbachev, I. V. Lerner, and V. I. Fal'ko. Quantum transport thermometry for electrons in graphene. *Phys. Rev. Lett.*, 102:066801, Feb 2009.

[72] T. Yamamoto, T. Noguchi, and K. Watanabe. Edge-state signature in optical absorption of nanographenes: Tight-binding method and time-dependent density functional theory calculations. *Phys. Rev. B*, 74:121409, Sep 2006.

[73] M. M. Müller, M. Kosik, M. Pelc, G. W. Bryant, A. Ayuela, C. Rockstuhl, and K. Słowik. Modification of the optical properties of molecular chains upon coupling to adatoms. *Phys. Rev. B*, 104:235414, Dec 2021.

[74] S. A. Mikhailov. Theory of the giant plasmon-enhanced second-harmonic generation in graphene and semiconductor two-dimensional electron systems. *Phys. Rev. B*, 84:045432, Jul 2011.

[75] M. M. Müller, M. Kosik, M. Pelc, G. W. Bryant, A. Ayuela, C. Rockstuhl, and K. Słowik. Energy-based plasmonicity index to characterize optical resonances in nanostructures. *J. Phys. Chem. C*, 124(44):24331–24343, Nov 2020.

[76] The physics of solid state chemistry. In *Festkörperprobleme 17*.

[77] Luca Bursi, Arrigo Calzolari, Stefano Corni, and Elisa Molinari. Light-induced field enhancement in nanoscale systems from first-principles: The case of polyacenes. *ACS Photonics*, 1(10):1049–1058, 2014.

[78] J. Zuloaga, E. Prodan, and P. Nordlander. Quantum description of the plasmon resonances of a nanoparticle dimer. *Nano. Lett.*, 9(2):887–891, Feb 2009.

[79] E. M. Purcell. Spontaneous emission probabilities at radio frequencies. *Phys. Rev.*, 69:681, 1946.

[80] A. F. Koenderink. On the use of Purcell factors for plasmon antennas. *Opt. Lett.*, 35(24):4208–4210, Dec 2010.

Appendix A

Including Pauli exclusion principle in the model

The dissipation with use of the Lindblad operators as described in Eq. 3.9 should normally be performed using $\tilde{\rho} = \rho$. However, as was mentioned in Section 3.4 in the main body of the thesis, in our case such choice leads to severe breaking of the Pauli exclusion principle, as shown in the left panel in Fig. 3.7. This appendix presents several approaches which we have tried to overcome this problem.

The first attempt consisted in evolving the system in time and at each timestep:

1. Converting Coulomb interaction matrix and density matrix into energy basis.

2. Iterating over all diagonal elements of the density matrix in energy basis. If a given energy state has occupation higher than or equal 2: Set on-site values of Coulomb matrix elements corresponding to the states that have occupations exceeding 2 to a very large value to induced depopulation of these states.

3. Converting the new Coulomb back to site basis and continue evolution in site basis.

Unfortunately, this method led to a very irregular evolution and did not solve the problem, as presented in Fig. A.1.

The second approach we have tried to prevent breaking the Pauli principle involved modifying the emission rates γ_{ij} while evolving the system in time. During the time evolution, when the occupation on some energy state $|j\rangle$ reached 2, we shut down all decay rates into this state by setting $\forall_i \gamma_{ij} = 0$. This approach works well for evolution
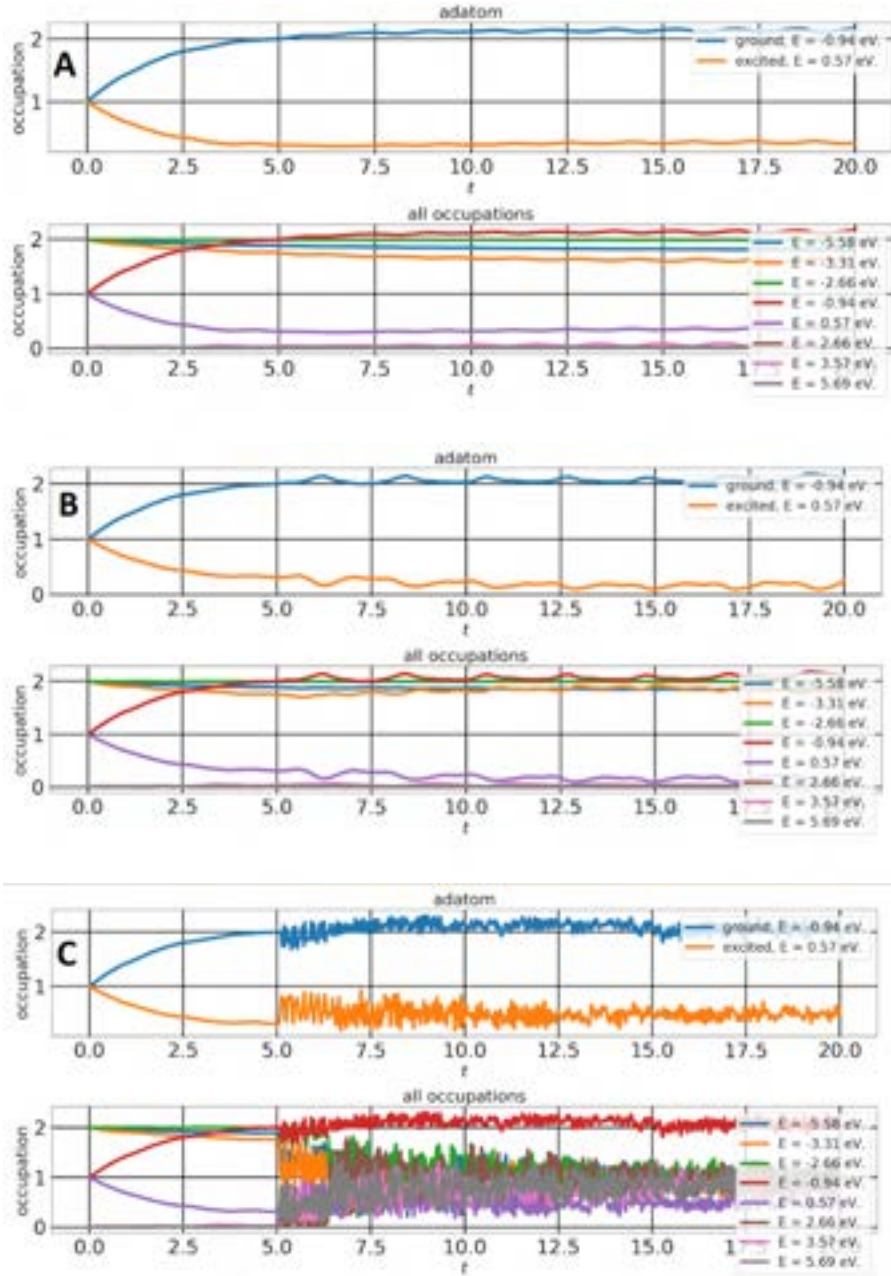
Figure A.1: Demonstration of attempts to prevent breaking the Pauli principle while evolving with a Lindblad decoherence term. The system under consideration is a benzene ring with an adatom with energies ± 1 eV attached to one carbon atom with coupling strengths $t_e = 4t$, $t_g = 0$. The dissipation is included using the Lindblad propagation as described in Eq. 3.9 with $\tilde{\rho} = \rho$. Subfigure A shows the evolution without using the correction mechanism. In Subfigures B and C the Coulomb matrix elements corresponding to states with occupations exceeding 2 were set to: 1000 eV (B), 10000 eV (C). This method causes very irregular evolution, and still does not enforce the Pauli exclusion principle.

without external illumination. However, occupations were sometimes still exceeding 2 when we included external electromagnetic field. Therefore, it is not sufficient for all the cases we wanted to explore and we continued to look for another solution of the problem.

Finally, we took the attempt which is mentioned in the main part of the thesis, in Section 3.4. It consists in choosing a particular expression for $\tilde{\rho}$ in Eq. 3.9. Normally, one should use just $\tilde{\rho} = \rho$. We tried to substitute the usual formula with one which leads to a similar type of dissipation as the phenomenological approach, i.e. $\tilde{\rho} = \rho - \rho^{sc}$. This method has solved the problem of occupations which exceed the value of 2, while still working well to model spontaneous emission in the system. We tested this solution numerically for a great deal of hybrid systems and did not encounter any case which would break the Pauli principle.

Appendix B

Eigenstate distribution for zigzag-edged nanoflakes and with phase factor included

This Appendix contains figures which present the probability amplitudes that the electron of a given eigenstate (energy) is located at given sites in real space. In the main text, in Figs. 4.6 to 4.8 absolute values of the amplitudes are shown for armchair-edged triangles. Here, we present absolute values of the probability amplitudes for zigzag-edged nanoflakes. We also show the armchair-edged amplitudes including their sign.
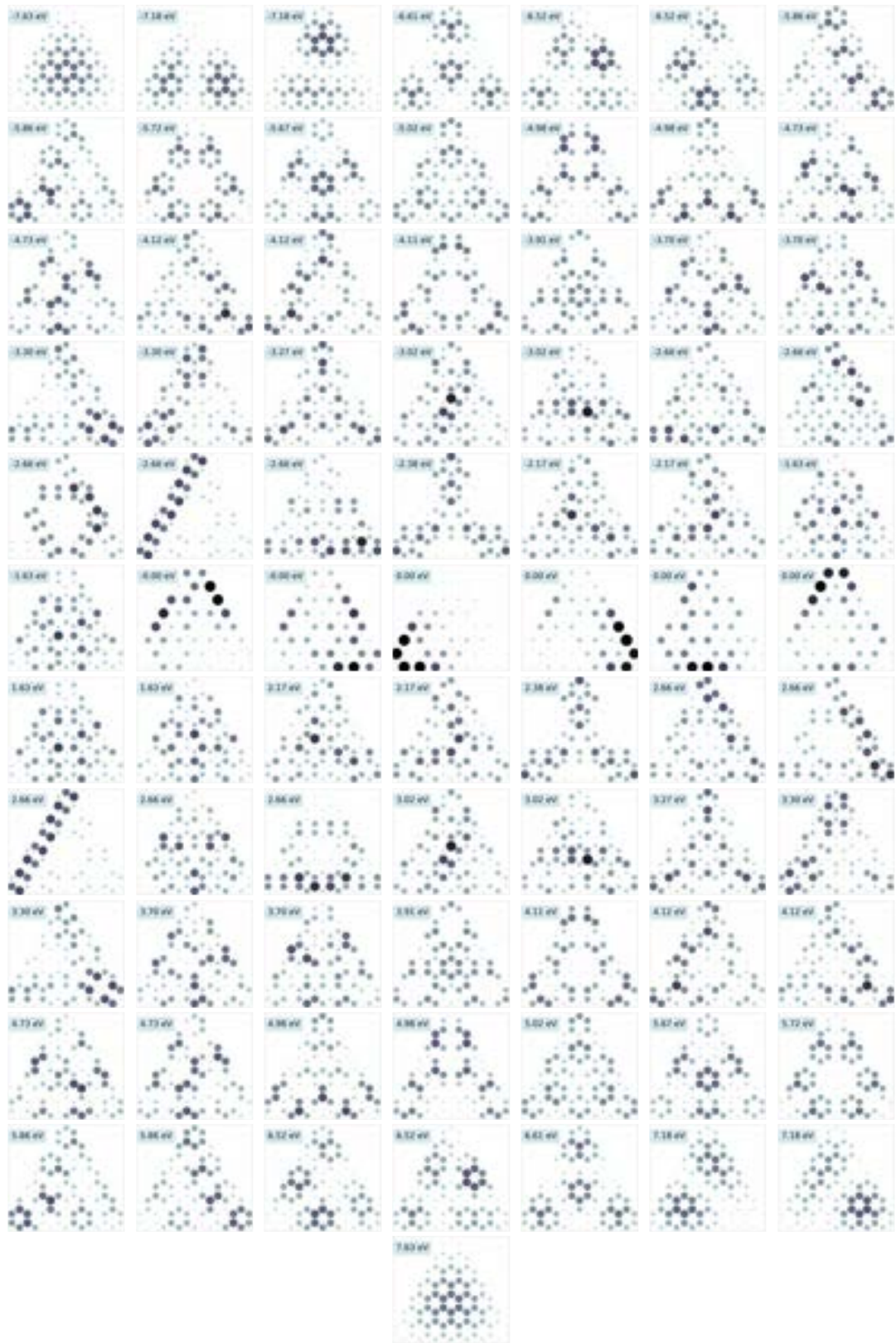
Figure B.1: Distribution on sites in real space of eigenstates of a 78-atom (1.48 nm) zigzag-edged triangular graphene nanoflake. The phase factor is neglected for clarity.
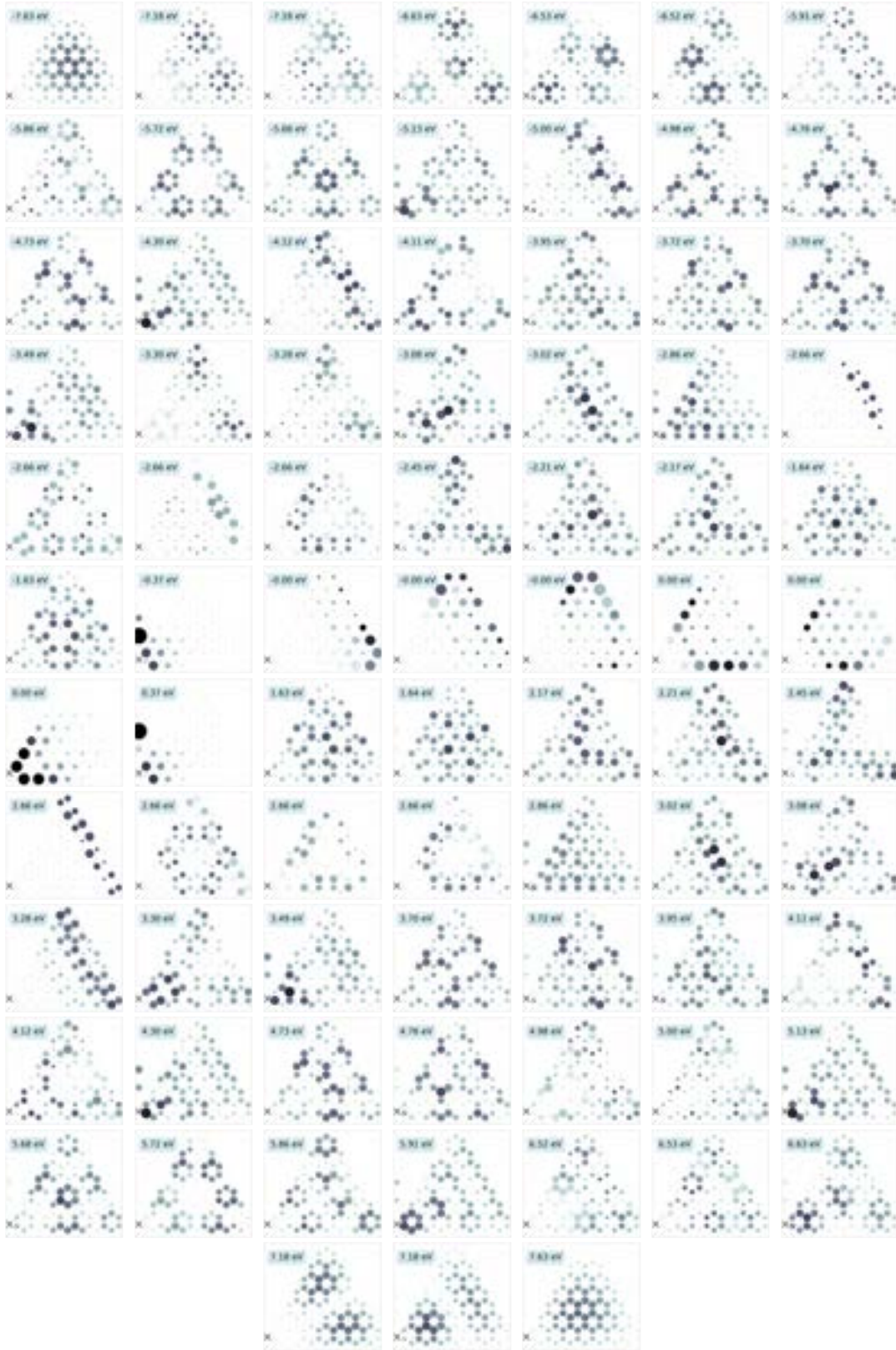
Figure B.2: Distribution on sites in real space of eigenstates of a 78-atom (1.48 nm) zigzag-edged triangular graphene nanoflake with an adatom attached in the lower-left corner of the nanoflake (location denoted with an X mark) with coupling strengths $t_e = t_g = 2\,\mathrm{eV}$. The phase factor is neglected for clarity.
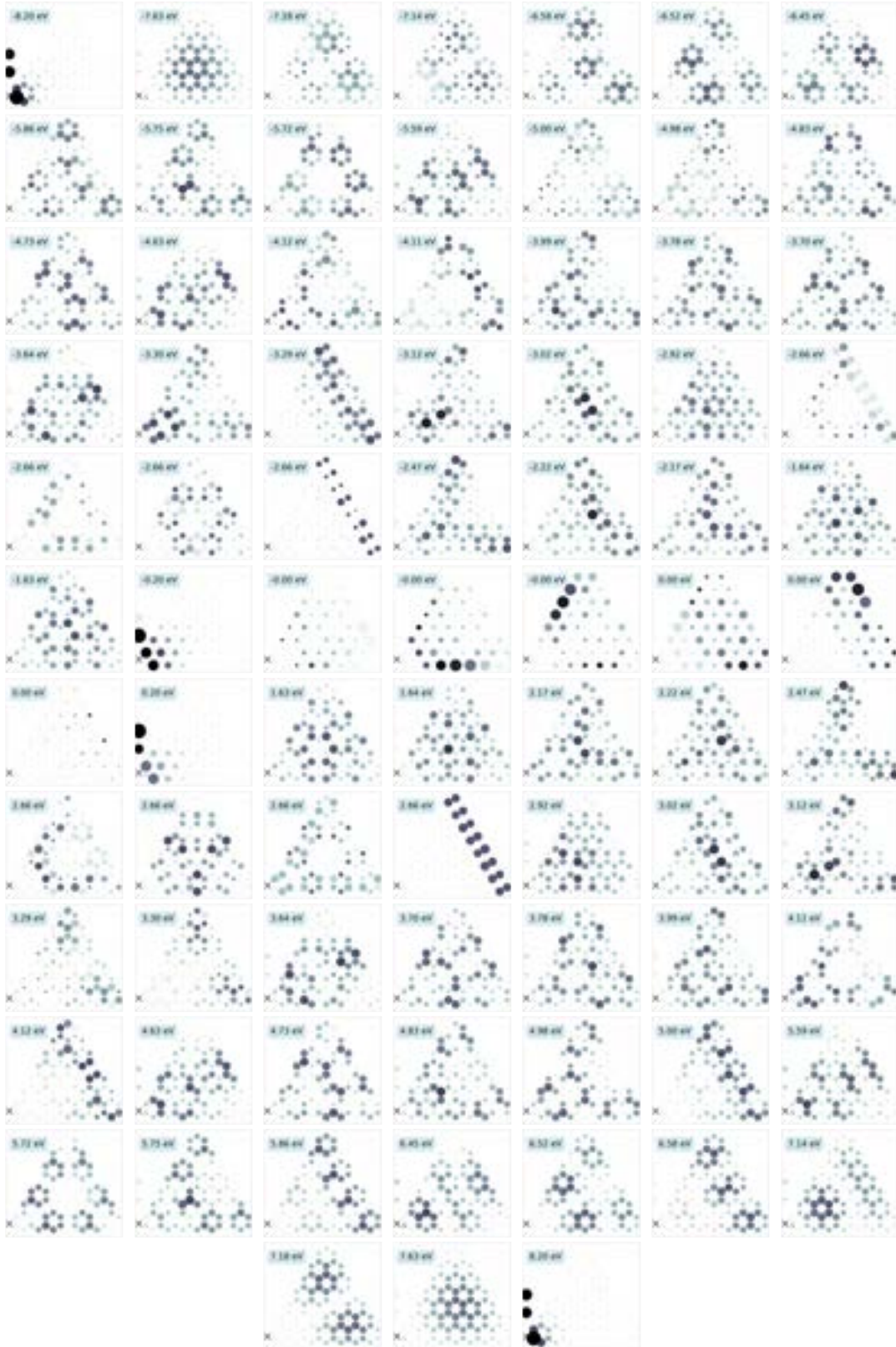
Figure B.3: Distribution on sites in real space of eigenstates of a 78-atom (1.48 nm) zigzag-edged triangular graphene nanoflake with an adatom attached in the lower-left corner of the nanoflake (location denoted with an X mark) with coupling strengths $t_e = t_g = 5\,\text{eV}$. The phase factor is neglected for clarity.
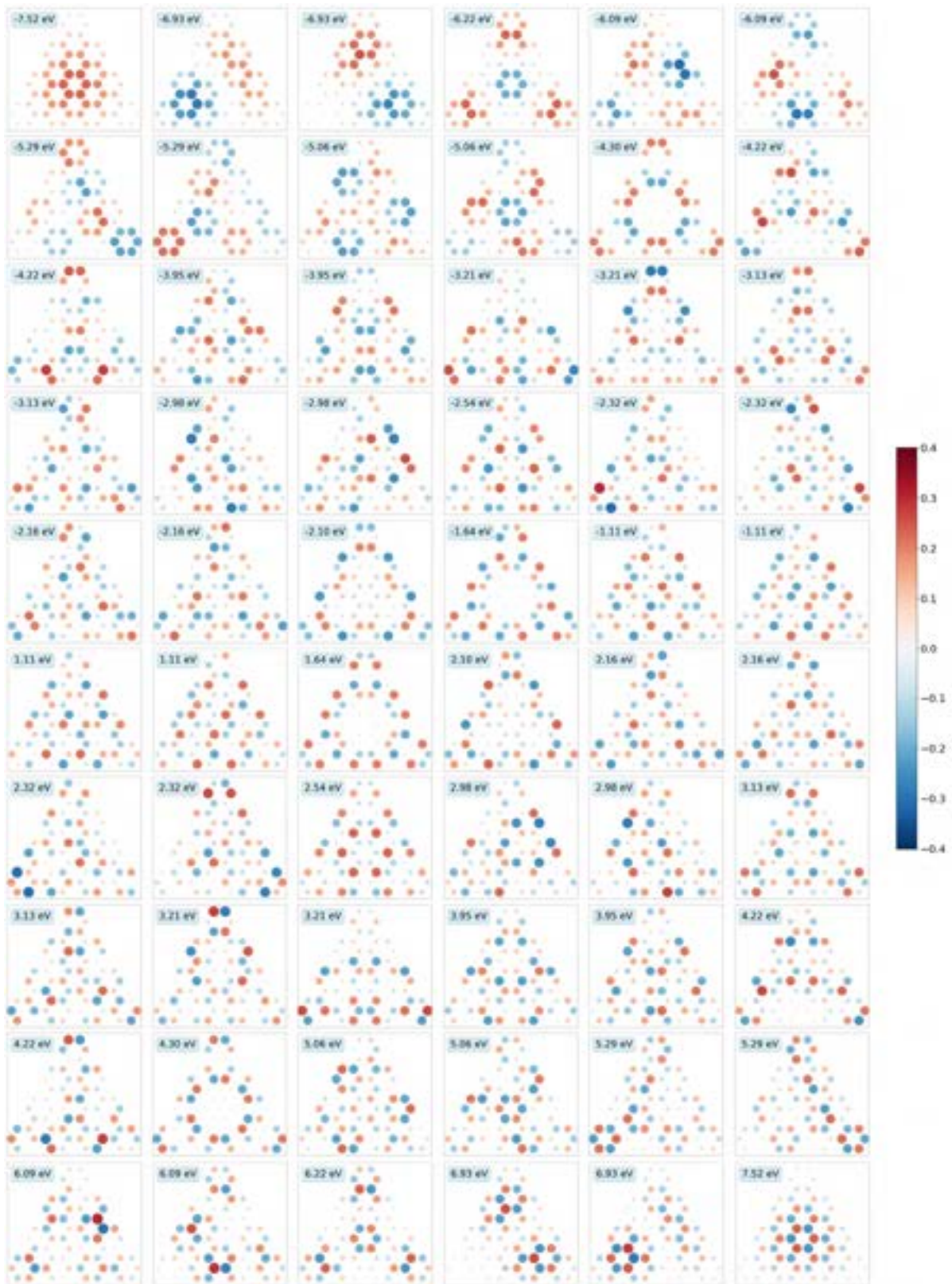
Figure B.4: Distribution on sites in real space of eigenstates of a 60-atom (1.56 nm) armchair-edged triangular graphene nanoflake.
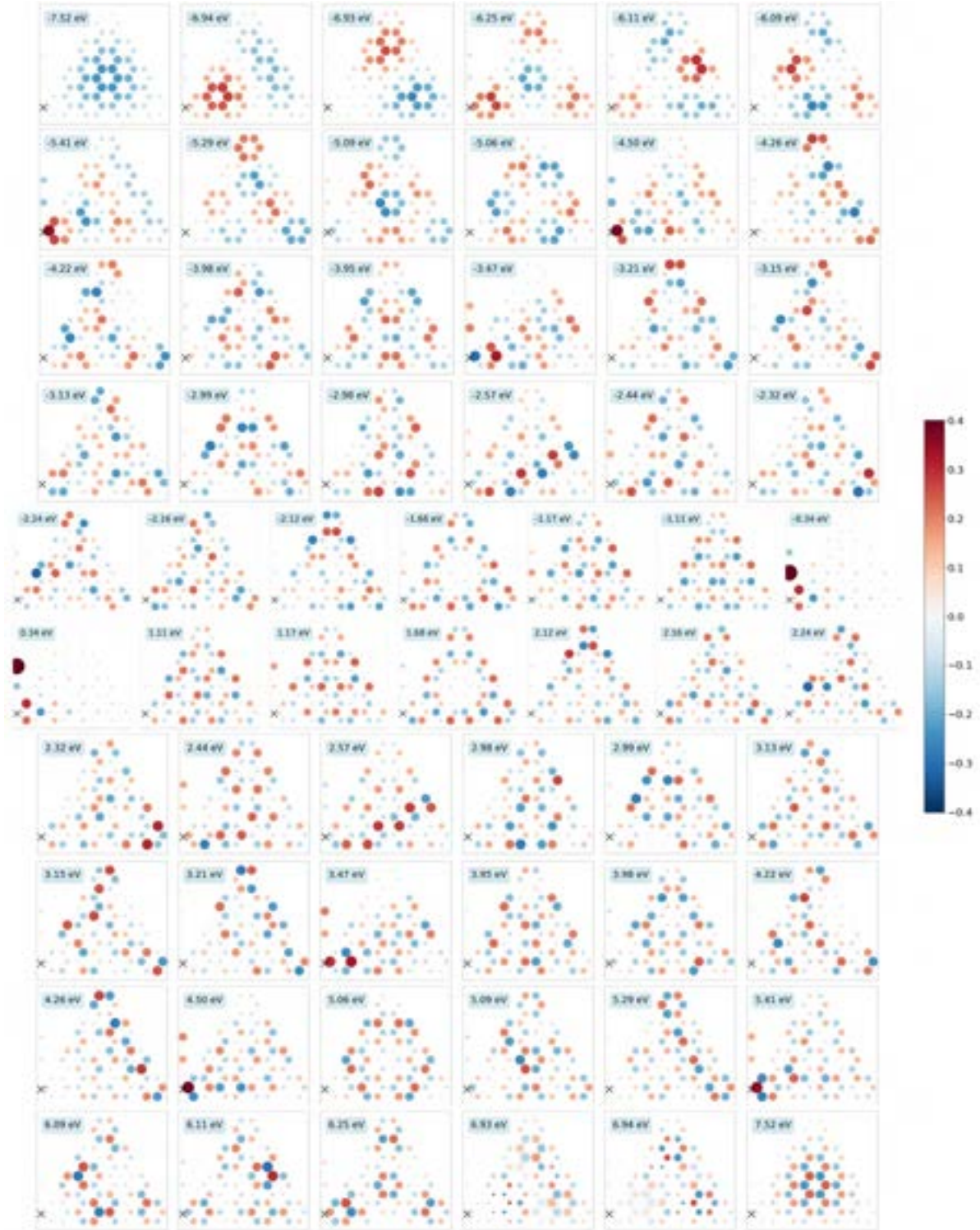
Figure B.5: Distribution on sites in real space of eigenstates of a 60-atom (1.56 nm) armchair-edged triangular graphene nanoflake with an adatom attached in the lower-left corner of the nanoflake (location denoted with an X mark) with coupling strengths $t_e = t_g = 2\,\mathrm{eV}$.
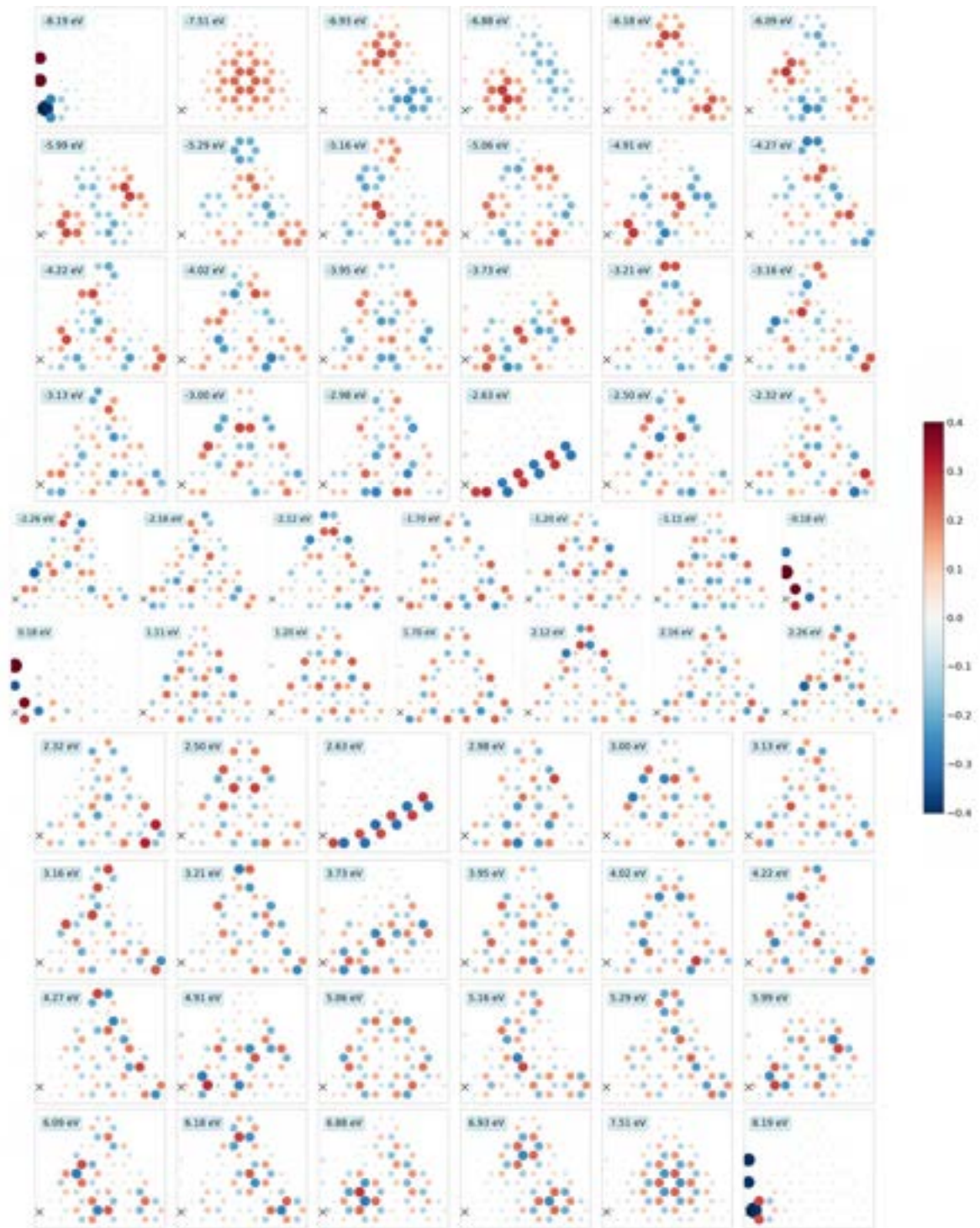
Figure B.6: Distribution on sites in real space of eigenstates of a 60-atom (1.56 nm) armchair-edged triangular graphene nanoflake with an adatom attached in the lower-left corner of the nanoflake (location denoted with an X mark) with coupling strengths $t_e = t_g = 5\,\mathrm{eV}$.

Appendix C

Numerical implementation of the framework: GRANAD toolbox manual

The entire framework presented in the thesis has been implemented in the Python programming language as a scientific toolbox. The code is freely available upon request from the author of this thesis. Figure C.1 contains a diagram which presents all modules of the toolbox together with the information about the classes and functions that are stored in each of them. Further below, we provide a manual in the form of simple usage examples. Each example consists of a short description of the used modules, code snippets with comments and a presentation of the expected results.
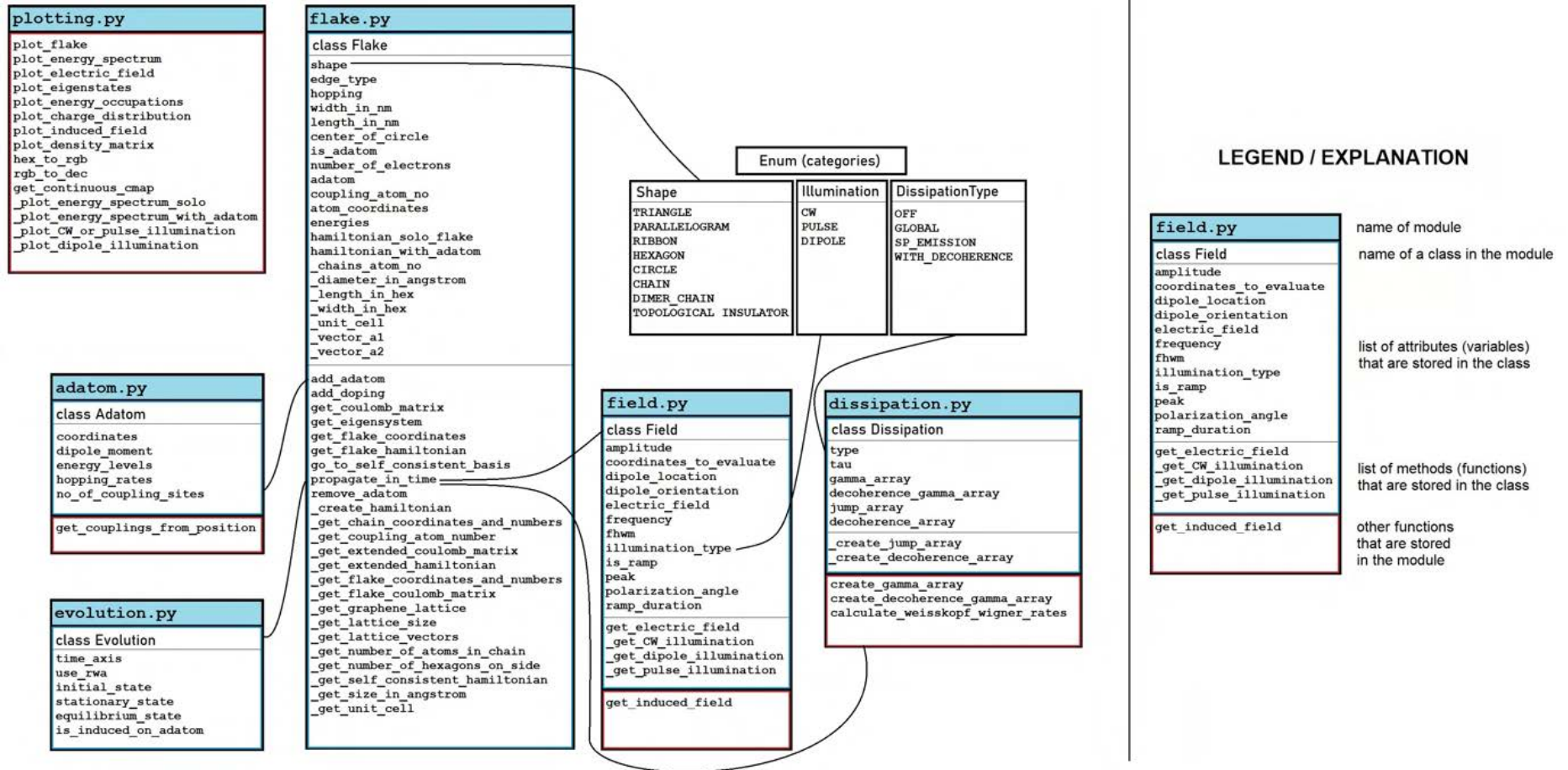
Figure C.1: A schematic representation of the GRANAD toolbox showing all of its modules, together with the information about classes and functions that are stored in each of them.

```python
from utils.flake import Flake
from utils.categories import Shape
from utils.plotting import plot_flake
```

Example 1: Setting up graphene nanoflakes

Example 1.1. Initialize a graphene flake
Example 1.2. Adding doping to the graphene flake

We will start with constructing a graphene flake.

First, you need to specify the parameters of the graphene flake you want to construct.

The `shape` and `width_in_nm` arguments are mandatory, others have default values as follows:

```
length_in_nm = None,
edge_type = 'ac',
center_of_circle = 'c_b',
hopping = -2.66,
verbose = True
```

Most shapes (the triangle, hexagon, circle, ribbon, chain, dimer chain, topological insulator) are parametrized only by one size parameter: `width_in_nm`.

If you choose one of these shapes, the value of `length_in_nm` will be ignored.

For a parallelogram you have to provide both the `width_in_nm` and the `length_in_nm`.

For a hexagon, please note that integer values of `width_in_nm` work best (other values might give distorted hexagons).

For a circle, you can choose the center of circle to positioned in the center of a hexagon (`h`), between two neighbouring atoms (`c-c`) or over an atom of a chosen sublattice (`c_a` or `c_b`).

The shape has to be a member of the `Shape` enum class. Available shapes and corresponding available arguments for each are:

```
Shape.TRIANGLE - width_in_nm, edge_type
Shape.PARALLELOGRAM - width_in_nm, length_in_nm, edge_type
Shape.RIBBON - width_in_nm, edge_type
Shape.HEXAGON - width_in_nm, edge_type
Shape.CIRCLE - width_in_nm, center_of_circle
Shape.CHAIN - width_in_nm
Shape.DIMER_CHAIN - width_in_nm
Shape.TOPOLOGICAL_INSULATOR - width_in_nm
```

and they can also be found in /utils/categories.py

Example 1.1. Initialize a graphene flake

Calling `Flake()`, will create the geometry, Hamiltonian of the flake and calculate the eigenvectors and corresponding energies.
At initialization the flake will have the following properties:

```
shape, length_in_nm, width_in_nm, hopping, edge_type, center_of_circle, is_adatom,
atom_coordinates, atom_numbers, atom_types, number_of_electrons,
hamiltonian_solo_flake, energies, eigenvectors, degeneracies
```

To see the current properties of a flake stored under `flake_1`, execute:

```
print(vars(flake_1).keys())
```

The recommended use of the programme is to **only use these properties to read values**, not to set them manually. If you want to modify the state of the flake, it is recommended to use corresponding built-in methods. For example, instead of manually changing `flake.number_of_electrons` one should run `flake.add_doping(10)` to increase the number of electrons by 10 (negative values for lowering the number of electrons are also allowed). Similarly, to include the adatom, you should not manually change the

property `flake.is_adatom` to True, but rather use the `flake.add_adatom()` method. This will be demonstrated in the next notebook (example02_include_adatom.ipynb).

```
In [2]:  flake_params = {'shape': Shape.TRIANGLE, 'width_in_nm': 1.5,
                         'edge_type': 'ac', 'center_of_circle': 'c_a',
                         'hopping':-2.66, 'verbose':True }
         flake_1 = Flake(**flake_params)

         print(f'\nThe properties of the flake at initializaiton are {vars(flake_1).keys()}.')

         plot_flake(flake_1)
```

A triangular flake has been cut from the lattice. The measured sidelength is 15.62 Angstrom.
There are 60 atoms in the flake. Number of atoms of type A = 30 and type B = 30.
In the Hamiltonian, 156 out of 3600 elements are nonzero.

The properties of the flake at initializaiton are dict_keys(['shape', 'length_in_nm', 'width_in_nm', 'hopping', 'edge_type', 'center_of_circle', 'is_adatom', '_unit_cell', '_vector_a1', '_vector_a2', '_length_in_hex', '_width_in_hex', 'atom_coordinates', 'atom_numbers', 'atom_types', 'hamiltonian_solo_flake', 'number_of_electrons', 'energies', 'eigenvectors', 'degeneracies']).
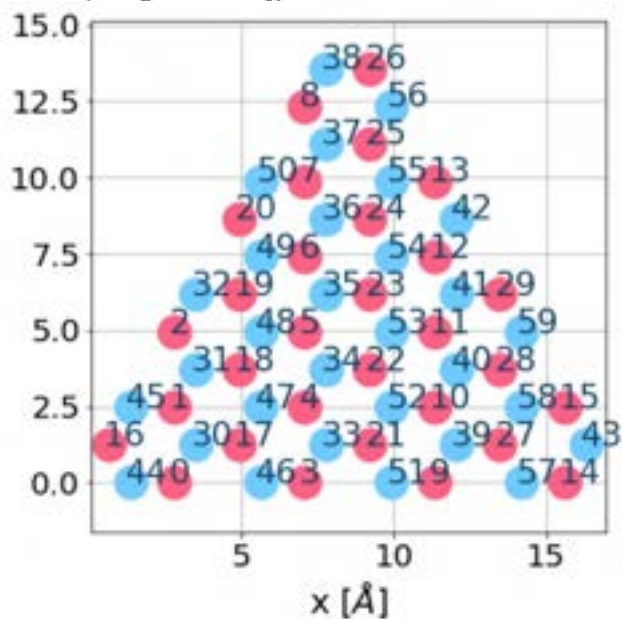
You can also call `Flake()` by specyfing the arguments directly in the function call.

```
In [3]:  flake_2 = Flake(Shape.HEXAGON, 2)
         plot_flake(flake_2)
```

A hexagonal flake has been cut from the lattice. The maximum width is 21.30 Angstrom.
There are 133 atoms in the flake. Number of atoms of type A = 67 and type B = 66.
In the Hamiltonian, 366 out of 17689 elements are nonzero.
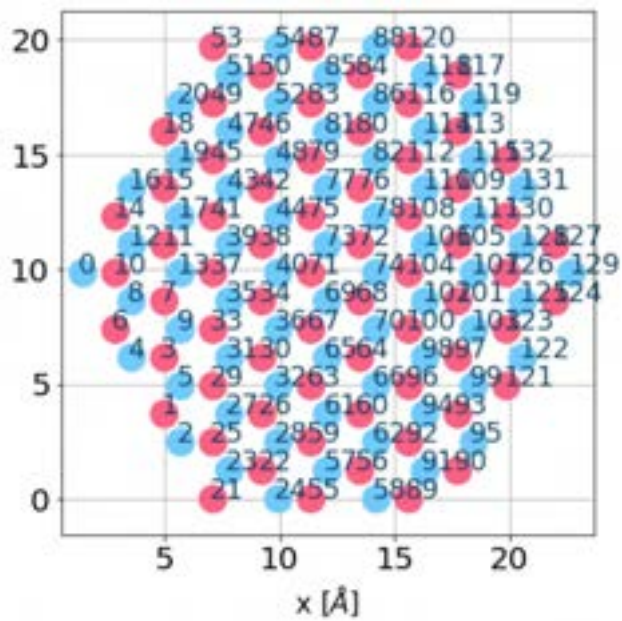
If you want to suppress printing the text information, use the `verbose = False` option.

```
In [4]: flake_3 = Flake(Shape.PARALLELOGRAM, 1, 2,
                        edge_type = 'only_zz', verbose = False)
        plot_flake(flake_3)
```
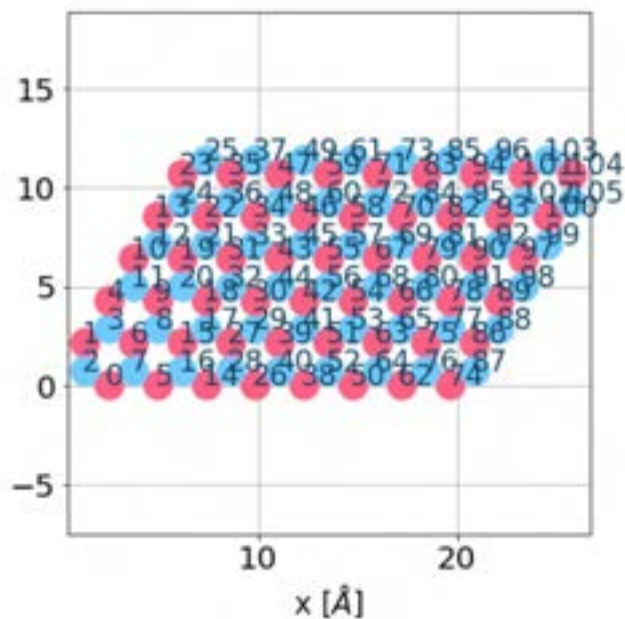

In dimer chains and topological insulators we have two different hopping values: $t_{strong} = 1.3t = 3.458$ eV and $t_{weak} = 0.7t = 1.862$ eV.

In the plots of these structures, one can see lines connecting pairs of atoms.

The thickness of these lines corresponds to the hopping strength between the atoms (thicker line means a larger hopping value).

```
In [5]: flake_4 = Flake(Shape.TOPOLOGICAL_INSULATOR, 2, verbose = False)
        plot_flake(flake_4, font_size=100)
```
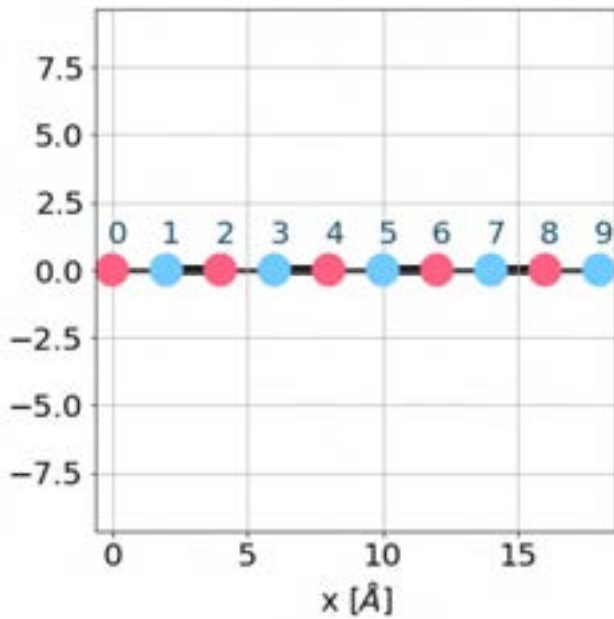
You can customize the flake plots with additional arguments:

- color,
- show_labels (determines if the numbers of atoms are shown),
- grid,
- figsize,
- fontsize,
- atom_size.

In [6]:
```python
flake_6 = Flake(Shape.TRIANGLE, 1.5)
plot_flake(
    flake_6,
    color='#154360',
    show_labels=False,
    grid=False,
    figsize=(5,5),
    font_size = 16,
    atom_size = 1100)
```

A triangular flake has been cut from the lattice. The measured sidelength is 15.62 Angstrom.
There are 60 atoms in the flake. Number of atoms of type A = 30 and type B = 30.
In the Hamiltonian, 156 out of 3600 elements are nonzero.
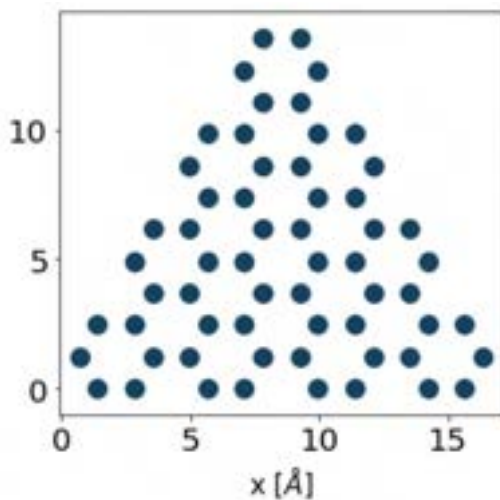
Example 1.2. Adding doping to the graphene flake

Now, we will demonstrate how to add or remove electrons from the flake.

You can **add** electrons (positive number means we increase the number of electrons) **or remove** electrons from the flake.

Note that the total number of electrons should not exceed 2 electrons per site,

so if you try to add to many electrons, the code will throw an exception.

```python
flake_2 = Flake(Shape.HEXAGON, 1)

print(f'\nThe number of electrons in the flake initially is {flake_2.number_of_electrons}.')
flake_2.add_doping(20)
print(f'The number of electrons in the flake after adding 20 electrons is {flake_2.number_of_electrons}.')
flake_2.add_doping(-10)
print(f'The number of electrons in the flake after removing 10 electrons is {flake_2.number_of_electrons}.')
flake_2.add_doping(100)
```

```
A hexagonal flake has been cut from the lattice. The maximum width is 9.94 Angstrom.
There are 34 atoms in the flake. Number of atoms of type A = 17 and type B = 17.
In the Hamiltonian, 86 out of 1156 elements are nonzero.

The number of electrons in the flake initially is 34.
The number of electrons in the flake after adding 20 electrons is 54.
The number of electrons in the flake after removing 10 electrons is 44.
```

```
In [1]:  from utils.flake import Flake
         from utils.adatom import Adatom, get_couplings_from_position
         from utils.categories import Shape
         from utils.plotting import plot_flake
```

Example 2: Attaching an adatom

Example 2.1. Attaching an adatom to the graphene flake (fixed hopping rates)
Example 2.2. Attaching the adatom with hoppings determined from its position

---

In this example, we will see how to attach an adatom to the graphene flake.

First, we need to initialize a graphene flake, as shown in Example 1.1.

```
In [2]:  flake_params = {'shape': Shape.TRIANGLE, 'width_in_nm': 1.5,
                         'edge_type': 'ac', 'hopping':-2.66, 'verbose': False }
         flake_1 = Flake(**flake_params)
```

Next, we need to create an adatom object using the `Adatom` class.

To couple the adatom to the flake, use the flake's `add_adatom` method. The parameters of the adatom are:

- `energy_levels` - list of the energies of the adatom's states (levels) in eV
- `hopping_rates` - hopping values between the flake and the energy levels in eV: `hopping_rates[0]` contains the hopping rate between the flake and the adatom state which has energy `energy_levels[0]`. The hopping_rates can be defined manually to some constant value as shown in Example 2.1. or they can be determined from the adatom's position using the function `get_couplings_from_position` (this is demonstrated in Example 2.2).
- `coordinates` - the coordinates of the adatom in the XY plane. In our model we assume that the adatom lies in the same plane as the graphene flake, however please note that this is just and approximation and in general not true. In reality, the adatom is located close to the flake's surface but slightly above it.
- `dipole_moment` - transition dipole moment between the two adatom states.

Please note that after adding an adatom, some of the properties will generalize to describe the entire system, whereas others remain the properties of the flake. New properties will also get created. Specifically:

- `is_adatom` will become True when the adatom is present
- `coupling_atom_no` will store the number of the carbon atom in graphene which is the nearest neighbour of the adatom, in our model we always assume that the adatom only couples to ONE particular graphene site (to the nearest one)
- `hamiltonian_solo_flake` will contain the Hamiltonian of the solo flake, whereas `hamiltonian_with_adatom` will contain the Hamiltonian of the entire hybrid flake+adatom system
- `energies, eigenvectors, degeneracies, number_of_electrons` will contain the values for the entire hybrid flake+adatom system
- `atom_coordinates, atom_numbers, atom_types` will contain the coordinates, atom numbers and atom types of the solo flake only

Example 2.1. Attaching an adatom to the graphene flake (fixed hopping rates)

```
In [3]:  adatom_params = {
             'energy_levels': [1,-1],
             'hopping_rates': [2.0, 2.0],
             'coordinates': [3,8],
             'dipole_moment' : (0,1,0)}
         adatom_1 = Adatom(**adatom_params)
         flake_1.add_adatom(adatom_1)
         plot_flake(flake_1)
```
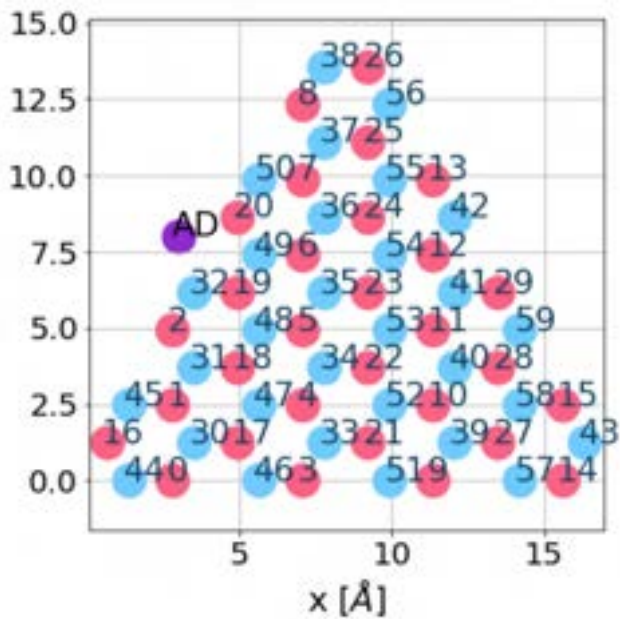
To remove the adatom, you can use the `remove_adatom` method. This will set:

```
self.is_adatom = False
self.adatom = None
self.coupling_atom_no = None
self.hamiltonian_with_adatom = None
```

and revert the values of `energies`, `eigenvectors`, `degeneracies`, `number_of_electrons` to the values for the solo flake.

To obtain the same effect, you can also just re-initialize the flake.

```
In [4]:  flake_1.remove_adatom()
         plot_flake(flake_1)
```
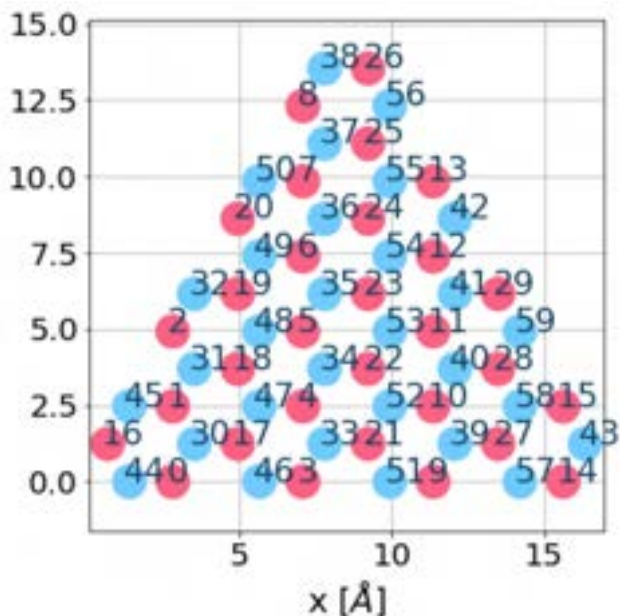

Example 2.2. Attaching the adatom with hoppings determined from its position

To obtain hopping rates based on the distance between the adatom and the nearest carbon atom in the flake, we first need to construct the geometry of the system.
Therefore, the first step is to create a Flake and an Adatom (with arbitrary hopping rates in the first place).

Then, we can determine the hopping rates from position using the function `get_couplings_from_position`.

Finally, we recreate the Adatom object using the newly obtained hopping rates and attach this adatom to the flake.

In [5]:
```python
flake_params = {'shape': Shape.TRIANGLE, 'width_in_nm': 1.5, 'edge_type': 'ac'}
flake_2 = Flake(**flake_params)

# First create the geometry of the system using some arbitrary values
# for the hopping rates, e.g. [0, 0]:
adatom_params = {'energy_levels': [1,-1], 'hopping_rates': [0, 0],
                 'coordinates': [3,8], 'dipole_moment' : (0,1,0)}
adatom_2 = Adatom(**adatom_params)
flake_2.add_adatom(adatom_2)
print('Hopping rates at initialization: ')
print(adatom_2.hopping_rates)

# Now, calculate the hopping rates based on the distance
# between the adatom and the nearest carbon atom in the flake.
atom_carbon_couplings = get_couplings_from_position(
    flake_2.coupling_atom_no, adatom_2.coordinates,
    flake_2.atom_coordinates, flake_2.hopping)

# Finally, create an adatom with the distance-based hopping rates.
adatom_params = {'energy_levels': [1,-1], 'hopping_rates': atom_carbon_couplings,
                 'coordinates': adatom_2.coordinates, 'dipole_moment': (0,1,0)}
adatom_2 = Adatom(**adatom_params)
flake_2.add_adatom(adatom_2)
print('Hopping rates found based on the flake-adatom distance: ')
print(adatom_2.hopping_rates)
```

```
A triangular flake has been cut from the lattice. The measured sidelength is 15.62 Angstrom.
There are 60 atoms in the flake. Number of atoms of type A = 30 and type B = 30.
In the Hamiltonian, 156 out of 3600 elements are nonzero.
Hopping rates at initialization:
[0, 0]
Hopping rates found based on the flake-adatom distance:
[-1.4401706768789142, -1.4401706768789142]
```

```
In [1]:  import numpy as np
         from utils.categories import Illumination, Shape
         from utils.field import Field
         from utils.flake import Flake
         from utils.plotting import plot_electric_field
```

Example 3: Setting up external electric field (illumination)

To define an external illumination, you have to provide four mandatory arguments: `time_axis, illumination_type, frequency, amplitude`.

The time_axis can be created as a `numpy` linspace or by defining an `Evolution` object. The unit of time is $\hbar$/eV = 0.658 fs.

The `illumination_type` has to be a member of the Illumination enum and can be:

- continuous wave (`Illumination.CW`)
- Gaussian pulse (`Illumination.PULSE`)
- dipolar source (`Illumination.DIPOLE`)

The variables `frequency` and `amplitude` should contain real numbers. The amplitude unit is eV/Angstrom.

Depending on the chosen illumination type, there are many additional parameters which one can specify.

- For the continuous wave you **have to** provide a `polarization_angle` (by default set to 90), the angle is defined such that `polarization_angle=0` corresponds to x-polarized illumination and `polarization_angle=90` to y-polarized illumiation. For the CW you also **can** provide additional arguments to make the field ramp up slowly instead of turning it on suddenly. This can be achieved by setting `is_ramp = True` and then providing the point in time when the field starts to ramp up (`time_ramp`) and the `ramp_duration` .
- If you choose the Gaussian pulse you **have to** provide additional arguments, i.e. the point in time when the pulse should occur (`peak`) and the full width at half maximum of the Gaussian pulse (`fwhm`).
- For the dipole illumination you also **have to** provide additional arguments: `dipole_orientation` , `dipole_location` and `coordinates_to_evaluate` .

```
In [2]:  time_axis = np.linspace(0,20,1000)
         field_1 = Field(time_axis, Illumination.PULSE, 5, 0.01, peak = 2, fwhm = 2)
         plot_electric_field(field_1)
```
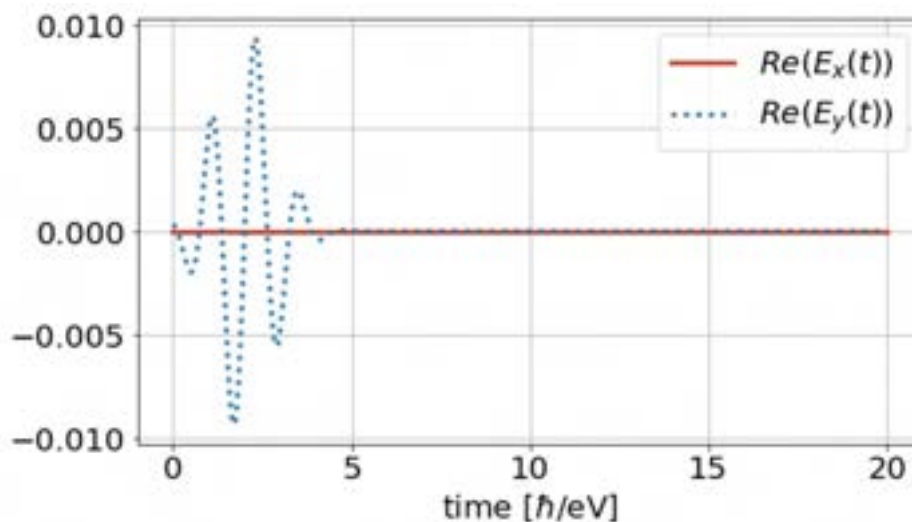
Similarly as before, you can provide the field parameters as a dictionary.

```
In [3]:  field_params = {
             'illumination_type':Illumination.CW,
             'frequency': 2,
             'amplitude': 0.01,
             'polarization_angle': 90}

         field_2 = Field(time_axis, **field_params, is_ramp=True, time_ramp=3, ramp_duration=3)
         plot_electric_field(field_2)
```
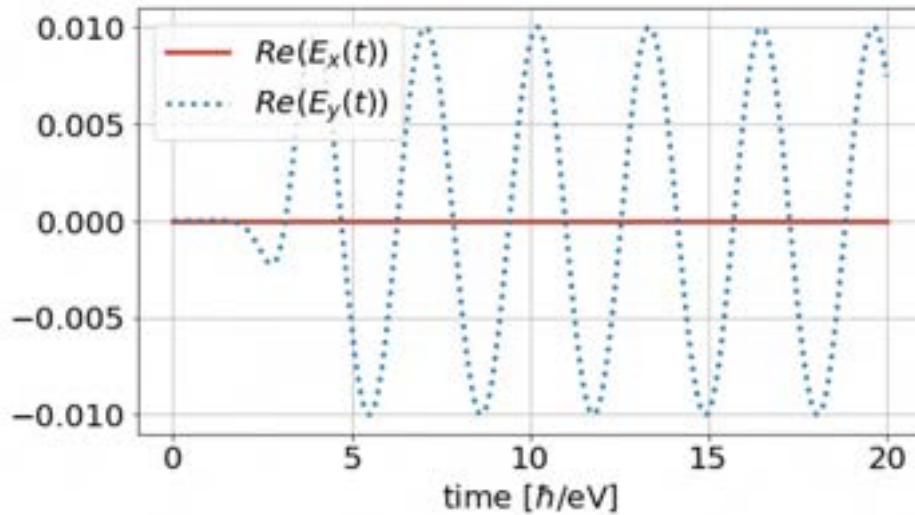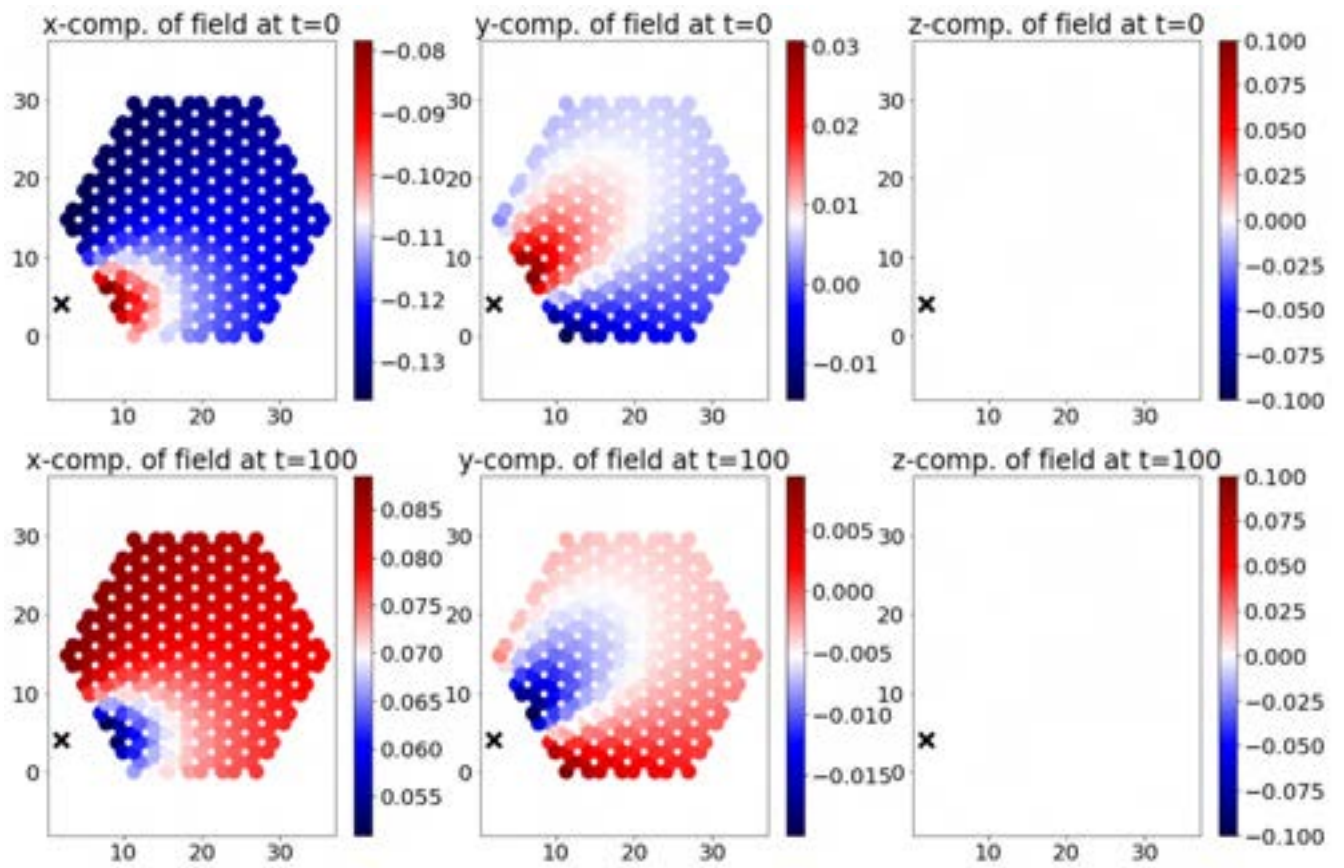

To demonstrate the dipole illumination, we need to first get a set of coordinates where the field will be evaluated, since in this case the electric field depends not only on time but also on the location in real-space. Thus, we will first construct a flake and then use its coordinates as the coordinates where the field should be evaluated.

In the plots, the black X mark indicates the location of the dipole source.

```
In [4]:  field_params = {'illumination_type':Illumination.DIPOLE,
                         'frequency': 2, 'amplitude': 0.01,
                         'dipole_orientation':'x', 'dipole_location':[2,4,0]}

         flake_1 = Flake(Shape.HEXAGON, 3)
         field_3 = Field(
             time_axis, **field_params, coordinates_to_evaluate=flake_1.atom_coordinates)
         plot_electric_field(field_3)
         plot_electric_field(field_3, at_timestep = 100)
```

A hexagonal flake has been cut from the lattice. The maximum width is 32.67 Angstrom.
There are 296 atoms in the flake. Number of atoms of type A = 148 and type B = 148.
In the Hamiltonian, 838 out of 87616 elements are nonzero.

x-comp. of field at t=0   y-comp. of field at t=0   z-comp. of field at t=0

x-comp. of field at t=100   y-comp. of field at t=100   z-comp. of field at t=100

```
In [1]:  from utils.flake import Flake
         from utils.adatom import Adatom
         from utils.categories import Shape
         from utils.plotting import plot_energy_spectrum, get_continuous_cmap

         import numpy as np
         import matplotlib.pyplot as plt
```

Example 4: Plotting eigenenergies of graphene nanoflakes and hybrid systems

Example 4.1. Energy spectrum of a pristine graphene nanoflake and a graphene nanoflake with an adatom.
Example 4.2. Shift of energy levels in a graphene nanoflake due to gradual coupling of an adatom.

___

Example 4.1. Energy spectrum of a pristine graphene nanoflake and a graphene nanoflake with an adatom.

First, we will create two identical flakes (flake_1 and flake_2) as described in Example 1.
Next, we will attach an adatom to flake_1 as shown in Example 2.
Last, we will plot the energy spectrum of both flakes to compare the flake without the adatom and with the adatom.

```
In [2]:  flake_params = {'shape': Shape.TRIANGLE, 'width_in_nm': 0.7,
                         'length_in_nm': None, 'edge_type': 'ac',
                         'center_of_circle': 'c_a', 'hopping':-2.66, 'verbose': False}
         adatom_params = {'energy_levels': [1,-1], 'hopping_rates': [4.0, 4.0],
                          'coordinates': [3,8], 'dipole_moment' : (0,1,0)}

         flake_1 = Flake(**flake_params)
         flake_2 = Flake(**flake_params)

         adatom_1 = Adatom(**adatom_params)
         flake_1.add_adatom(adatom_1)

         plot_energy_spectrum(flake_2)
         plot_energy_spectrum(flake_1)
```
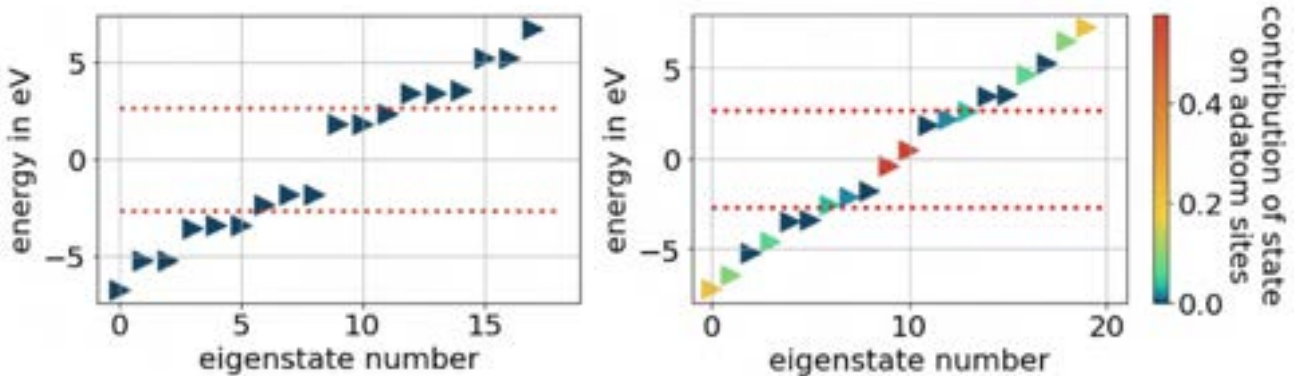

To create custom variations of the plots, you can use the standard `matplotlib` library to plot the `energies` property of the flakes.

Example 4.2. Shift of energy states due to gradual coupling of an adatom

```
In [3]:  fig = plt.figure(figsize=[5.5,6])
         iter_range = 200
         discr = 0.02

         flake_params = {'shape': Shape.TRIANGLE, 'width_in_nm': 0.7,
                         'edge_type': 'zz', 'verbose': False }

         for ratio in range(iter_range):

             atom_carbon_couplings = [discr*ratio, discr*ratio]

             adatom_params = {
                 'energy_levels': [0.25, -0.75],
                 'hopping_rates': atom_carbon_couplings,
                 'coordinates': [3,7.5],
```

```
                'dipole_moment' : (0,1,0)}
        flake_4 = Flake(**flake_params)
        adatom_4 = Adatom(**adatom_params)
        flake_4.add_adatom(adatom_4)

        adatom_contribution = np.zeros((len(flake_4.energies)))
        for i in range(len(flake_4.energies)):
            adatom_contribution[i] = np.abs(
                flake_4.eigenvectors[i][-2])**2 + np.abs(flake_4.eigenvectors[i][-1])**2

        hex_list = ['#154360', '#2874A6', '#1ABC9C', '#58D68D', '#F4D03F', '#CB4335']
        data_to_plot = flake_4.energies
        plt.scatter([atom_carbon_couplings[0]]*len(data_to_plot), data_to_plot,
                    s = 2, marker='D', c = adatom_contribution,
                    cmap=get_continuous_cmap(
                        hex_list, float_list=[0, 0.02, 0.05, 0.1, 0.3, 1]),
                    linewidths = 2, vmin=0, vmax=1)

plt.xticks([0,1,2,3,4,5,6])
plt.yticks([-8, -6, -4, -2, 0, 2, 4, 6, 8])
plt.vlines(
    0.5, np.min(data_to_plot), np.max(data_to_plot),
    linestyles = 'dotted', colors = 'k',linewidth = 2)
plt.vlines(
    2.0, np.min(data_to_plot), np.max(data_to_plot),
    linestyles = 'dotted', colors = 'k',linewidth = 2)
plt.vlines(
    3.5, np.min(data_to_plot), np.max(data_to_plot),
    linestyles = 'dotted', colors = 'k',linewidth = 2)

plt.xlabel('coupling $t_e=t_g$ (eV)')
plt.ylabel('energy (eV)')
plt.grid()
plt.colorbar()
plt.tight_layout()
plt.show()
plt.close(fig)
```
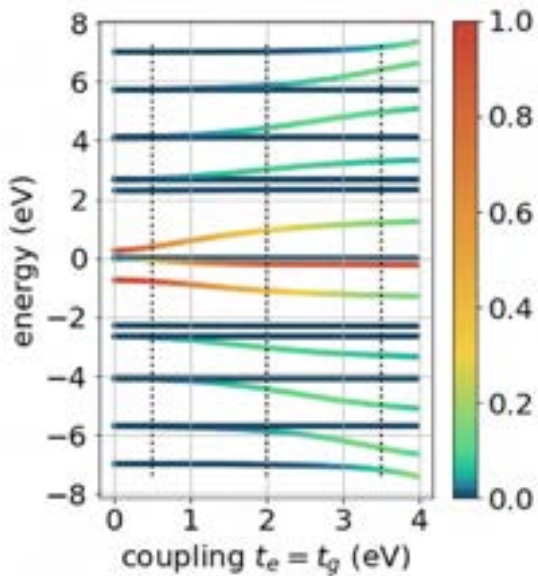
```
In [1]:  from utils.flake import Flake
         from utils.adatom import Adatom
         from utils.categories import Shape
         from utils.plotting import plot_eigenstates
```

Example 5: Distribution of eigenstates on the sites in real space

Here, we will create plots which show the distribution of eigenstates on the sites in real space.

First, we will create a triangular graphene flake as described in Example 1.
Next, we will attach an adatom to flake_1 as shown in Example 2.
Last, we will plot the eigenstate distribution in real space.

The adatom levels are always shown on the left side from the flake.

If you specify a `filename`, all the eigenstates of the flake will be saved under this filename with corresponding state numbers.
To determine how many plots will be printed out on screen, set the parameter `amount_to_show`.

```
In [2]:  flake_params = {'shape': Shape.TRIANGLE, 'width_in_nm': 2.4}
         adatom_params = {
             'energy_levels': [0.5,-0.5],
             'hopping_rates': [2.0, 2.0],
             'coordinates': [11,22],
             'dipole_moment' : (0,1,0)}

         flake_1 = Flake(**flake_params)
         adatom_1 = Adatom(**adatom_params)
         flake_1.add_adatom(adatom_1)

         plot_eigenstates(flake_1, states_to_show = [62,63])
```

```
A triangular flake has been cut from the lattice. The measured sidelength is 24.14 Angstrom.
There are 126 atoms in the flake. Number of atoms of type A = 63 and type B = 63.
In the Hamiltonian, 342 out of 15876 elements are nonzero.
```
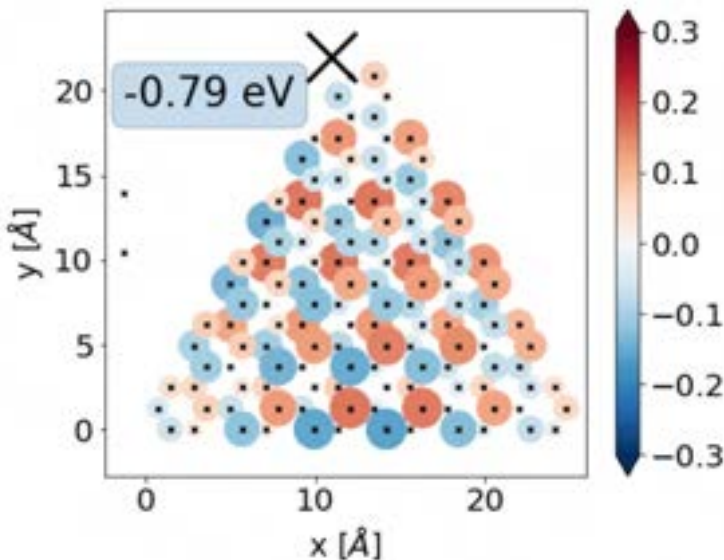
```
In [1]:   from utils.adatom import Adatom
          from utils.categories import Shape, Illumination
          from utils.evolution import Evolution
          from utils.field import Field
          from utils.flake import Flake
          from utils.plotting import plot_energy_occupations
          from utils import maths
```

Example 6: Time evolution of the graphene nanoflake + adatom system.

Now we will look at the time evolution of a graphene nanoflake coupled to an adatom with two energy levels.
Again, the parameters of both subsystems can be specified in the dictionaries below.

For the evolution, you have to specify:

- the total simulation time (`end_time`) and in how many timesteps the total evolution should be divided
  (`number_of_timesteps`) for integration etc.
- `initial_state` : the initial state for time evolution, by default "0" (the ground state of the system),
- `stationary_state` : the stationary state for dissipation, by default "0" (the ground state of the system),
- `equilibrium_state` : the equilibrium state with respect to which the induced potential at each timestep is calculated by default
  "0" (the ground state of the system),
- `use_rwa` : whether the Rotating-Wave Approximation should be used,
- `is_induced_on_adatom` : whether the field induced (scattered back) from the flake should be added on the adatom site. This
  option will be important for calculating the spontaneous emission with the Green's tensor method.

The initial, stationary and equilibrium state can be chosen from the integers 0-9, which are defined as presented below.
0: ground state, no transition excited
1: HOMO - LUMO excited
2: HOMO - (LUMO+1) excited
3: HOMO - (LUMO+2) excited
4: (HOMO-1) - LUMO excited
5: (HOMO-1) - (LUMO+1) excited
6: (HOMO-1) - (LUMO+2) excited
7: (HOMO-2) - LUMO excited
8: (HOMO-2) - (LUMO+1) excited
9: (HOMO-2) - (LUMO+2) excited

```
In [2]:   flake_params = {'shape': Shape.TRIANGLE, 'width_in_nm': 0.7,
                          'length_in_nm': 0.7, 'edge_type': 'ac', 'verbose': False}

          adatom_params = {'energy_levels': [0.5,-0.5], 'hopping_rates': [2.0, 2.0],
                           'coordinates': [3, 7.5], 'dipole_moment' : (0,7.5,0)}

          field_params = {'illumination_type' : Illumination.CW, 'frequency': 2,
                          'amplitude': 0.05, 'polarization_angle': 90}

          evolution_params = {'end_time': 50, 'number_of_timesteps': 500_000,
                              'initial_state': 0, 'stationary_state': 0, 'equilibrium_state': 0,
                              'use_rwa': True, 'is_induced_on_adatom': True}
```

To see Rabi oscillations between the two adatom levels, we have to make sure that we illuminate the structure with a resonant
frequency, i.e. with a frequency which is equal to the energy difference between the two levels which have the largest contribution on
the adatom sites. This is made by first getting the adatom levels' indices (`excited_idx` and `ground_idx`) and then setting the
frequency to the difference of corresponding energies:

```
excited_idx, ground_idx = maths.get_adatom_states_index(flake_1.energies, flake_1.eigenvectors)
field_params['frequency'] = flake_1.energies[excited_idx] - flake_1.energies[ground_idx]
```

```
flake_1 = Flake(**flake_params)
adatom_1 = Adatom(**adatom_params)
flake_1.add_adatom(adatom_1)

excited_idx, ground_idx = maths.get_adatom_states_index(
    flake_1.energies, flake_1.eigenvectors)
field_params['frequency'] = flake_1.energies[excited_idx] - flake_1.energies[ground_idx]

evolution_1 = Evolution(**evolution_params)
field_1 = Field(evolution_1.time_axis, **field_params)

site_occupation, energy_occupation, *_ = flake_1.propagate_in_time(
    evolution_1, field_1, print_iterations = 100_000)
```
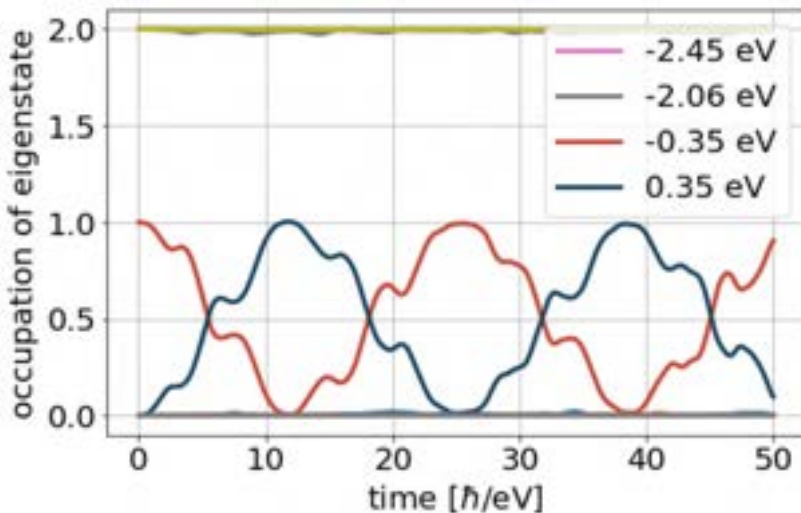
```
------------------------------------------------------------
****** TIME: 0/500000
Working fine, timestep: 10.
------------------------------------------------------------
****** TIME: 100000/500000
------------------------------------------------------------
****** TIME: 200000/500000
------------------------------------------------------------
****** TIME: 300000/500000
------------------------------------------------------------
****** TIME: 400000/500000
This run took 250.87591767311096 seconds
```

```
plot_energy_occupations(
    energy_occupation, evolution_1.time_axis, flake_1.energies,
    ground_index = ground_idx, excited_index = excited_idx,
    plotting_threshold=0.025, figsize=(8,5))
```


To obtain a simpler picture, we could look at the case where the Coulomb interaction is neglected by setting the argument `coulomb_strength=0`. This will allow us to see just "pure" Rabi oscillations, without the beating (some additional frequencies), which are caused by Coulomb interactions in the flake. We could also fix the frequency to an off-resonant value to see detuned behaviour.

```
In [1]:  from utils.adatom import Adatom
         from utils.categories import Shape, Illumination, DissipationType
         from utils.dissipation import Dissipation, create_gamma_array, create_decoherence_gamma_array
         from utils.evolution import Evolution
         from utils.flake import Flake
         from utils.plotting import plot_energy_occupations
         from utils import maths
```

Example 7: Dissipation in the graphene nanoflake+adatom system.

Example 7.1. Including dissipation with a phenomenological damping term.
Example 7.2. Including dissipation with Lindblad operators.

The dynamics of the hybrid system is described via the single-electron master equation

$$\frac{\partial}{\partial t}\rho(t) = -\frac{i}{\hbar}[H(\rho(t),t),\rho(t)] - \mathcal{D}[\rho(t)] \tag{1}$$

The Hermitian Hamiltonian accounts for the reversible processes in the system, with the nonlinearity related to the inclusion of the Coulomb interactions. Dissipation effects can be taken into account in the term $\mathcal{D}[\rho(t)]$, which we consider in one of the two forms described below and refer to as *phenomenological* and *Lindblad* approaches.

This notebook presents how one can include dissipation in the modeled system. There are two ways in our model in which one can describe decay in the system:

1. The phenomenological approach (`DissipationType.GLOBAL`) : It is a simple robust way to generate dissipation in the system. It only needs two parameters. For more details, see example 7.1 below.
2. The Lindblad method: A more complex treatment of dissipation with the use of quantum-mechanical Lindblad operators. We can use only jump operators, which will cause spontaneous emission (`DissipationType.SP_EMISSION`) or we can include both jump and decoherence operators, which will generate both spontaneous emission and decoherence of the diagonal elements (`DissipationType.WITH_DECOHERENCE`). For more details, see example 7.2 below.

Example 7.1. Including dissipation with a phenomenological damping term.

The phenomenological damping term has a relatively simple form and interpretation:

$$\mathcal{D}[\rho(t)] = \frac{1}{2\tau}(\rho(t) - \rho^{sc}). \tag{2}$$

First, we need to create a flake (see notebook `example01_initialize_flakes.ipynb`).
Next, we will create an adatom and couple it to the flake (see notebook `example02_include_adatom.ipynb`).
Then, we will define an external field (see notebook `example03_set_up_and_plot_electric_field.ipynb`).
Finally, we need to define the parameters of the time evolution (see notebook `example06_rabi_oscillations.ipynb`).

In the four dictionaries in the next cell, we can specify all the parameters of the flake, adatom, field and evolution.

```
In [2]:  flake_params = {'shape': Shape.TRIANGLE, 'width_in_nm': 0.7,
                         'edge_type': 'ac', 'verbose': False}

         adatom_params = {'energy_levels': [0.5,-0.5], 'hopping_rates': [2.0, 2.0],
                          'coordinates': [0,1], 'dipole_moment' : (0,7.5,0)}

         field_params = {'illumination_type' : Illumination.CW, 'frequency': 2,
                         'amplitude': 0.05, 'polarization_angle': 90}

         evolution_params = {'end_time': 0.1, 'number_of_timesteps': 1_000,
                             'initial_state': 1, 'stationary_state': 0, 'equilibrium_state': 0,
                             'use_rwa': True, 'is_induced_on_adatom': True}
```

Next, we will need to specify parameters of the dissipation. In the case of phenomenological dissipation we only need to specify one parameter;

- `tau` - mandatory, the rate of decay.

In [3]:
```python
dissipation_params = {
    'type': DissipationType.GLOBAL,
    'tau': 0.2
    }
```

Next we run an evolution without external field but with the defined dissipation.

In [4]:
```python
flake_1 = Flake(**flake_params)
adatom_1 = Adatom(**adatom_params)
flake_1.add_adatom(adatom_1)

evolution_1 = Evolution(**evolution_params)
dissipation_1 = Dissipation(flake_1, **dissipation_params)

site_occupation, energy_occupation, *_ = flake_1.propagate_in_time(
    evolution_1, None, dissipation_1, print_iterations = 1_000)
```
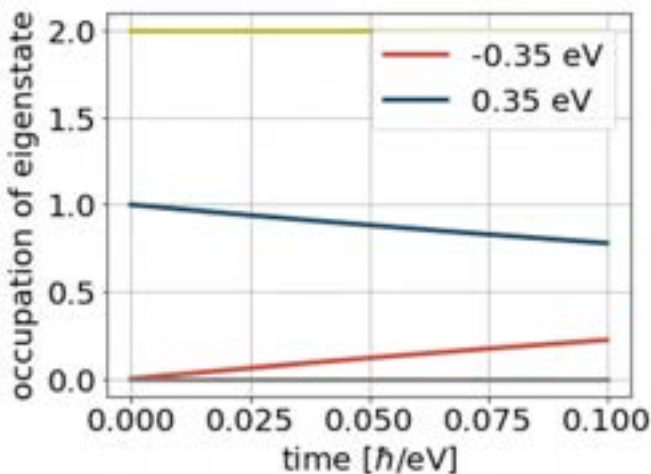```

****** TIME: 0/1000
Working fine, timestep: 10.
This run took 0.4397139549255371 seconds
```

In [5]:
```python
excited_idx, ground_idx = maths.get_adatom_states_index(
    flake_1.energies, flake_1.eigenvectors)

plot_energy_occupations(
    energy_occupation, evolution_1.time_axis, flake_1.energies,
    ground_index = ground_idx, excited_index = excited_idx,
    plotting_threshold=0.025, figsize=(6,4.5))
```

Example 7.2. Including dissipation with Lindblad operators.

Again, we need to create a flake, create an adatom and couple it to the flake,
define an external field and define the parameters of the time evolution.

In [6]:
```python
flake_params = {'shape': Shape.TRIANGLE, 'width_in_nm': 0.7,
                'edge_type': 'ac', 'verbose': False}

adatom_params = {'energy_levels': [0.5,-0.5], 'hopping_rates': [2.0, 2.0],
                'coordinates': [0,1], 'dipole_moment' : (0,7.5,0)}

field_params = {'illumination_type' : Illumination.CW, 'frequency': 2,
                'amplitude': 0.05, 'polarization_angle': 90}
```

```
evolution_params = {'end_time': 0.1, 'number_of_timesteps': 1_000,
                    'initial_state': 1, 'stationary_state': 0, 'equilibrium_state': 0,
                    'use_rwa': True, 'is_induced_on_adatom': True}

flake_1 = Flake(**flake_params)
adatom_1 = Adatom(**adatom_params)
flake_1.add_adatom(adatom_1)
```

Next, we will need to specify parameters of the Lindblad-based dissipation.
We can choose to use only jump operators (`DissipationType.SP_EMISSION`)
or both jump and decoherence operators (`DissipationType.WITH_DECOHERENCE`).

In the case of `DissipationType.SP_EMISSION` we need to specify one parameter:

- `gamma_array`; a 2D array that at position (i,j) stores the transition rate for the jump operator between states i and j

In the case of `DissipationType.WITH_DECOHERENCE` we need to specify two parameters:

- `gamma_array`; a 2D array that at position (i,j) stores the transition rate for the jump operator between states i and j
- `decoherence_gamma_array`: 1D array which at position i stores the value of the decoherence rate for state i

In [7]:
```
gamma_array = create_gamma_array(flake_1, 0.3, "all")
decoherence_gamma_array = create_decoherence_gamma_array(flake_1, 0.3)

dissipation_params = {
    'type': DissipationType.WITH_DECOHERENCE,
    'gamma_array': gamma_array,
    'decoherence_gamma_array': decoherence_gamma_array}
```

Next we run an evolution without external field but with the defined dissipation.

In [8]:
```
evolution_1 = Evolution(**evolution_params)
dissipation_1 = Dissipation(flake_1, **dissipation_params)

site_occupation, energy_occupation, *_ = flake_1.propagate_in_time(
    evolution_1, None, dissipation_1, print_iterations = 1_000)
```
```
---------------------------------------------------------------
****** TIME: 0/1000
Working fine, timestep: 10.
This run took 17.000746250152588 seconds
```

In [9]:
```
plot_energy_occupations(
    energy_occupation, evolution_1.time_axis, flake_1.energies,
    ground_index = ground_idx, excited_index = excited_idx,
    plotting_threshold=0.025, figsize=(6,4.5))
```